GRAVITY SUCKS, MORE OR LESS
TECHNIQUES & APPLICATIONS OF PRECISION GRAVITY MEASUREMENTS

by

Paul Gettings

A dissertation submitted to the faculty of
The University of Utah
in partial fulfillment of the requirements for the degree of

Doctor of Philosophy

in

Geophysics

Department of Geology and Geophysics

The University of Utah

December 2011

THE UNIVERSITY OF UTAH GRADUATE SCHOOL

SUPERVISORY COMMITTEE APPROVAL

of a dissertation submitted by

Paul Gettings

This dissertation has been read by each member of the following supervisory committee and by majority vote has been found to be satisfactory.

Chair: David S. Chapman

Richard G. Allis

Robert B. Smith

D. Kip Solomon

Brian J. McPherson

THE UNIVERSITY OF UTAH GRADUATE SCHOOL

FINAL READING APPROVAL

To the Graduate Council of the University of Utah:

I have read the dissertation of Paul Gettings in its final form and have found that (1) its format, citations, and bibliographic style are consistent and acceptable; (2) its illustrative materials including figures, tables, and charts are in place; and (3) the final manuscript is satisfactory to the Supervisory Committee and is ready for submission to The Graduate School.

Date

David S. Chapman
Chair: Supervisory Committee

Approved for the Major Department

D. Kip Solomon
Chair/Director

Approved for the Graduate Council

Fixme fixme
Dean of The Graduate School

ABSTRACT

This is the abstract for all three papers

abstract for techniques paper

abstract for nebraska

abstract for geysers 4-D grav

CONTENTS

CHAPTER 1

INTRODUCTION

Repeated high-precision gravity measurements track changes in vertical position and mass under stations. If gravity changes due to vertical motion are removed, gravity changes reflect only mass changes under stations. These changes can provide insight into changes of geologic or engineering interest; for example, changes in storage of groundwater aquifers [*Pool and Eychaner*, 1995; *Pool*, 2008], natural seasonal mass changes [*Goodkind*, 1986; *Keysers et al.*, 2001], steam field changes under exploited geothemal resources [*Allis and Hunt*, 1986; *Arnet et al.*, 1997; *Sugihara*, 2001; *Nordquist et al.*, 2004; *Sugihara and Ishido*, 2008], or combined mass and elevation changes on volcanic or tectonic systems [*Jachens et al.*, 1981; *Arnet et al.*, 1997; *Battaglia et al.*, 1999; *Jousset et al.*, 2000; *Ballu et al.*, 2003; *Vigouroux et al.*, 2008]. Precision gravimetry can also be used for detailed investigation of geologic structures, although this has been little used historically.The applicability of gravity (change) data is controlled by the precision of the measurements, which determines the minimum position and mass changes resolvable.

Previously reported techniques (see chapter 2 for a list) focused on using manually-recorded gravimeters and many loops of single or multiple gravimeters. In contrast, the techniques presented in Chapter 2 are designed to produce optimum precision from a single automatic-recording meter with minimal looping. Techniques for designing station networks, acquiring time-series data, and processing gravity readings for monitoring and exploration projects are covered. Included is a discussion of a new terrain correction code suitable for comuting terrain corrections world-wide.

Chapter 3 reports on a short monitoring study of an agricultural area in western Nebraska that is being used as a test bed for groundwater monitoring by various geophysical techniques. The monitoring project is used as a test case for data fusion in model construction. Gravity surveys were completed on a network of 18 stations over 4 months from July to October 2003, with coincident GPS campaigns (which showed no deformation) and groundwater monitoring at wells. The gravity and water level changes are used to infer an optimum study-wide specific yield of the shallow alluvial aquifer. Depending on whether the model construction use airborne EM for a basement topography or a fixed, deep saturated zone base, the optimum specific yield is 0.20 or 0.35. Misfit in models is consistent with the typical gravity change precision of 10 μGal.

To produce models using airborne EM results as basement topography to localize modeling into an alluvial aquifer, it is necessary to find a method for converting from geographically-reference isolines (elevation countours) to a regular grid for model construction. Various techniques for "uncountouring" the isolines and gridding observed data are compared to find the best techniques for the particular data sets of this project; gravity and groundwater levels are gridded from sparse observations using an equivalent sources method [*Cordell*, 1992], and the isolines gridded using a multiquadric surface fit [*Hardy*, 1971].

Combination of the groundwater, gravity, basement topography, and surface elevation data is done through constructing numerical models based on adaptively-sized columns of blocks. The gravity effect of the model, using an assumed constant specific yield across the entire model space, is computed at all gravity stations and gridded as if observed gravity changes. The predicted gravity change grid is compared to the observed gravity change grid using a RMS difference; a grid search of specific yields produces a misfit surface and an optimum specific yield.

Chapter 4 presents the results of gravity monitoring at The Geysers geothermal system in northern California between 2000 and 2011. Gravity change over the geothermal reservoir is sensitive to elevation and mass changes in the reservoir and cap rocks; when gravity measurements are coupled with high-precision GPS measurements to determine surface deformation, the gravity changes can be corrected to reflect only the mass changes under each station. Thus, combined gravity and

GPS monitoring can provide insight into saturation, temperature (via thermal contraction), mass balance, and steam-field boundary changes over time. While many of these changes can be detected in other ways (e.g. production well monitoring, microseismic networks, or InSAR) across the reservoir, gravity monitoring can play a crucial role in systems with challenging access, large spatial extent, or deep sources, such as The Geysers. Despite being the largest produced geothermal system in the world, The Geysers does not have a particularly well-defined boundary for the overall system. Multiple operators and a long production history combine to make delineation of the maximum extent of production changes, reservoir boundaries, and well interference difficult at best. To help address the challenges of where and how The Geysers reservoir is changing at depth and on the surface, gravity and GPS monitoring began in fall 2000 and continued to early spring 2011.

CHAPTER 2

HIGH-PRECISION GRAVITY DATA ACQUISITION

2.1 Introduction

The applicability of gravity (change) data is controlled by the precision of the measurements, which determines the minimum position and mass changes resolvable. Measurement precision is controlled by acquisition and processing technique, and the precision of vertical deformation information. This chapter focuses on optimizing acquisition and processing techniques; vertical deformation data can be acquired using various GPS units and processing flows, or from InSAR, leveling, or other less common options.

Previously reported measurement techniques [*Whitcomb et al.*, 1980; *Jachens et al.*, 1981; *Dragert et al.*, 1981; *Allis and Hunt*, 1986; *Hunt and Kissling*, 1994; *Andres and Pederson*, 1993; *Arnet et al.*, 1997; *Battaglia et al.*, 1999; *Furuya et al.*, 2003; *Sasagawa et al.*, 2003; *Ferguson et al.*, 2007] generally use manually-recorded gravimeters, typically LaCoste & Romberg model "D" meters (1 μGal reported precision); *Whitcomb et al.* [1980] and *Furuya et al.* [2003] are notable exceptions, where multiple model "G" gravimeters ($\sim$10 μGal reported precision) were used to speed surveying over large areal and elevation extents. *Sasagawa et al.* [2003] and other sea-bottom monitoring projects use a 3-sensor gravimeter derived from Scintrex CG-3Ms to conduct highly automated ocean-bottom gravimetry. All techniques generally use multiple loops of one or more gravimeters to address instrument drift and tare concerns; *Sasagawa et al.* [2003] use a single loop of three sensors at once. The multiple occupations and/or gravimeters also allow for statistics (typically averaging or linear least-squares fitting) to be applied to reduce measurement errors. *Ferguson et al.* [2007] uses a CG-3M, but with a custom-built computer interface for logging and real-time analysis. The looping and analysis scheme of *Ferguson et al.* [2007] is very similar to those presented above for LaCoste & Romberg G meters, with low-order polynomial instrument drift functions (typically linear or cubic) fit from repeated station occupations.

In contrast, the techniques presented here are designed to allow for large networks to be rapidly measured using a single instrument, with minimal looping. This allows for maximal station counts for a project, while minimizing costs (instrument and field support). To achieve maximum return with minimal cost, the instrument operators are required to adhere to a relatively strict regimen for acquisition and processing of data.

The rest of this chapter consists of sections on the design of projects, station networks and repeat schemes, and algorithms for raw data processing.

2.2 Station Network Design & Repeat Schemes

Designing station networks always involves a trade-off between the number of stations and the time available to occupy the network. For the discussion here, we will assume that only one instrument is available, although the extension to multiple instruments is straight-forward.

2.2.1 Network Design

Station networks must be designed to capture the signal of interest. Given a restriction on the total number of stations that any project can occupy in its available time, this capture requirement will mean placing stations to maximize signal information with the minimum number of stations.

Station networks will typically cover either rectangular or circular regions, often with areas of high station density (near a source or sink of interest) and other areas with few stations (far from sources of interest). The dense station areas must be designed to capture (perferably on all sides) the signal of interest, and so should bracket the source of interest. Far-flung stations can generally be far more sparse, but should also surround the source(s) of interest to allow for regional/natural signal capture. Do not make the mistake of placing all stations on the target source, and neglecting nearby and far-flung stations; the resulting data set will be inadequate for most interpretation tasks.

Station spacing, in the densest regions, need not be less than the depth of the signal. Higher density will not reveal more information, as the nature of the gravity field is such that deep sources produce smooth, broad signals at the surface. Hence, keep the dense station spacing no tighter than half the depth of the source.

Far-flung stations should be as close as practical, but sufficiently far that the source will not influence the stations during the project lifetime. In hydrologic projects, this typically results in far-flung stations 2-8 km from the sources. For geothermal investigations, far-flung stations may be 30+ km from the production field. Do not choose all far-flung stations to be in different hydrologic and/or meteorologic regions than the sources, as the signals at such stations adds considerable complexity to interpretation.

Regular grids of stations are convenient for interpretation, but typically require too many stations to cover the region of interest to be practical. Thus, most projects will likely end up with networks that resemble collections of sparse rings and clusters. Irregular geometry generally does not greatly complicate interpretation, and increases the area that can be covered in a given time, or reduces the number of days required to measure the target signal.

Using the repeat occupation schemes presented in this manual, and assuming easy road transit between stations (1-5 min driving between stations), 11-15 unique stations can be occupied in one day, including time for commuting from the office/hotel to the field site. As an example, a project that can afford 1-3 days in the field for each campaign can have a network of 10-35 stations total. The stations per day rate is the critical factor in network design for any project, and determines the trade-off between number of stations and days in the field per campaign.

Summary

1. Networks need to cover sources of interest **and** far-flung regions for regional control. This requirement is relaxed to allow a network to only cover the source of interest if absolute gravity measurements are available during a project, as the absolute control can remove the need for far-flung/"stable" stations.

2. Projects need to first determine how many days per campaign are feasible, and then compute the maximum number of stations in the network.

3. Given a maximum number of stations, place stations in an irregular geometry to maximize the chances of capturing sources and regional/natural signals.

4. With the repeat schemes in this manual, 11-15 unique stations/day is the maximum that can be occupied.

5. Station spacing closer than about half the source depth is generally a waste of station occupations.

2.2.2 Station Repeat Schemes

Field data will have nonlinear instrument drifts due to transport effects, errors in Earth tide corrections, instrument tares, or other uncorrected noise. To measure and correct this nonlinear noise, it is necessary to have repeated occupations of stations in a single survey; by assuming gravity at a given station is static during a campaign, we can use repeated occupations to remove noise and improve our estimate of the true gravity field.

Choosing the scheme for repeating occupations of stations during a campaign is a critical part of project design, and is worth spending some time to get correct. The goal is a station occupation scheme (or schedule) that will allow at least two occupations of all stations in a network, 4-5 occupations of a local base station for each day of a campaign, and minimum transport time between stations.

To illustrate the general repeat schedule for a day of stations, assume a single day network of 11 stations, plus the office (called `O`). Name the stations by letters

(A-K). Measurements taken at the office/hotel before moving in the morning, and after returning at night, will be used to tie multiple days together, hence station O is critical to all projects.

Measurements at station O must be taken before significant transport of the gravity meter; there is no way to determine instrument drift before the first measurement. Thus, ensure the gravity meter is stored overnight next to station O to allow a measurement without transport at the start of the next field day.

For any repeat scheme, it is highly recommended to write down the station order, in complete detail. Repeat schedules are complicated, and not easy to rebuild from scratch in the car!

2.2.3 Regional Networks

The general procedure to develop a station repeat scheme, given a regional network (one that covers a region, **not** a line), is to break the entire survey into chunks of 11-15 unique nearby stations for each day. A centrally-located station is chosen as the *local base*, which will be occupied at least 4 times in the day.

A general repeat scheme for 11 stations is:

```
O-A-B-C-D-E-A-F-G-H-I-J-K-A-B-C-D-E-F-A-G-H-I-J-K-A-O
```

27 occupations total, which would require ∼9 hours of measuring, typically.

Note that station A is occupied 5 times. If time is short, the **fourth** occupation (second to last occupation) could be omitted as each occupation after the first full loop of stations is closing repeat loops. In no case can the final measurements of A or O be omitted, as these loops are used to provide overall drift during the day and tie together multiple days.

For a network with 15 stations (A-P), use the repeats of A to ensure that there are not many hours between a repeat during the first full loop of all stations:

```
O-A-B-C-D-E-A-F-G-H-I-J-A-K-L-M-N-P-
  A-B-C-D-E-F-G-H-I-J-K-L-M-N-P-A-O
```

35 occupations total, which would require ∼12 hours of measuring, typically.

For such a large number of stations, station `A` must be occupied 5 times to create sufficient looping early in the day, before the loop closures during the second tour of the daily network. As with smaller networks, the last measurements of `A` and `O` are critical for tieing multiple campaign days together and tracking long-term meter drift during a campaign.

2.2.4 Linear Networks

The general procedure to develop a station repeat scheme, given a linear network (one that is a line), is to break the line into chunks of about 4 unique stations, and then stitch multiple chunks together into a day of 11-15 stations.

Because the network is a long line, efficient loops are best done by a modified ladder technique where a chunk of stations are measured from the start, then measure back to the start, then jump back to the end of the line.

For example, a day with 12 stations (`A-L`) plus the office (`O`), broken into 3 chunks of 4: `A-D`, `E-H`, and `I-L`

```
O-A-B-C-D-E-
            D-C-B-A-F-E-G-H-I-J-
                                I-H-G-F-K-J-L-K-L-A-O
```

27 occupations total, which would typically require ∼9 hours.

Note the overlaps between chunks, which prevents any two chunks from being disconnected; the goal is to have every chunk have at least one station overlap with the next chunk, and every station has at least two occupations in the day.

The final measurements of stations `A` and `O` are critical in linear networks, for the same reasons as with regional networks.

2.2.4.1 Preferred Repeat Schedules

To investigate how different repeat schemes affect the ability of a drift function inversion to recover a drift function, synthetic drift functions were built for a Monte Carlo study.

A polynomial function is used as the basis of the synthetic drift function; polynomials tested ranged from linear to cubic, to achieve basic drift function shapes ranging from a line to a peak-to-trough. Uniformly-distributed random values were added to each drift function at each station occupation. Different repeat schedules were used in drift function inversions, with the resulting drift function compared to the input synthetic data. The RMS difference between input and recovered drift functions at each station is scaled by the maximum range of the drift function, and the result plotted against the maximum range of polynomial divded by the range of the random error; the resulting plot (figure 2.1) shows a unitless RMS difference vs. unitless fraction of random error.

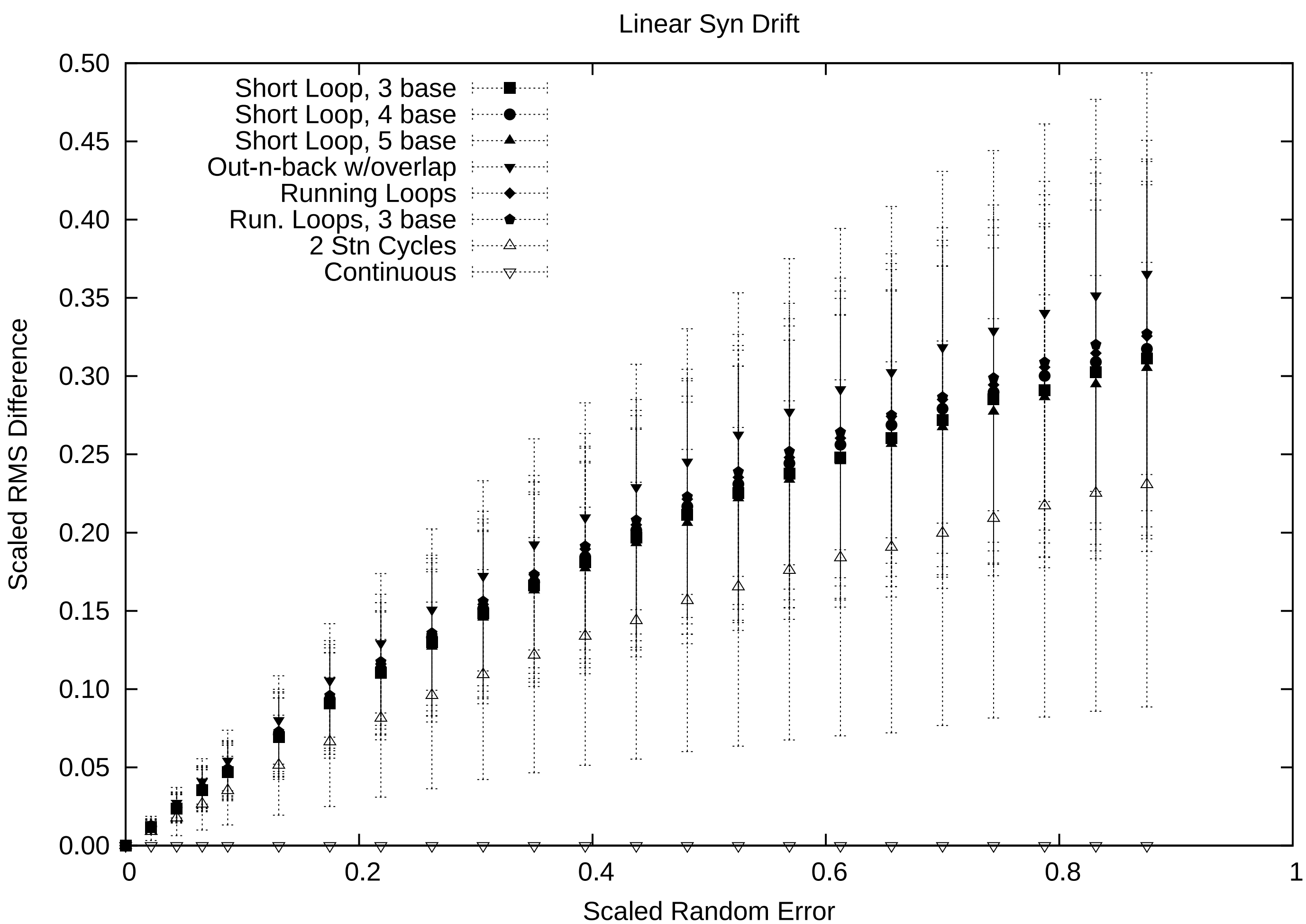

Figure 2.1. Average scaled RMS difference vs. fraction of random error. Results are for 10 000 trials.

Eight repeat schemes were tested: (1) short loops (as described above) with three base occupations, (2) short loops with 4 base occupations, (3) short loops with 5 base occupations, (4) out-and-back with overlap (see above for linear networks), (5) running loops, (6) running loops with 3 base occupations, (7) two station cycles, and (8) single station continuous. The last scheme is a check on the drift inversion algorithm - no field campaign would use repeated occupations of one station.

All repeat schemes correctly recover the input synthetic polynomial for no random error. As the random error grows, the continuous repeats perfectly recover any drift function. Two station cycles are next best, with scaled differences growing to 0.25 when the random error is nearly equal to the linear rate.

2.2.5 Reference Stations

To handle instrument drift between surveys, one or more stations are assumed "stable," meaning no gravity change over time. The apparent gravity changes at the reference station(s) provide a correction to the measured gravity changes to compute gravity changes for interpretation. Any signals at the reference stations are superimposed (in an inverted manner) on all other gravity stations. In general, reference stations should be determined by the location of absolute gravity measurements during campaigns; gravity changes at reference sites are then directly measured, and the sites need not be stable.

In practice, many projects will need to use the far-flung stations as a set of reference stations, holding the average to zero. A suite of far-flung stations also provides a measure of the variability in natural signals, and will remove regional signals. Removing appropriate regional signals can be used to enhance the signal of interest. However, far-flung stations that are too distant, or in a different hydrologic or meteorologic region, will complicate interpretation.

2.2.6 Example Networks & Repeat Schemes

Here are two example networks and their repeat schemes. The first example is taken from an artificial recharge project based around infiltration of surface water into a deep aquifer using a small area of ponds. The second example is from Yellowstone National Park, where two lines of stations are being used to measure gravity change related to volcanic changes in the deep magma chamber; the large extent of the project and short field campaigns dictate the use of lines of stations, rather than a grid.

2.2.6.1 Weber River Aquifer Storage & Recovery

The Weber River ASR project was a multi-year infiltration experiment to determine the feasibility and limits of recharging the deep municipal-supply aquifer under the South Ogden urban area using surface water poured into 5 acres of infiltration ponds. As part of the overall project, the University of Utah used repeated high-precision gravity measurements on a network of 30 stations to track the infiltration and migration of the water. Figure 2.2 shows the network of stations used for the project. Stations were generally located on existing concrete structures; stations WRP01 (labelled 01 on the figure) and WRP28 were built using a 12" paving stone over a 12" deep hole filled with cement, with two 24"-long pieces of 3/8" rebar driven into the ground out of the poured cement. Stations WRP26 and WKRP were destroyed during the project by construction, but replaced with WRP30 and WKRD. Ideally, WRP30 and WKRD would have been occupied before the loss of WRP26 and WKRP, but this wasn't possible. Western stations were dropped early in the project to add more central stations once migration to the south, and not west, was observed. Thus, out of 30 stations located, no more than 25 needed to be occupied during any campaign.

To occupy the 25 stations of a campaign required two field days for gravity and two additional days for precision GPS. An example repeat schedule from actual field notes for the first day:

```
WBB115-WKRD-WRP05-WRP06-WRP07-WRP27-WRP08-WRP29-WKRD-
            WRP09-WRP02-WRP01-WRP11-WRP04-WRP28-WKRD-
            WRP05-WRP06-WRP07-WRP27-WRP08-WRP29-WKRD-
            WRP09-WRP02-WRP01-WRP11-WRP04-WRP28-WKRD-WBB115
```

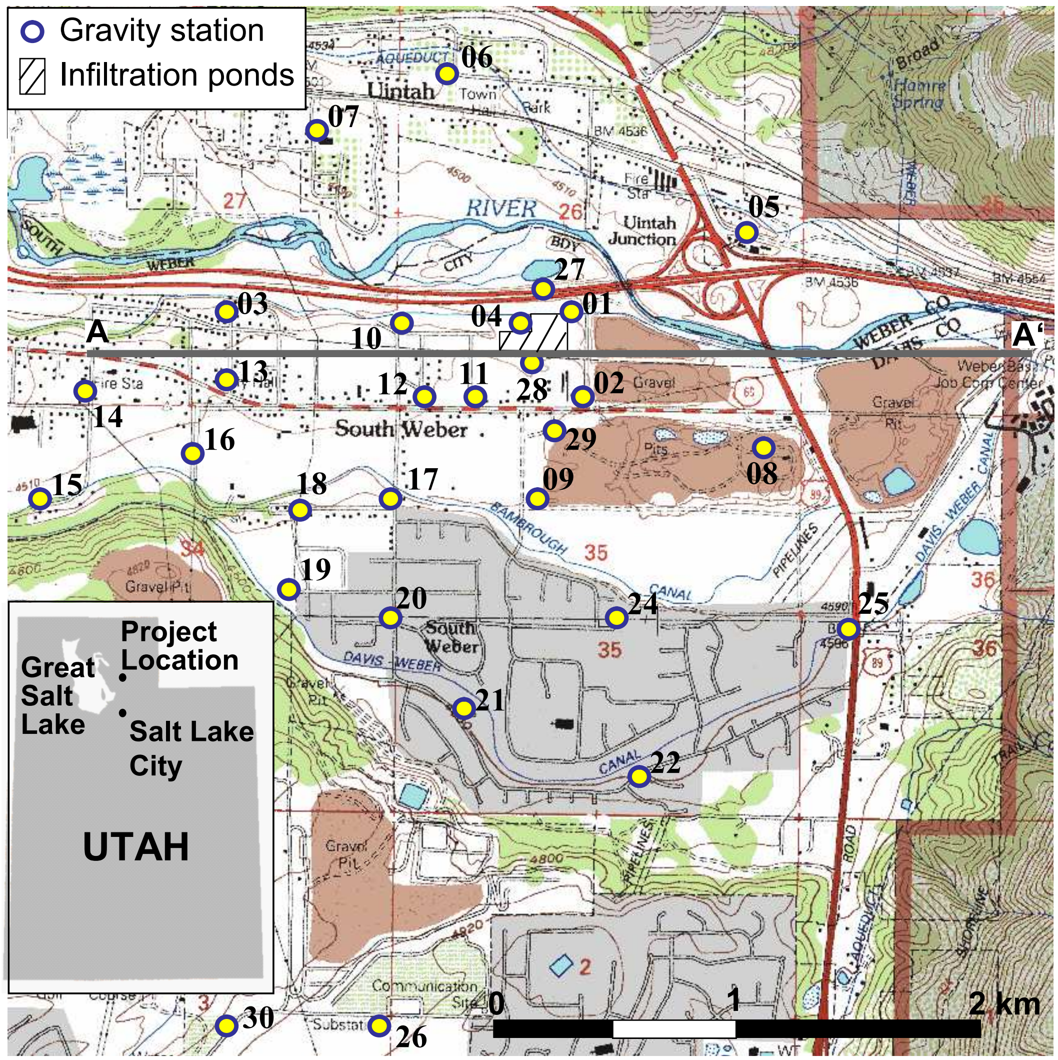

Figure 2.2. Station map for the Weber River Aquifer Storage & Recovery project gravity network. Station names have had a common "WRP" removed from the front for clarity. Note the tight station spacing at the source of interest (the infiltration ponds) and the far-field stations for natural background and instrument drift control. Stations WKRP and WKRD are ~9 km east of WRP05.

And for the second day:

```
WBB115-WRP12-WRP10-WRP13-WRP16-WRP17-WRP18-WRP19-WRP12-
      WRP24-WRP20-WRP21-WRP22-WRP25-WRP30-WRP12-
      WRP10-WRP13-WRP16-WRP17-WRP18-WRP19-WRP12-
      WRP24-WRP20-WRP21-WRP22-WRP25-WRP30-WRP12-WBB115
```

Note the five occupations of WKRD or WRP12, and the overall loop between WBB115 for each day, which is the long-term storage location of the gravity meter.

2.2.6.2 Yellowstone National Park Caldera Lines

Yellowstone National Park, one of the world's best-studied hot spots, has recently been showing rapid uplift in certain portions of the park [*Chang et al.*, 2007]. To help determine the cause of the uplift (magma intrusion? pressure changes? hydrologic changes?), a new gravity monitoring program was begun on a couple of existing gravity networks which are located along roads crossing the main deformation zone. Figure 2.3 shows the stations of one such line, as an example of a linear network. In the case of the Yellowstone project, the stations were chosen by recovering all the old gravity benchmarks possible, to allow comparison with the measurements from the 1970's to 1990's. By using fixed benchmarks (e.g. NGS benchmarks on bedrock, etc.) with good field notes for exact meter positions, and assuming station 11mdc stable between campaigns, it is possible to tie together measurements over 30 years to look at long-term changes in the park!

Due to the linear nature of the network, campaigns use a ladder repeat schedule such as:

```
11mdc-13mdc-hollis-lc58-22mdc-y367-
  22mdc-lc58-hollis-11mdc-13mdc-24mdc-y367-
z367-kaygee-f11a-e11a2-arbee-27mdc-
  arbee-e11a2-f11a-kaygee-z367-24mdc-27mdc
```

This is for a single day; the plotted line takes two days to fully occupy, with the second following a similar repeat pattern to the first, starting with 11mdc and then

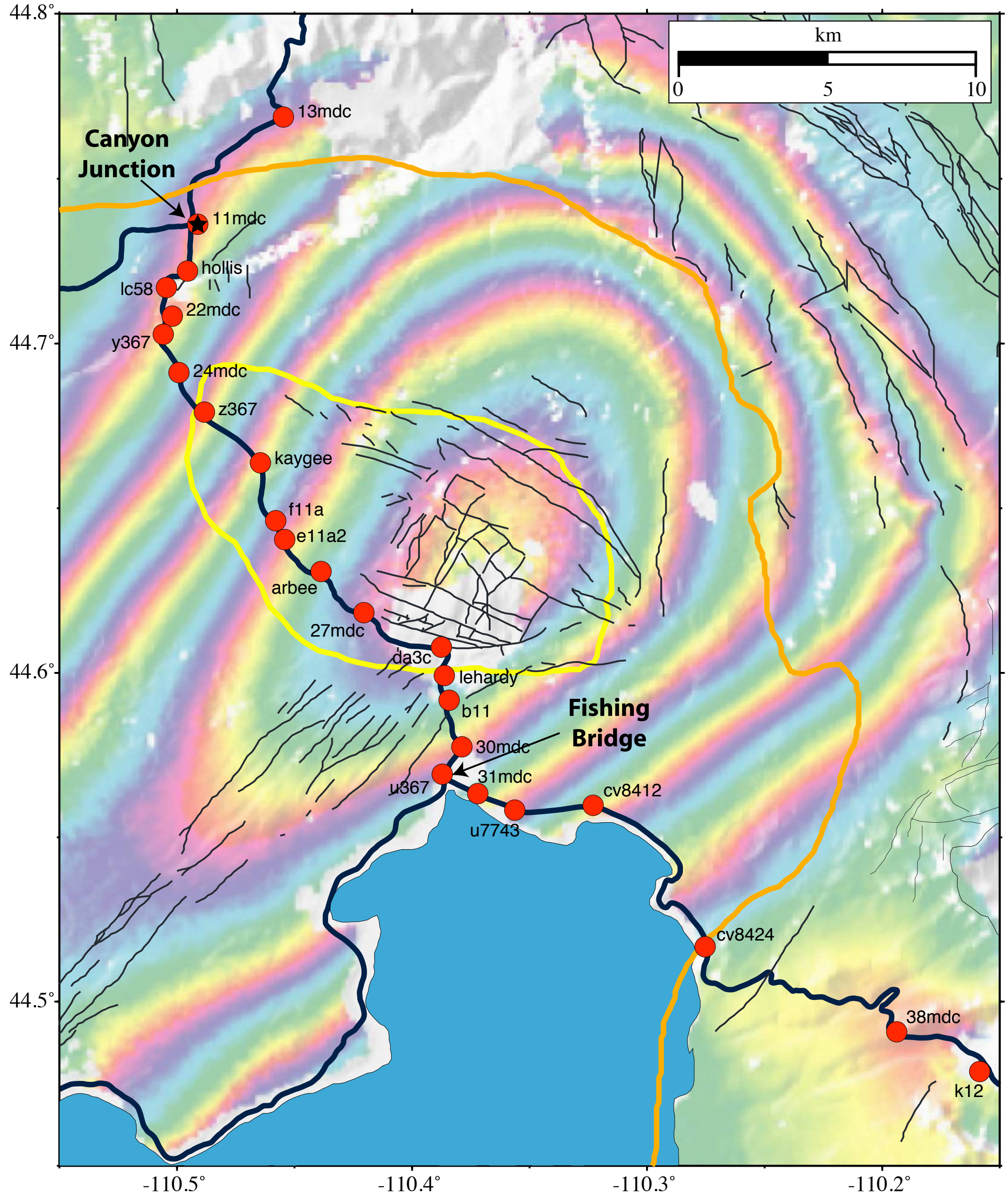

Figure 2.3. Station map of one of the Yellowstone gravity lines being used for investigation of the sources of Yellowstone's recent deformation. Note the linear nature of the station network, making the most efficient looping techniques ladders. Background is an InSAR image of deformation, with the 600 ka caldera outline in orange, and the main deformation zone in yellow. Station 11mdc, with the star, is used as a stable reference between campaigns.

da3c to k12 and back in segments. Note that at the end of the line (38mdc and k12), the repeat schedule flops back and forth to get 2 readings of each station without having to drive the entire line again:

```
...-cv8424-38mdc-k12-38mdc-k12-cv8424-cv8412-11mdc
```

This sort of trick allows for two occupations of all stations in the line, while minimizing driving without measurements.

2.3 Gravimeter Storage & Long-Term Drift

In the experience gained so far, it is critical to store gravity meters in such a way that they are continously available for field work, and are given a chance to "age" as quickly as possible. Thus, relative gravity meters should be stored level, on wall power with an attached battery (in case of power failure), and reading/recording. The storage location must be stable, quiet, and secured since the meters will be left unattended for long periods.

The collected long-term drift data are valuable in checking the functioning of the meter, and in learning the expected daily drift rates for a meter. Since every meter is unique, drift data for each meter is required. Also note that if the meter is recording up until a field campaign, there is no need to start or end a campaign day with occupations of the base, as the long-term data can be used instead. Add the long-term drift data to the field data after downloading, and save an untouched backup of the downloaded data.

The settings for long-term drift measurements are identical to those for field measurements (see section A.2) except the `Read Time` should be increased to 180 or 240 s.

Download and check the drift rates for the meter every 1-4 weeks. This will also help catch impending temperature and tilt problems. A command-line utility (*cg5e_cmd.py*) has been included with the reduction software to parse CG-5 text data files and reformat into easily plotted files. Alternatively, load the CG-5 text file into *Excel* for plotting, or import the SGD-format data file into *Oasis montaj.*

It is recommended to store all the drift data for future reference, to help catch and interpret changes in the CG-5 drift rate, and to allow investigation of the long-term drift characteristics of the meter.

2.4 Gravimeter Transport

Transport of the gravity meter determines the success of projects. Rough transport will result in large apparent meter drifts, increased reading error, and possibly destruction of the sensor. After years of testing various transport schemes in vehicles and on foot, the following suggestions have been developed:

- Vehicle transport should be in a seat, with the seat belt used to strap the meter down under light compression. This helps keep the meter from tilting or bouncing on bumpy roads.
- The best seat for a gravity meter is the middle of the back seat in a four-door vehicle; this puts the meter closest to the geometric center of the vehicle, resulting in the least acceleration due to bumps and turns.
- If no backseat is available, put the meter in the passenger seat, and strap securely down.
- Don't let items hit the meter while in transport.
- Don't transport the meter on its side; keep it upright at all times.
- Typical car seats deal well with high-frequency vibration, such as from washboard roads. Thus, the real concern is sudden large bumps, such as from potholes or trenches when off-pavement.
- Slower travel with gentle ups and downs does not impact the gravity meter as much as sudden, sharp impacts. So, drive slowly over rough roads.
- Do not bump the meter into the car when putting it in, or taking it out, of the vehicle.

- Walking with the meter on a shoulder strap is worse than holding it in your hand, and trying to keep it stable. Don't let the meter bump against your leg when you walk; hold it away from your body.

- Backpacks are good for long-distance travel on foot, but vehicles are better if available.

2.5 Data Processing Theory & Algorithms

2.5.1 Station Occupation Processing Overview

Gravity data acquired as a time series, as advocated herein, passes through a number of processing steps to go from a time series of raw readings to a single gravity value for the occupation. These steps, in order, are:

- Temperature, voltage, tilt corrections

- Solid Earth tide corrections

- Automated QA, including detrending

- Time series processing (averaging or extrapolation)

- Elevation change correction

- Instrument drift correction

- Difference from reference station

2.5.1.1 Gravimeter Averaging Time

When acquiring high-precision gravity data using the techniques advocated here, the CG-3M or CG-5 gravimeter is set to record many 30 s averages. Other techniques have used varying occupation times and reading cycles [e.g. *Sugihara*, 1999; *Sasagawa et al.*, 2003; *Ferguson et al.*, 2007]. The 30-s reading cycle was chosen by inspecting the instantaneous (running) average of five 60-s cycles of a CG-3M (which has the same sensor as the newer CG-5) gravimeter; one such cycle

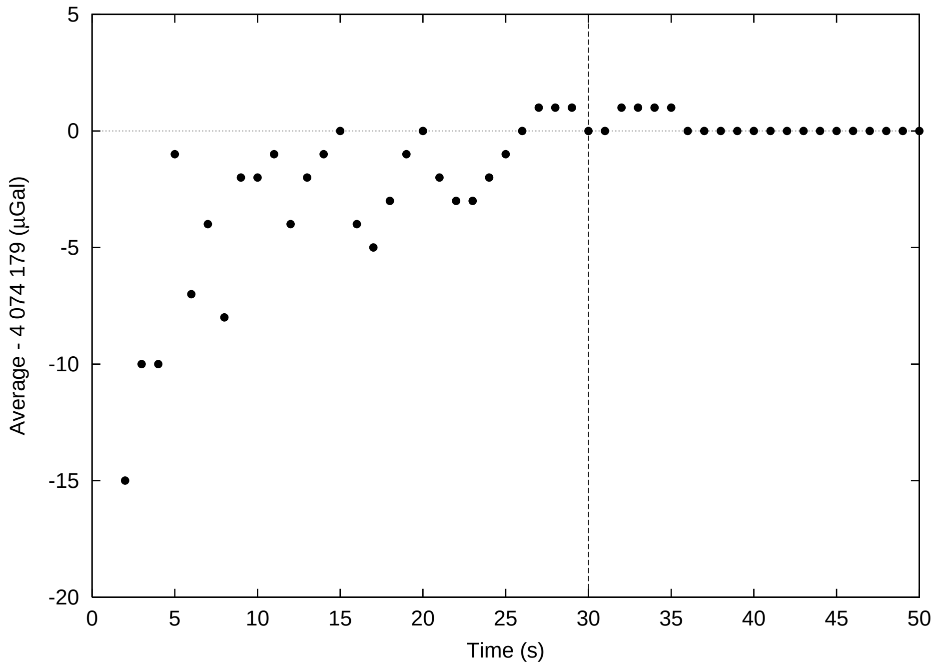

Figure 2.4. Instantaneous (running) average of gravity samples for one reading at a gravity station. Note the small change in the average after 30 s (vertical dotted line); variation is reduced to ~1 μGal.

is plotted in Figure 2.4. The running average is recomputed with every sample, along with the standard deviation. No corrections are applied to these statistics during the reading cycle, but are applied to the final average. In all five inspected cases, the instantaneous average reaches a value within 1 μGal of the final value within the first 30 s. It is more valuable to have more stored readings of shorter time, to improve statistical certainty and allow for finer-grained quality control in processing. Read times less than 30 s tend to run into problems with excessive standard deviations due to the short sampling. There is also a built-in minimum 3 s delay between measurement cycles due to the CG-5 and -3 design. This delay becomes steadily more important at shorter read times, as more of the meter's occupation time is spent waiting rather than reading. Thus, the 30 s read time is a balance. Acquisition using an Aliod gravimeter, which takes 1 s samples instead of averages, uses a 12 min time series as well, but processes the individual samples differently.

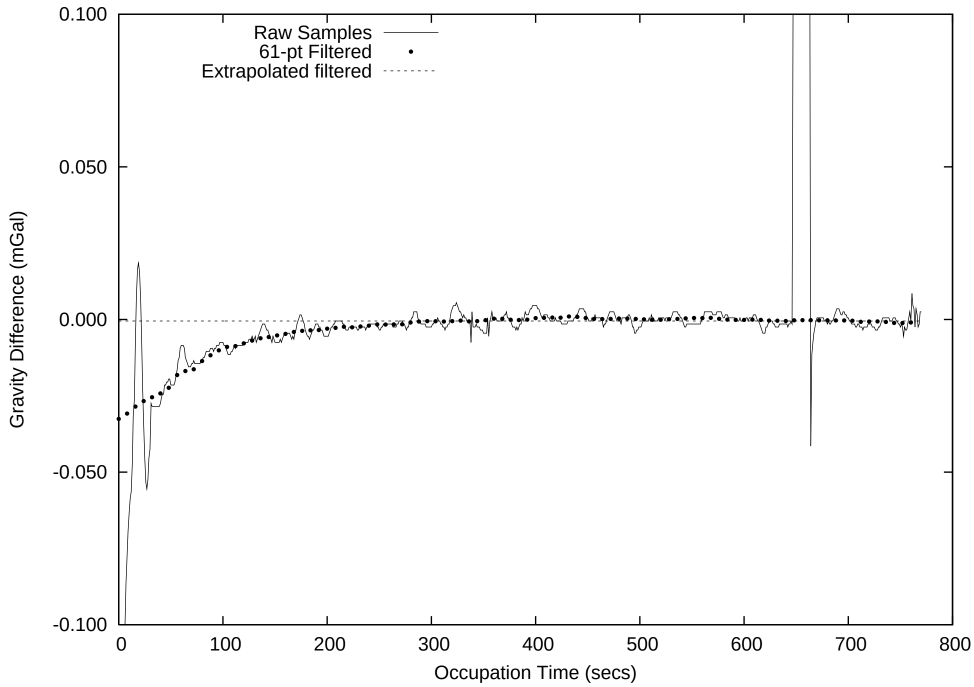

Figure 2.5. Raw, filtered, and extrapolated time series for station occupation 20 of 9 Oct 2007. The raw time series exhibits most of the common traits in Aliod-collected station data - rise from lower readings to higher, spikes from near-meter disturbances, and 30-60 s signals from environmental noise. Filtered time series uses an 8 s offset between points, with a 61-point centered window. Thiele extrapolation of the filtered series results in the constant value shown.

2.5.1.2 Station Occupation Length

Based on existing testing with real field conditions, stations should be occupied for a minimum of 10 min, with a good standard being a minimum of 12 min. Scintrex gravimeters show little transport effect after 3 min from start, but Aliod (zero-length spring meters) meters have some occupations with elastic relaxation (transport & unclamping) effects still noticeable after 10-12 min of measurements. However, given a standard field day with 35 occupations, lengthening occupations to 15 min adds 2 hrs to the field day, which may well be too long for accurate work. Hence, a compromise time of 12 min is adopted as with the CG-5.

An example raw station timeseries, with filtering and extrapolation results, is shown in Figure 2.5; the filtering and extrapolation procedure will be covered in greater detail later. The raw time series shows a distinct non-linear trend characteristic of elastic relaxation after unclamping. Due to the clamp holding the beam at the extreme low end of the range, the relaxation trends are always from lower gravity readings to higher. Note the large spike between 660 and 680 s. This spike, of ~2 mGal scale, is likely due to a near-meter disturbance (jogger running by the meter). Filtering is used to remove such spikes and decimate the data stream for numerical precision reasons before extrapolating to an infinite-time asymptote.

2.5.1.3 Temperature Compensation

Scintrex meters have both an automatic temperature regulation system, and a temperature readout system accurate to 1 mK. Due to the extreme sensitivity of the fused-quartz sensor to temperature, the meters apply a temperature correction automatically. Assuming the temperature readout circuits are working, Scintrex instruments require no processing for temperature changes.

An Aliod-equipped meter provides a coarse (0.1 C) temperature readout of the meter temperature for each measurement. According to the L&R literature, the temperature dependance of the metal zero-length spring is significantly less than that of the fused-quartz fiber in a CG-5 or -3. Hence, the relatively coarse temperature readings are used as a check of meter operation, not a source for compensation.

There is no data to indicate that a meter with apparently good voltage and temperature has significant temperature effects in the range of desireable field conditions (-10 to 30 C). Without a better temperature readout circuit, there is not enough precision in the Aliod data stream to produce a useful temperature correction to the data; instead, temperature measurements are useful only as a coarse quality control measure for removing/skipping data.

2.5.1.4 Voltage Fluctuations

Scintrex and Aliod instruments are not apparently affected by voltage drop during field use; battery voltages above 10.5 V are all that is required to maintain listed accuracy. With good batteries (typically 7-7.5 Ah), the meter and electronics should get at least 8 hours of measurements before needing a change. In conditions below 40 °F, battery life will be closer to 4 hours due to increased heating time.

Battery changes in an Aliod, unlike the CG-3M or CG-5, cannot be done without losing power for a second or so. This does not let the meter cool significantly, nor does it cause loss of constants in the electronics. Swapping batteries at 10.5-11 V is recommended for any instrument. Note that bad batteries will typically show good voltages for 4 hrs or so, and then drop from 11-11.5 V to 8-10 V in 5-10 min; this is an indication that the battery needs to be tossed and replaced with a new one.

Current data from readings with bad batteries where voltages dropped to <10 V show no gravity reading change with dropping voltage. Regardless, readings with voltages <10.5 V should be checked for consistency with previous, high voltage readings.

2.5.1.5 Tilt Corrections

Scintrex meters measure tilts in both directions, and apply a correction for non-zero tilt values. The correction is documented in the manual, and works for tilts up to at least 150 arcsec. Occasional check and adjustment of the zero-tilt setting, as specified in the manual, maintains the tilt error corrections.

Aliod-equipped meters provide a stream of cross and long level measurements, in counter units. Unlike the CG- series, these have not been converted to a displacement from maximum gravity in arcsec. The counter range is reported by L&R to be between [0, 65535]. There is a procedure in the Aliod manual for adjusting the levels to maximum gravity using the front display; this does not guarantee a maximum gravity counter value of 32767 or so.

Without testing to see how the gravity value changes depending on the deviation from "zero" (maximum gravity/nulled level galvo), a tilt correction can't be computed. To produce the necessary numbers, we need to know how many counter values are represented by 1 division on the galvo, and how much this affects the gravity reading. This is essentially determining the cross- and long-level sensitivities and zero errors as for the x,y tilt meters on the CG- series; however, the equations and procedures of the CG-3M manual can't be used unmodified!

A theoretical correction to the gravity values, given a tilt in cross- and long-level directions, can be derived from a coordinate rotation. Define ψ as the angle (in radians) to be rotated about the x axis, and θ as the angle (in radians) to be rotated about the y axis. Since we only measure a vertical component, rotations about the z axis are irrelevant and set to 0. Note that the angles ψ and θ are the angles we measure with the levels in the meter.

Now, compute a rotation from a theoretical, untilted frame to the tilted frame. By Euler's rotation theorem, we can compute a single rotation matrix A from the individual rotations about x, y, and z axes (B, C, D matrices) from $A = BCD$. Since there is no rotation about the z axis, $D = I$, and the resulting matrix is $A = BC$. B and C are defined as,

$$B = \begin{bmatrix} 1 & 0 & 0 \\ 0 & \cos\psi & \sin\psi \\ 0 & -\sin\psi & \cos\psi \end{bmatrix}$$

$$C = \begin{bmatrix} \cos\theta & 0 & -\sin\theta \\ 0 & 1 & 0 \\ \sin\theta & 0 & \cos\theta \end{bmatrix}$$

Hence,

$$A = \begin{bmatrix} \cos\theta & 0 & -\sin\theta \\ \sin\psi\sin\theta & \cos\psi & \sin\psi\cos\theta \\ \cos\psi\sin\theta & -\sin\psi & \cos\psi\cos\theta \end{bmatrix}$$

Application of this rotation matrix to an unrotated frame yields the rotated (measured) gravity value, g',

$$g' = g\cos\psi\cos\theta$$

since only the vertical component of the gravity field is measured. Hence, an unrotated gravity value can be computed from the measured angles and gravity values as

$$g = \frac{g'}{\cos\psi\cos\theta}$$

This is significantly different from the development of a tilt correction in the Scintrex manual, which is of unknown origin.

All that remains to implement a tilt correction for Aliod data is the mapping from level counter value to radians from local vertical. This will also require knowledge of the "zero" tilt counter value in the cross- and long-level directions. All of which must be empirically derived for each meter.

2.5.2 Solid Earth Tide Corrections

Raw time-series data have a solid Earth tide correction applied using the precise coordinates of each station from the parameter file and the formulas of *Tamura* [1987]; the Longman correction computed by the meter, if present, is first removed.

Solid Earth tides, generated by the gravitational deformation of the Earth, can generate gravity signals with peak-to-trough amplitudes in excess of 0.2 mGal. Computation of the tide can be accomplished starting with observations of the astronomical motion of the planets and Sun, with a result that is accurate to several μGal [*Longman*, 1959]. *Tamura* [1987] fits the amplitudes of a harmonic function to a set of predicted Earth tide potentials. The resulting function, with its empirically-derived constants, is accurate to better than 0.06 μGal [*Wenzel*, 1996]. Either Earth tide algorithm is of sufficient accuracy for high-precision gravity at the several μGal level, but the reduction package in this work uses the harmonic function. Both formulations require an assumed constant for the elastic response of the Earth to the applied stress. The constant has been taken as the standard value of 1.16.

Using the harmonic Earth tide correction from *Tamura* [1987] and correct positions and time offset, there are residual periodic signals evident in long-term records of meters on a fixed location in Salt Lake City, possibly due to loading effects of the Great Salt Lake. Figure 2.6 shows an example residual over time. These data were taken on a single station where a CG-3 was not moved for weeks, removing the possibility that the signals are short-term instrument effects. Attempts were made to remove the residuals by varying the time offset from GMT, the station position used for computation, and the Earth's elastic response parameter. Regardless of the shifts employed, the residuals remained, with peak-to-trough amplitudes of ∼5 μGal.

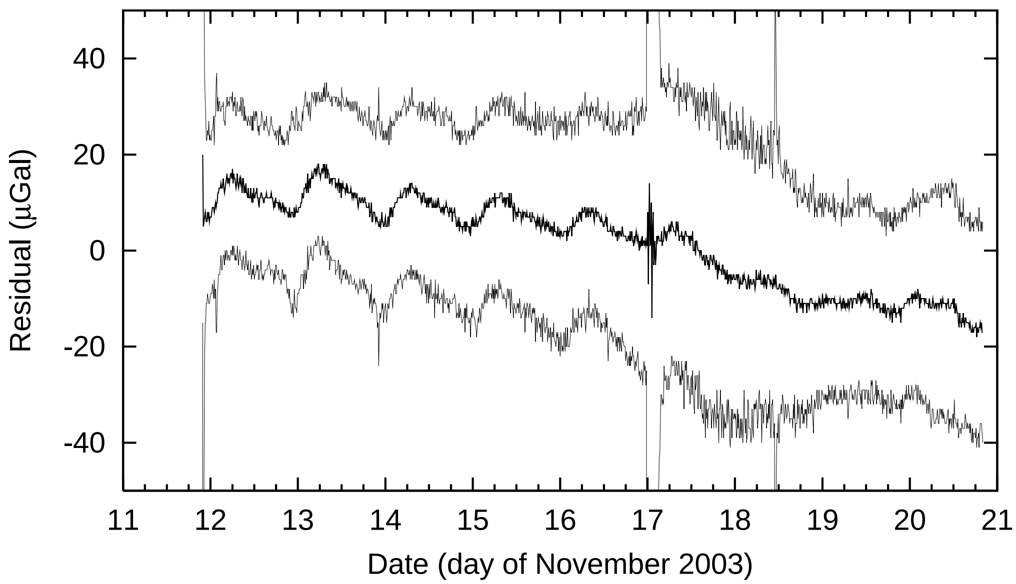

Figure 2.6. Residual gravity signal after removal of the overall average and Earth tide using *Tamura* [1987]. The heavy line is 540-second mean readings minus 4 687 480 μGal; light lines are residual mean plus or minus one standard deviation (σ). The large σ values (truncated at $\pm$50 μGal) indicate surface waves from a distant earthquake.

Applying a fast Fourier transform (FFT) to the time series gives an indication of the dominant frequencies of the residual signals. Using the residual data shown in Figure 2.6, the results are shown in Figure 2.7. The data from Figure 2.6 have been detrended by an additional -3 μGal/day to remove residual linear drift. Examination of the FFT power spectrum in Figure 2.7B shows highly variable power at the short (sub-day) periods, with increasing power with increasing period. The short-period power is dominated by the longer periods, and represents noise in the residual time-series of Figure 2.7A. Part of the noise is certainly due to the 1 μGal precision of meter measurements; note the residual time-series shows large numbers of quickly oscillating values different by only 1 μGal. There are four prominent "peaks" in the power spectrum, at periods of 0.5, 1, 3, and 9 days/cycle. While attempts to remove the residual signals by varying the Earth

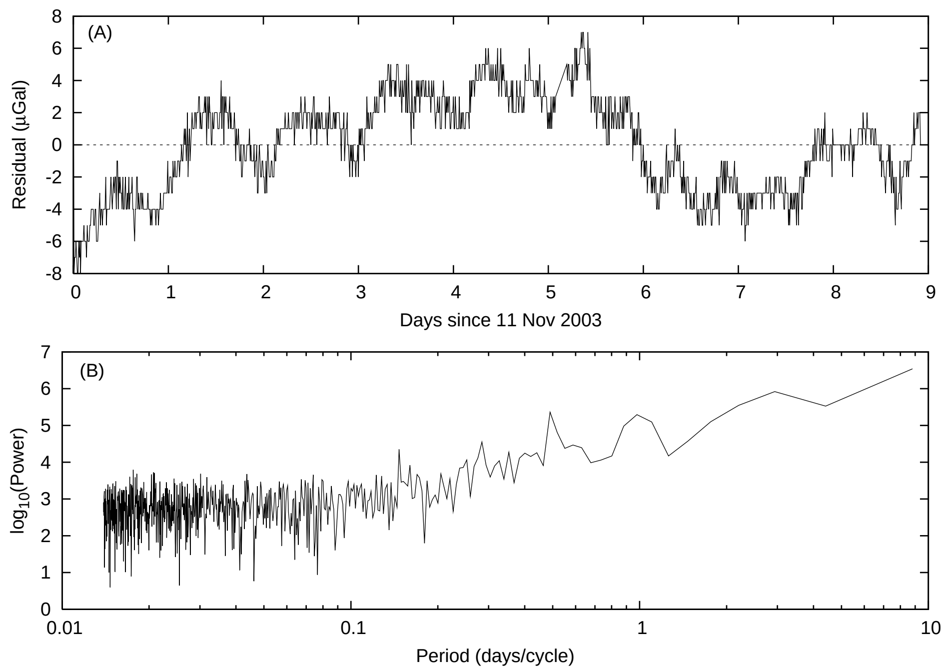

Figure 2.7. Investigation of dominant signal periods for Earth tide residual signals. (A) Residual gravity signal at a fixed site after removal of linear drift and Earth tides computed from [*Tamura*, 1987]. An additional -3 μGal/day drift has been removed compared to Figure 2.6. The sharp gravity changes during the large earthquake have been removed to focus on continuous signals, rather than the earthquake-induced surface waves. (B) Plot of the Fast Fourier Transform power spectrum of panel A as a function of period; the power is not normalized.

tide parameters proved unsuccessful, the long periods of the residual signals allow nonlinear instrument drift functions to remove residual Earth tide signals present in field data.

2.5.3 Station Time-series Analysis

Each occupation of a station results in a set of readings over approximately 12-15 min. This length of time was chosen to allow for any short-term effects of instrument transport to dissipate while maximizing the number of stations observable in a single field day. A 12-15 min time series also gives enough data to average out small random noise, such as intermittent vehicle traffic. For typical field handling of the instrument, transient effects in the CG-3M decay within 3-5 min, and may take up to 12 min or more in an Aliod-equipped L&R. Figure 2.8 plots the time-series of a

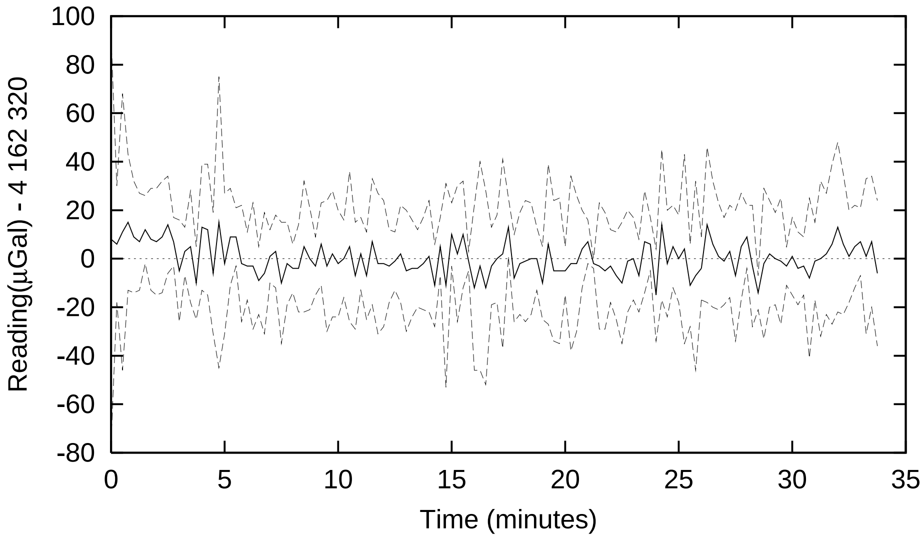

Figure 2.8. Time series of a long site occupation to test elastic relaxation properties of CG-3M gravimeter spring. Readings (heavy line) are shown with one standard deviation error envelope (light dashed lines), differenced from the average reading value. Note the elevated readings in the first three min, and the lack of noticeable trend after 5 min.

long site occupation to determine the relaxation characteristics of CG-3M 9711420. The light dashed lines indicate the envelope of one standard deviation (s.d.) of the measurements. Note the slightly elevated mean values (heavy line) in the first 3 min of measurement, and the near-zero means afterwards. There is no discernible trend in the data after the first 5 min; for a 15 min occupation, there would be at least 10 min of useful data after removing the first 3 to 5 min.

If particularly rough handling is suspected or known, 30 or 60 min occupations of a station are advisable. Figure 2.9 shows two time-series of CG-3M meter readings before and after an extreme shock where the meter was blown off the tripod by an exceptional wind gust. Error envelopes have been omitted for clarity in the plot, and both time-series have been differenced from the average reading of the "before" time series. The "after" time-series was taken immediately after the meter was restored to the tripod, 13 min after the extreme shock. Note the significant trends in the "after" time series for up to 20 min.

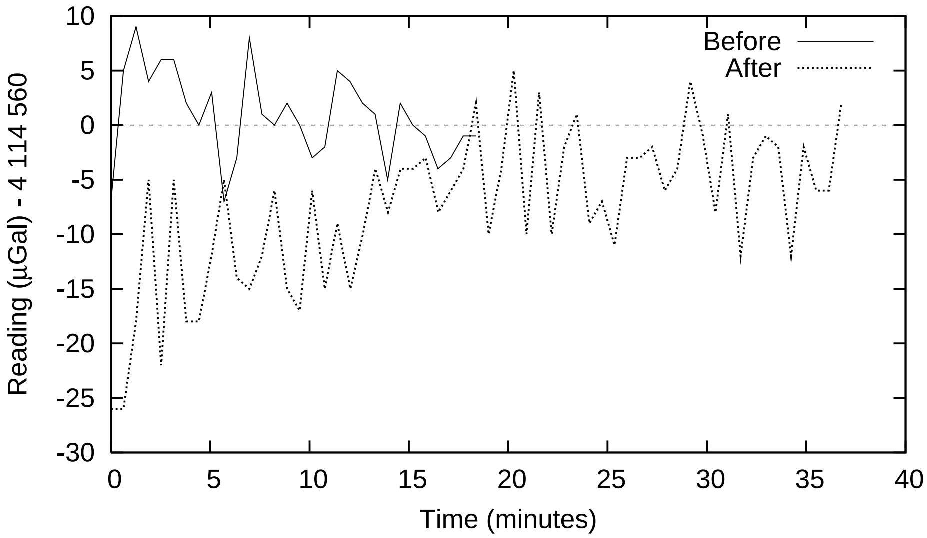

Figure 2.9. Time series before and after an extreme shock to the CG-3M meter. "Before" data taken from a station occupation previous to the severe shock. "After" data taken 13 min after shock at the same location. Error envelopes omitted for clarity.

Although recorded for testing the elastic relaxation of the gravimeter spring, the time-series in Figure 2.8 is typical of normal stations. The initial trend or deviation in the readings is most likely due to elastic relaxation of the spring from small shocks in transport between stations. The trend is no longer noticeable after the first 3 min, so the initial readings are discarded for the purposes of averaging and analysis. Although discarded from analysis, the data are valuable for checking the response of the instrument to transport between stations; large trends in the first few minutes can indicate particularly rough transport, and hence the data warrant closer inspection than at other stations.

2.5.3.1 Automated Quality Assurance

As an automated check of station occupations, the processing package computes a linear fit to each time-series of readings. If the slope of the linear fit is larger than a defined threshhold, chosen empirically to be 97.2 μGal/hr (based on inspection of field stations with noticeable trends), then the time series is detrended with the fit slope. The procedure excludes the first few (typically 3) min of data, and performs a weighted fit using the inverse of reading standard deviations. This effectively pivots the time-series about the 3 min reading to have no overall trend in the final 9 to 12 min of data. Linear trends in a station occupation time-series are typically due to incorrectly set tilt correction constants, with time-varying tilt of the meter. Since earlier readings have smaller tilt, the linear fit removes the effect of changing tilt while maintaining other signals in the time-series.

2.5.3.2 Time-series Averaging

After linear detrending, the time-series is converted to a single value using a weighted average, where the weights (w_i) are taken to be the inverse square of the standard deviations (s.d.) of the readings (g_i). The formulas used to compute the average and two standard errors of the mean are:

$$\begin{aligned}\bar{g} &= \frac{\sum w_i g_i}{\sum w_i} \\ \bar{\sigma} &= 2\left(\frac{\sum w_i}{N}\right)^{-1/2}\end{aligned}$$

where overbars denote average values, w_i is the weight of the ith data point, g_i is the gravity value of the ith point, and N is the number of readings in the time-series.

The weighted average is a robust number, but it does include the possibility of unnecessarily down-weighting good data. The downweighting problem comes from the use of the s.d. as the weight; it has been noted in long-term drift records that some sources of noise, such as earthquakes, do not significantly change the mean reading, but strongly affect the s.d. For the case of earthquakes, the s.d. can vary by as much as an order of magnitude. When these data are used in the weighted average, it receives a small weight due to the large s.d., even though the reading value is still quite accurate.

Attempts to improve on the scheme of a weighted average of 15 min time-series included testing with both exponential function fitting and rational function extrapolation algorithms. It was hoped that by using an alternate algorithm, it would be possible to obtain a long-duration (15 min) result from a short (8 min)

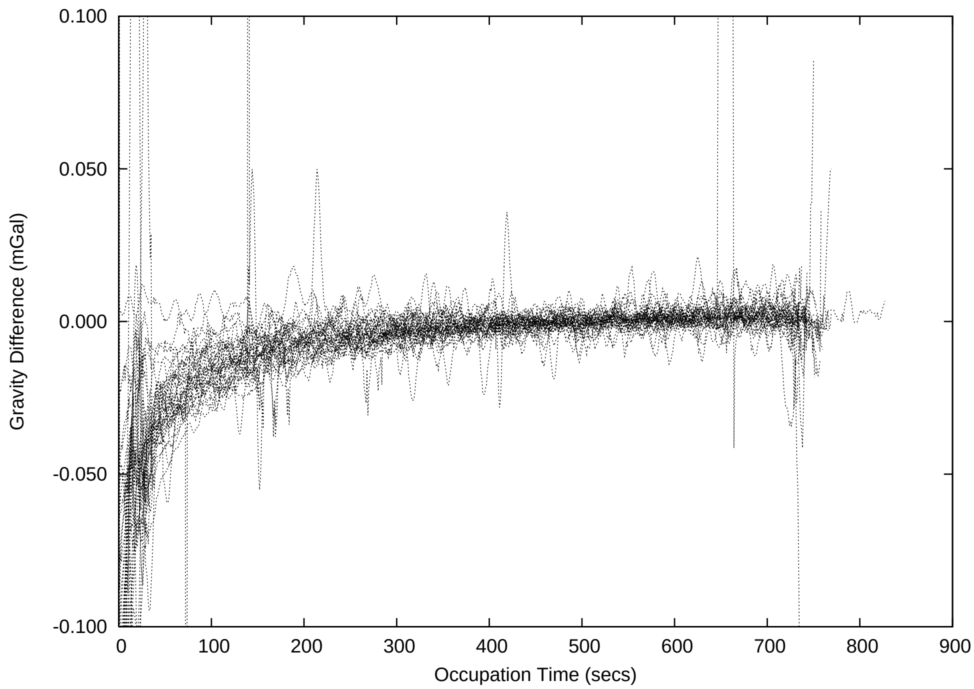

Figure 2.10. Time series of 35 stations from 9 Oct 2007, without filtering. All stations are shown relative to their despiked station average. Gravity range held at [-0.100, 0.100] mGal to enhance detail. Note the strong trends in the first 300 sec due to elastic relaxation (unclamping), except for one station that was taken after the meter was left unclamped overnight. Large spikes are also visible, which may be >2 mGal in size; these are removed by the despiking filter.

station occupation. Both schemes failed to produce results consistent with weighted averages in at least some real field data, and hence are not used with CG-5 data.

2.5.3.3 Sample Time-series Analysis

Aliod time series are significantly different from the Scintrex gravimeter data, and require a significantly different processing approach. Aliod-generated data show much longer relaxation times, typically in the 5-10 minute range. Although this leaves little (or no) data in a 12 min occupation for using a simple average, extrapolation techniques allow useful, accurate gravity determinations from a 12 min occupation. Figure 2.10 plots the raw time series of 35 stations from 9 Oct 2007, relative to their despiked averages. The stations show significant trends in the first 300 sec, with some stations having visible trends to 700+ sec. One station, which was taken after leaving the meter unclamped overnight, shows no consistent trend, reinforcing the conclusion that the trends are due to transport and (mostly) unclamping. Note that the large spikes in many stations are due to near-meter disturbances, and the spikes may be >2 mGal in magnitude. The despiking filter detailed below was applied before averaging, to center all stations near zero.

Note that due to the longer relaxation time of the Aliod meter, linear detrending, as with CG-5 or CG-3M data, is not advisable for sample data; early time readings are more likely incorrect due to elastic relaxation from unclamping, and hence detrending tends to severely underestimate the gravity reading at a site, possibly by as much as 0.1 mGal.

Raw gravity sample series are first corrected for Earth tides. Samples are then filtered for spikes and decimated to a maximum of 100 points covering the time span of the station occupation. The filtered, decimated series is then extrapolated to infinite time for the station reading.

2.5.3.4 Despiking Filter

The raw time series is first despiked using a multiple-pass despiking filter. For each point in the series, a centered window (truncated to series length) of (typically) 61 points is used to find the local average (S_i) and standard deviation (σ_i). Then, all points where $|s_i - S_i| > N\sigma_i$ are replaced with S_i; the multiplier N is found from interpolation of Chauvenet's table for data rejection using the actual width of the window for the point i. This procedure (find S_i, σ_i, replace s_i where $|s_i - S_i| > N\sigma_i$) is repeated until no points are replaced, up to 5000 times. The resulting series is used as the despiked series for further filtering and extrapolation.

Note that the ability of the despiking filter to remove spikes is strongly dependant on the choice of window size; small windows will leave residual spikes, and very large windows take long times to compute. By inspecting the test data, spikes are at most 15-30 seconds wide. Thus, a 61 point window (30 points on either side) was chosen to gain maximum despiking with minimum computation time.

2.5.3.5 Series Decimation

Due to the finite precision of a computer, and the need to use the (e^j, S_j) series for extrapolation, it is impractical to use a sequence of more than ∼500 points ($exp(500)$ is at the limit of a double-precision float). Thus, the 700+ point series from a 12 min occupation must be reduced in size. Moreover, Thiele extrapolation is quite sensitive to trends in the end of the provided series. To minimize short-term trends in the series, and decimate the data to a maximum of 100 points, the despiked time series is filtered as follows:

The despiked time series, typically 720-800 points long, is decimated to at most 100 points by computing an offset of

$$O = \mathrm{ceil}(N/100)$$

where N is the number of points in the original series. A moving average filter, with a 61-point centered window, then starts at the first point and marches through the despiked series moving O points each time. Windows are truncated at series boundaries, so beginning and ending points are averaged over a window of 31-60 points. Note that the window is much larger than O, so neighboring filtered points have significant overlap in their windows; this leads to a smoother filtered series, which is desireable.

The result of the moving average filter is a series of at most 100 points which is quite smooth, and fairly resistant to trends at the end of the time series.

2.5.3.6 Thiele Extrapolation of Filtered Series

The despiked, decimated, filtered time series is then used as the input to a Thiele extrapolation to estimate the infinite-time gravity reading.

Thiele extrapolation [*Stenger*, 1993] is a procedure for estimating the value of a function at infinity given some number of points at finite values. It uses a constructed rational function (computed as a "ρ-table") to represent the function at known points, and the value of the rational function is found at infinity. Since the algorithm needs only a set of known points, it can be applied to series of data as well as analytic functions.

For the Thiele algorithm to be accurate, it is necessary and sufficient for the sequence to have a limit at infinity, and for the sequence to approach that limit "sufficiently" fast. Here, "sufficiently" rapid convergence is achieved if

$$S - S_j = O(e^{-j\alpha}) \text{ as } (j \rightarrow \inf) \tag{2.1}$$

or

$$S - S_j = O(\frac{1}{Cj^{\alpha}}) \text{ as } (j \rightarrow \inf) \tag{2.2}$$

where S is the sequence value at infinity, S_j is the sequence value for some j, $O()$ indicates the order operator, and C and α are constants. For the case of exponential convergence (equation 2.1), it is necessary to apply the Thiele algorithm to the sequence (e^j, S_j); algebraic convergence uses the sequence (j, S_j). Based on the results of the exponential function inversion testing, it is apparent that station time series do converge at a rate of $O(e^{-j\alpha})$ and hence the algorithm can be accurately applied.

Note that algebraic convergence is only sufficient if a sequence is **monotonic**. As gravity time series are never monotonic, algebraic convergence is not sufficient, and only exponential convergence can be used. In practice, attempts using an algebraic sequence result in divide-by-zero errors, as the non-monotonic nature of the sequence causes entries in the ρ-table to be opposite in sign, equal in magnitude, which results in a divide by zero. Also note that since the sequence (e^j, S_j) has to be used, there is a limit of ~500 points in a sequence, as e^{500} is at the limit of a double-precision float, and overflow errors occur.

While the sequence to be extrapolated must converge within an exponential envelope, the sequence cannot have any repeated elements; that is, if $S_j = S_{j+1}$ for any j, the algorithm will result in a divide-by-zero when constructing the rational function table. To prevent this, the filtered gravity sequence is examined, and adjacent repeated values are removed. To prevent divide-by-zero due to adjacent, nearly-equal values becoming equal in finite precision results, the equality test is relaxed to remove adjacent points that are within a specified tolerance (defaulting to 10^{-7}). This particular case is commonly encountered in a raw time series filtered to at most 100 points, where the window offset is small (e.g. 5 points) with a relatively large window (e.g. 61 points) - the averaging of two points nearby can result in averages that are strictly different, but at the limits of machine precision; the construction of the rational function then creates a difference less than machine precision, and a divide-by-zero results.

Testing the algorithm with a data set of 746 CG-3M station time series yields results close to weighted averages in most cases. The difference between the result of the Thiele algorithm and the weighted average is shown in Figure 2.11. A total of 100 series have differences greater than 5 μGal, or about 13%. Only 30 series (4%) have a difference greater than 10 μGal. Moreover, the extrapolation algorithm remained finite for all stations, even those with consistent trends. Trends which cause a large difference (>10 μGal) in the extrapolation result compared to an average generally exceed the 97 μGal/hr detrending threshhold typically used.

Extrapolation is more likely to underestimate the gravity value than overestimate; the distribution in Figure 2.11 is weighted towards the negative numbers. Figure 2.12 shows a histogram of trend value, in μGal/hr, for all the test series. Note the symmetrical peak, which is centered around -27 μGal/hr. This shifted distribution influences the Thiele extrapolation results by causing the extrapolation to more often underestimate the weighted average result. These trends would not be removed by the analysis algorithm, as they are not above the 97 μGal/hr threshhold.

One reason for using the Thiele algorithm is to test if it is possible to extrapolate essentially the same value for a short time series as for a longer one. If possible, this would reduce the minimum time spent reading a station, and allow more stations to be occupied in a day, increasing the number of stations that can be used in a study. To test the difference between extrapolation with short and long time series, the full 15 min series were truncated after 16 records (~8 min) and input to the Thiele algorithm. Figure 2.13 shows the histogram of differences between the extrapolation results and averages. The general shape is the same as for full time-series results, but the peak has widened; more series are showing significant

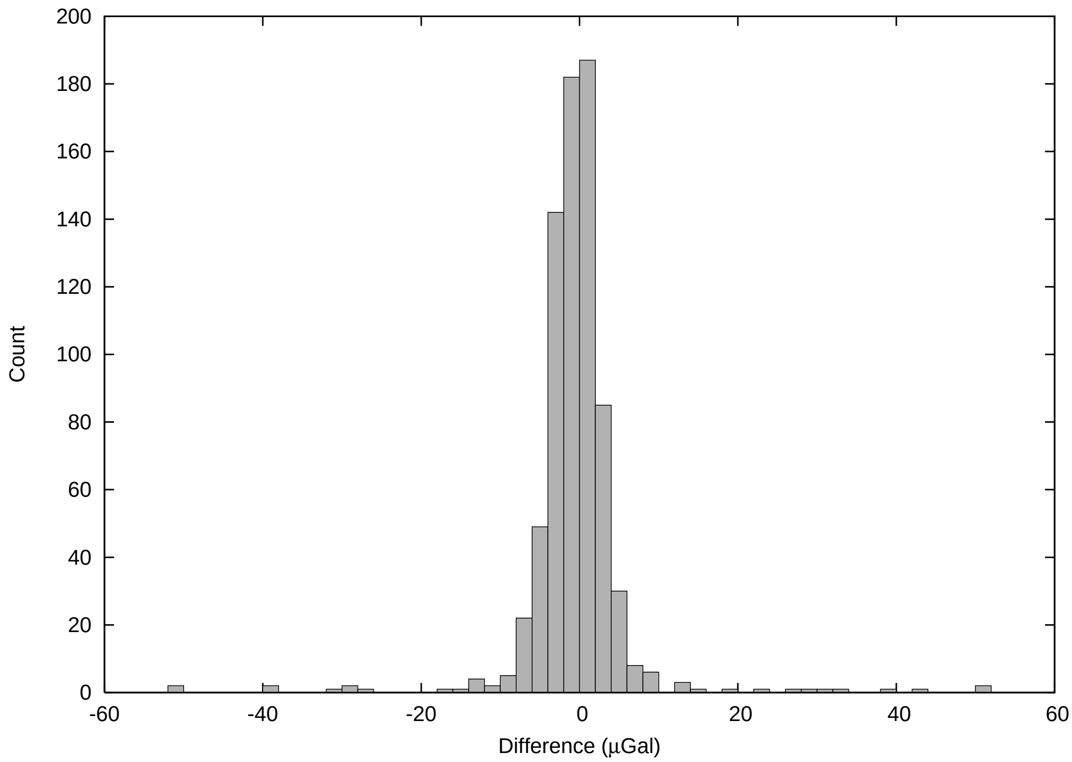

Figure 2.11. Histogram of differences between Thiele extrapolation result and weighted average for full time series. Of the 746 time series, 100 have a difference >5 μGal. Note the strong central peak and greater number of negative differences; extrapolation is more often underestimating the gravity compared to a weighted average.

differences. Of the 746 series, 165 (22.1%) have differences >5 μGal in magnitude, and 46 (6.2%) are different by more than 10 μGal. While larger than for full 15 min series, the number of stations significantly different from averages is still acceptable. A survey using shortened time series would have larger error bounds, as there is a reasonable chance that the extrapolation result is up to 5 μGal different from a 15 min average. If a survey can acccept accuracy at the 10 (or larger) μGal level, Thiele extrapolation with 8 min series will allow larger networks.

2.5.3.7 Thiele Extrapolation Error Analysis

Error analysis of the Thiele algorithm shows preservation of input error. That is, if the error of the input data is 3 μGal, the error in the Thiele algorithm result

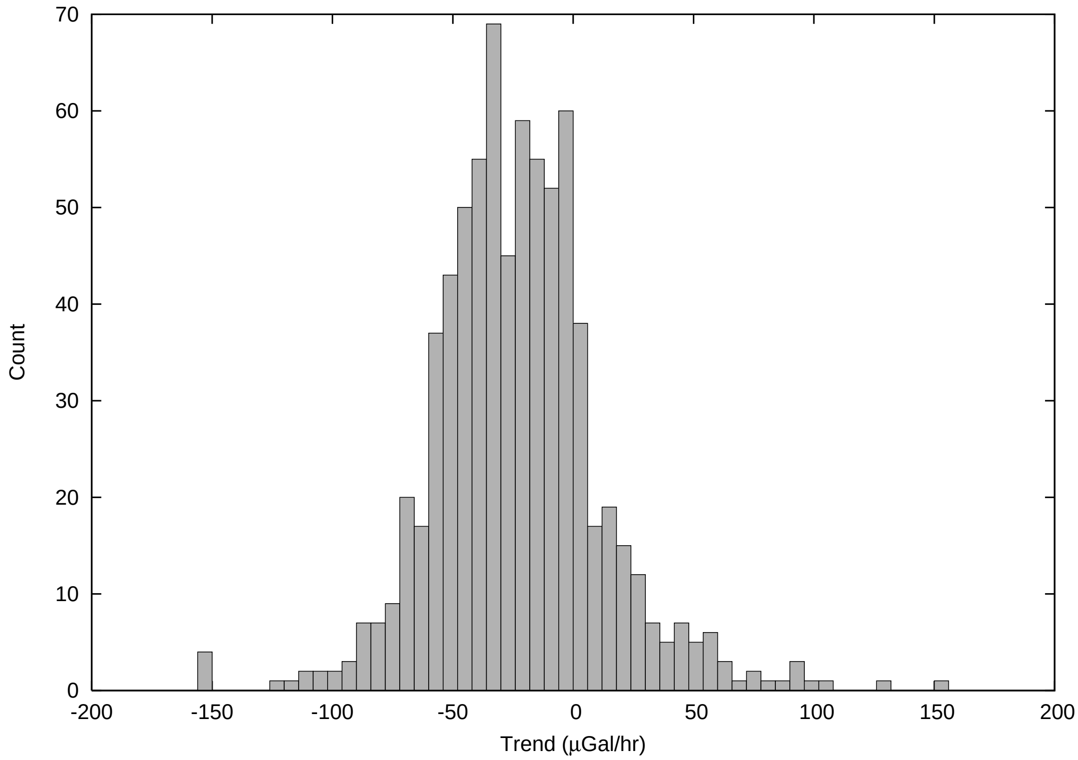

Figure 2.12. Histogram of trend values for all test series. Trends are reported in 6 μGal/hr intervals. Values above or below ± 150 μGal/hr are collected in the ± 150 μGal/hr bins. Note the peak, which is centered around -27 μGal/hr, not 0. This shift is the origin of the asymmetry in differences between extrapolation results and averages, shown in Figure 2.11.

is 3 μGal. A Monte Carlo scheme was used for error analysis due to the complexity of an analytical treatment. One million realizations of a random time series of 18 points provided the test data for the Thiele algorithm. Comparison of the Thiele output to the a priori average yields the error data set. The standard deviation of this error data set is a measure of error in the Thiele algorithm. Comparison of the Thiele error s.d. to the s.d. of the input data indicates if the Thiele algorithm preserves, reduces, or increases input data error. For white noise error about a constant or sinusoidal mean, the Thiele algorithm preserves the error level in the input data.

Regardless of input error level, 6% of the generated time series converge to a point >3 s.d. from the a priori mean. Upon inspection, these series all show a

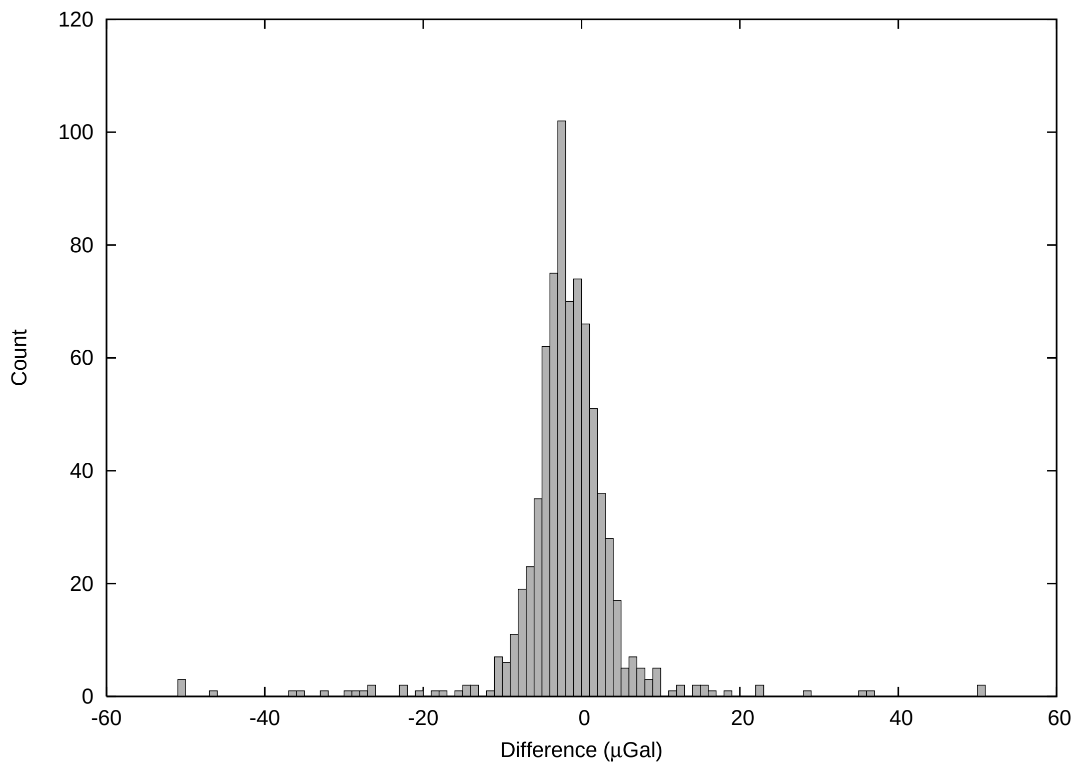

Figure 2.13. Histogram of differences between weighted average of full time series, and Thiele extrapolation on 16 record (<8 min) time series. Of the 746 time series, 165 have a difference >5 μGal.

distinct trend in the final four or more data points. This relatively large linear trend at the end of the time series causes the spurious result of the Thiele algorithm, and is one reason for the linear fitting quality check during CG-3M data processing, and the despiking/decimating filters in Aliod processing. In practice, none of the test data has a large trend in only the final points, and hence linear detrending prevents Thiele algorithm results from exhibiting this behavior.

2.5.4 Elevation Change Corrections

Station locations, while assumed to have static topography over a monitoring project lifetime, are quite likely to have varying elevations. Exploitation-induced elevation changes are known to occur in geothermal fields [*Allis and Hunt*, 1986], and seasonal elevation changes are seen in ground water reservoirs [*Merteens et al.*, 1998]. These changes are known to reach 5 cm per year, and may be larger in some systems. Given a typical vertical gravity gradient of -0.3086 mGal/m, elevation changes translate to a possible gravity effect of 15 μGal. Hence, it is desirable to have elevation control on all stations during a project, and the elevations should have an absolute accuracy of better than 3 cm.

After averaging the time-series, the station occupations are corrected for known elevation changes. The correction is computed from a constant global gradient of -3.086 μGal/cm. Local vertical gradients can vary from the typical free-air gradient [e.g., *Arnet et al.*, 1997], but this variation, while potentially exceeding 1 μGal/cm, is assumed to be small in most situations. Large changes in vertical gradient can always be handled using a post-reduction correction, or by mapping the gravity effect at the actual vertical gradient into an effective elevation change at the standard gradient. Moreover, a change of 1 μGal/cm in the vertical gradient, with subsidence of a few centimeters, causes an error still within the acceptable error bound of 5 μGal.

Measurements of the gradient using multiple heights at a fixed point suffer from the limited range of available heights [*Butler*, 1984], and extremely local terrain effects; for example, stations located on large cement blocks have measured vertical gradients significantly different from the free-air correction, but the measured gradients do not accurately reflect the gravity effect of ground subsidence. The cement block moves with the ground, and the actual gravity effect is closer to the free-air correction than the local gradient. Hence, for the relatively small elevation changes of concern in most monitoring projects, the global gradient of -3.086 μGal/cm is assumed.

To compensate for elevation changes, it is necessary to have elevation changes between surveys that are accurate to 3 cm vertically, and preferable to have accuracy of better than 1 cm vertically. Several methods are available to obtain this information, among them leveling differential GPS, and InSAR. Leveling is the historical method, but is labor intensive and slow. Differential GPS is relatively quick and cheap, and can be sufficiently accurate. InSAR is best suited for projects of large extent, as the acquisition cost and processing are more intensive than differential GPS on small projects.

2.5.5 Instrument Drift

Instrument drift corrections are inherently empirical calculations, although historically they have been handled by fitting simple theoretical functions to gravity differences. Unfortunately, no particular continuous function is necessarily the best choice for modeling gravimeter drift, making the choice of function part of the craft of gravity measurements. For exploration gravity, with acceptable accuracy of 100 μGal, linear drift models are often used for each campaign day. Previously reported high-precision techniques used large numbers of reoccupations and/or multiple gravity meters to help detect nonlinear instrument drift and tares [e.g. *Whitcomb et al.*, 1980; *Jachens et al.*, 1981; *Dragert et al.*, 1981; *Allis and Hunt*, 1986; *Hunt and Kissling*, 1994; *Andres and Pederson*, 1993; *Budetta and Carbone*, 1997; *Battaglia et al.*, 1999; *Sasagawa et al.*, 2003; *Ferguson et al.*, 2007], which were removed by fitting of low-order polynomial functions (sometimes with least-squares adjustment [e.g. *Jachens et al.*, 1981]). The maximum useful complexity in the drift function is set by the available drift information in the campaign, in the form of station reoccupations.

The fundamental assumption of all campaign drift functions is that the value of gravity should not change at a single station over the length of a single campaign. Under this assumption, repeated occupations of stations in a single campaign allows measurement and correction for instrument drift, regardless of cause.

Repeat schemes for a project should create many repeats of a daily local base (which may change each campaign day!) with 4 or more occupations throughout the day, particularly in the early loops. The extra repeats of a local base station allows a better representation of highly nonlinear drift curves with any drift function, but particularly the "staircase" function used in the reduction package. Early repeats of the local base station also allows identification of possible tares in the early part of the campaign day; such tares will be removed by the staircase drift function, but only if they can be correctly located within a loop.

It is important to note the first station in a campaign has zero drift by assumption; there is no information in the campaign data to indicate possible errors in the first station. For this reason, a very quiet station must always be used as the first occupation of a campaign, such as a location where the gravity meter has been undisturbed for at least 12 hours.

For processing campaigns of abritrary length and complexity, we have developed a drift function based on arbitrary offsets between stations; a chain of offsets forms a "staircase" function. By construction, the staircase function is nonlinear, discontinuous, handles arbitrary length campaigns, and does not assume an *a priori* functional form of the drift curve. A schematic staircase function is shown in Figure 2.14. The offsets between readings can be viewed as stair steps or linear trends; the drift function is only computed at station occupations, so the behavior of the function between station occupations is irrelevant. The stair step formulation simplifies the equations (developed below), but both views are equally correct. The staircase function produces effectively zero residuals for all campaigns and is therefore error-preserving.

2.5.5.1 Math of the Staircase Drift Function

We construct a staircase drift function as follows. First, we label all station occupations with a number, i, starting from 1. We define n as the total number of station occupations in the survey; thus, there are $N = n - 1$ intervals between ocupations. Let g_i be the gravity reading and t_i the time of the ith occupation. For every interval between two sequential occupations, we define τ_k as the midpoint time; note that there are N such times.

The drift function, $F(t)$, is defined as

$$F(t) = \sum_{k=1}^{N} C_k(t)\delta_k, \qquad (2.3)$$

where $C_k(t)$ is the coefficient for the kth interval taken from the set $\{0, 1\}$, and δ_k is the drift for that interval. Note that the length of the interval is not used, nor

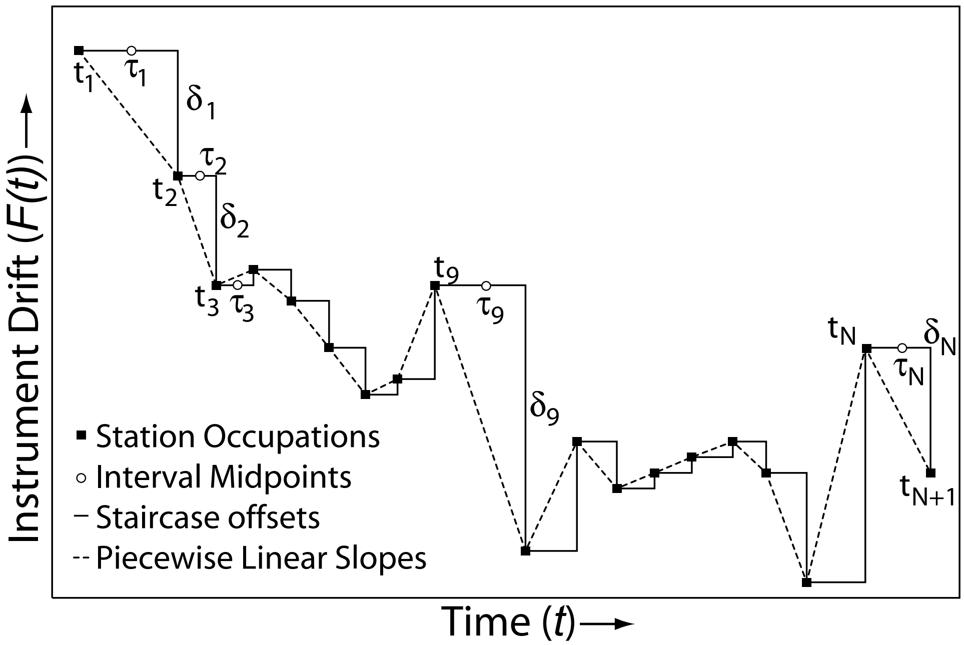

Figure 2.14. Schematic drift curve representation by the staircase drift function. Labels refer to the mathematical development in the text; δ_i is the drift for the ith interval, t_i the time of the ith occupation, and τ_i is the midpoint time of the ith interval.

are there any constraints on the change between sequential δ_k values. Thus, the function $F(t)$ is immediately applicable to surveys of arbitrary size and duration.

The value of $C_k(t)$ is found from

$$C_k(t) = \begin{cases} 0 & t < \tau_k \\ 1 & t \geq \tau_k \end{cases} \tag{2.4}$$

We label stations and repeat occupations with subscripts, so the first occupation of station A becomes A_0, the first repeat of station A becomes A_1, the second A_2, etc. Next, we construct a mapping, $\Gamma(\alpha_k) = i$, where α_k varies over all stations (α) and occupations of the station ($k = (0, 1, \ldots)$), and i represents the occupation number; this mapping is used below to build the drift observation equations.

A set of δ_k must be found such that the equation set

$$D_{\Gamma(\alpha_k)\Gamma(\alpha_{k+1})} = [g_{\Gamma(\alpha_{k+1})} - F(t_{\Gamma(\alpha_{k+1})})] - [g_{\Gamma(\alpha_k)} - F(t_{\Gamma(\alpha_k)})] \tag{2.5}$$

is minimized for all α_k (stations and repeated occupations).

This inversion problem is generally under-determined; there are $n-1$ unknowns, and at most $n/2$ equations. Additional equations result from noting that the difference between stations should be constant over a campaign. Hence, we construct additional difference of differences equations:

$$D_{\Gamma(\alpha_k)\Gamma(\alpha_{k+1})\Gamma(\alpha_j)\Gamma(\alpha_{j+1})} = D_{\Gamma(\alpha_{k+1})\Gamma(\alpha_{j+1})} - D_{\Gamma(\alpha_k)\Gamma(\alpha_j)}, \tag{2.6}$$

where k and j can vary over all stations that have repeated occupations. To remove redundant equations, only differences that are forward in time are used; that is, only pairs of stations where the time of occupation $\Gamma(\alpha_j)$ is later than that of occupation $\Gamma(\alpha_k)$. Also note that if a station has multiple repeated occupations, these are used by forming the above equation once for each repeat with the original occupation. If the survey does not have enough repeated stations, the problem may still be under-determined even with the differences of differences. Results of an under-determined system may still be valid; in all work so far, inversion matrices have been nonsingular even with an under-determined problem.

Define M as the total number of equations; the number of equations for repeated occupations plus the number of equations for interstation differences. To solve the (most likely) over-determined minimization problem, it is convenient to recast it into a matrix form and add data weighting factors. The vectors $\hat{m}$ and $\hat{d}$ are defined by

$$\hat{m} = [\delta_1, \delta_2, \ldots, \delta_N]^T \tag{2.7}$$

$$\hat{d} = [D_{\Gamma(A_0)\Gamma(A_1)}, D_{\Gamma(B_0)\Gamma(B_1)}, \ldots, D_{\Gamma(A_0)\Gamma(A_1)\Gamma(B_0)\Gamma(B_1)}, \ldots]^T \tag{2.8}$$

and the $M \times N$ operator matrix $\hat{A}$ is defined by

$$\hat{A} = [A_{lm}], \tag{2.9}$$

where A_{lm} is chosen according to the following algorithm. If l is a row with an equation for a repeated occupation, then

$$A_{lm} = \begin{cases} 1 & t_i < t_m < t_{i'} \\ 0 & \text{otherwise} \end{cases} \tag{2.10}$$

where i is the occupation and i' the repeated occupation represented by the lth row.

If row l is a difference of differences equation, then

$$A_{lm} = \begin{cases} -1 & t_i < t_m < t_j \\ 0 & t_{i'} < t_m < t_j \\ 1 & t_{i'} < t_m < t_{j'} \\ 0 & \text{otherwise} \end{cases} \tag{2.11}$$

where i, i', j, and j' are the occupations and repeats represented by the lth row. Define the square $M \times M$ data weighting matrix by

$$\hat{W} = [W_{ll}] \tag{2.12}$$

where W_{ll} is computed by the following algorithm: If row l is a repeated occupation equation,

$$W_{ll} = \frac{1}{\sqrt{\sigma_i^2 + \sigma_{i'}^2}} \tag{2.13}$$

otherwise,

$$W_{ll} = \frac{1}{\sqrt{\sigma_i^2 + \sigma_{i'}^2 + \sigma_j^2 + \sigma_{j'}^2}}. \tag{2.14}$$

where i, i', j, and j' are the occupations and repeats represented by the lth row.

The matrix equation to be solved is

$$\hat{W}\hat{A}\hat{m} = \hat{W}\hat{d}. \tag{2.15}$$

As the operator is linear, the problem can be solved in a direct linear least-squares inversion, which can be written in matrix notation as

$$\hat{m} = (\hat{A}^T\hat{W}^2\hat{A})^{-1}\hat{A}^T\hat{W}^2\hat{d} = \hat{Q}^{-1}\hat{A}^2\hat{W}^2\hat{d}, \tag{2.16}$$

where $\hat{Q}$ is the diagonal matrix found from the singular value decomposition of $\hat{A}$.

Once $\hat{m}$ is found by equation 2.16, the drift for any station can be computed from a specialization of equation 2.3. As the drift function is always being computed on an interval boundary,

$$F(t_k) = F(k) = \sum_{i=1}^{k-1} \delta_i. \tag{2.17}$$

For stations that have no repeats, the inversion process (being a least-squares process) assigns a drift value that is a linear interpolation between the nearest repeated stations.

2.5.6 Reference Station

To handle instrument drift between surveys, one or more stations are assumed "stable," meaning no gravity change over time. The apparent gravity changes at the reference station(s) provide a correction to the measured gravity changes to compute actual change. Any signals at the reference stations are superimposed (in an inverted manner) on all other gravity stations. Since in the inter-mountain West, a known-stable site is generally not available, it is common to pick a set of reference stations, whose average will be held at zero. In general, reference stations should be determined by the location of absolute gravity measurements during campaigns; gravity changes at reference sites are then directly measured, and the sites need not be stable.

2.6 Checking Reduced Data

2.6.1 Quality Check of Reduced Data

Reduced data should always be inspected using an instrument drift plot and a reduction/processing log; particular care should be exercised when dealing with occupations that were detrended. Also, if computing instrument drift, compare a linear daily rate for stations and repeats. Linear rates will fluctuate even on good days, due to the extrapolation of short intervals to 24 hr periods. However, occupation pairs with drift rates that are differing signs or more than 30 times different than all the other pairs are suspect.

The most useful plot for checking the reduction results is a pre-drift arrow plot; an example is shown in figure 2.15. For a typical field day, this plot should show station pairs following one of 2 patterns: (1) small random drift at the 10-20 μGal level, or (2) predominantly linear drift over the entire day (parallel pairs) with random shifts at the 10-20 μGal level. Station pairs with radically different arrows than the others are suspect. However, drifts less than 10 μGal are approaching instrument noise (2-5 μGal precision in each station) and should be ignored regardless of patterns.

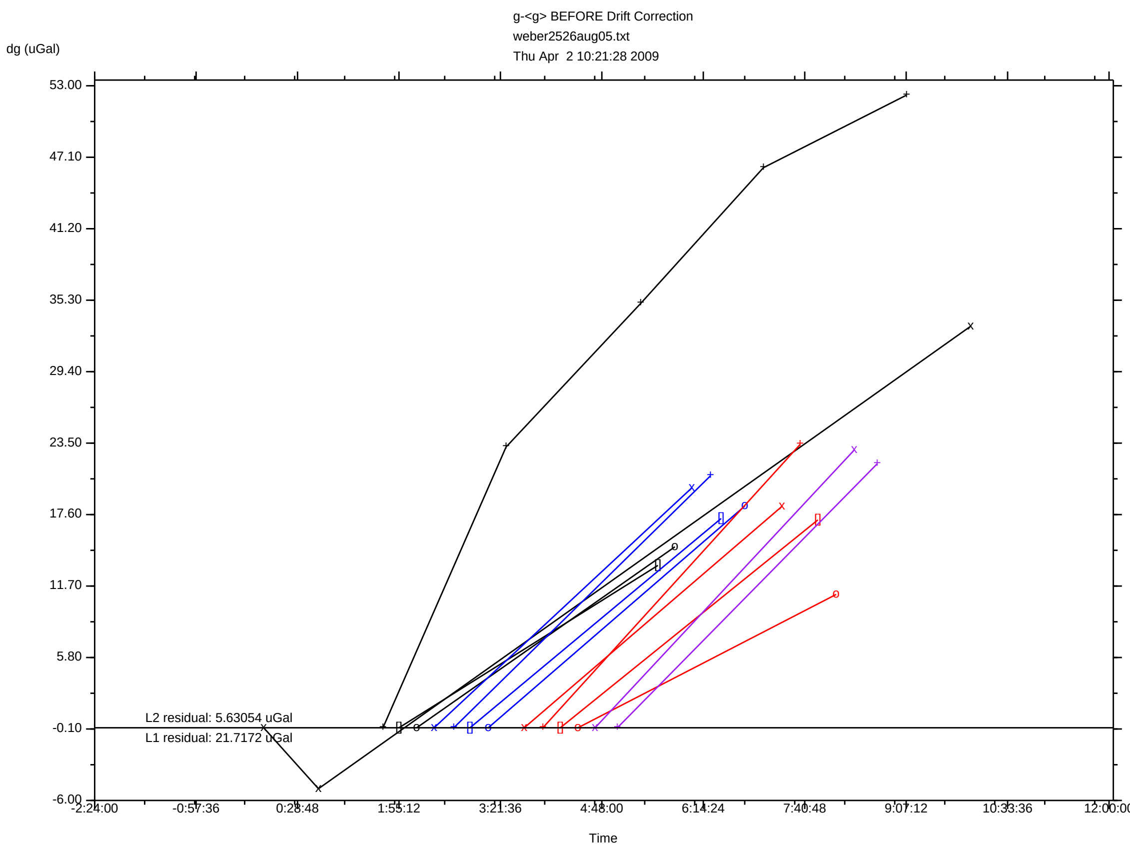

Figure 2.15. Example pre-drift station repeat arrow plot, with stations and repeats shown as connected strings of stations; markers and line color differentiate the strings. L1 and L2 show the L1 and L2 norms of the repeats; smaller numbers indicate smaller overall drift. All station strings start at 0 relative gravity, as gravity values are referenced to the first station in a string. Times are in hours since the first station in the data. Gravity differences represent instrument drift, residual Earth tides, etc.

Drifts of milligals (1000s of μGal) generally indicate a mistake in processing where a station repeat pair as been incorrectly assigned (station A' is actually B', and B' is actually A'). In one case, this check has led to noting that the field book was wrong! After finding what stations should be repeats, fix the processing files/flow, then re-run the reduction from the start.

Other station pairs that are suspect need to be inspected individually. Inspection of the raw time-series may help explain why a station pair shows a large drift. In some cases, multiple occupations may be being claimed as a single station occupation. In other cases, particular occupations are noticeably worse than others due to external factors such as traffic or weather.

Fixing the recorded data file to break apart multiple occupations being claimed as a single occupation, or removing the bad occupation before rerunning the data processing allows further quality checking of a campaign. Skipping a poor-quality station occupation is only viable if there is a good occupation of the station, and a different occupation is clearly problematic (erratic gravity values, etc.). Always choose the best station time-series to keep, even if the kept station is the repeat of the first occupation.

If more than 10% of stations in a data file have problems due to intermittently faulty measurements, it is unlikely to be possible to simply skip stations and not lose all occupations of some stations or cripple the drift computations with few repeats. In this case, try fixing the collected data using a temperature correction or sample removal option (for faulty sensor temperature readings) or linear detrending (for faulty tilt measurements). Note that if the gravity readings are possibly faulty, skip the occupation(s) and redo the campaign if necessary.

2.7 Exploration Gravity Procedures

Exploration gravity projects use the same general acquisition and processing techniques presented here, but there are some changes required by the large areas and allowed by the lower accuracy requirements.

This section presents the changes to the station repeat schedule and station occupation times that allow for large areas to be covered at acceptable accuracy.

2.7.1 Station Network Design

Unlike monitoring projects, the station network required for an exploration project will likely be sparse and relatively uniform. Networks will need to be designed with the end interpretative technique in mind, since acquiring sparse 2-D transects makes 3-D models nearly impossible, and grids are wasetful for a handful of 2-D transect models. Once the exploration area is known, the target must be identified in terms of size (lateral and thickness extent), depth of burial, and density contrast. These estimates need to be realistic enough to allow simple modeling to determine:

1. expected gravity signal at the surface, and therefore accuracy requirement; if accuracy of better than 0.05 mGal is needed, the exploration project will need to use the full monitoring-project techniques described in Chapter 2.2.

2. expected horizontal extent of signal, and therefore the station spacing needed to resolve it, which sets the number of stations to measure. Expect to only have time to put in a minimum number of stations at the maximum acceptable spacing.

3. vertical accuracy needed at stations, and thus the time-on-station for GPS measurements. This may require a second crew doing nothing but GPS, and a system for marking where gravity stations were placed!

4. how useful the existing gravity station database can be in the target area, and thus how many new stations will be needed, and where.

If stations must be reoccupied, such as 2 crews in the field - one for gravity and one for GPS, stations must be marked fairly exactly. Spray chalk and flagging will be helpful here. It is typically wasteful to install a true monument, as these stations will not be measured over many months or years. If doing combined gravity and

GPS at once, stations need not be marked on the ground at all! With modern GPS receivers and processing, stations can be put at any convenient location, rather than requiring spot elevations or benchmarks. Thus, it is advantageous to perform GPS and gravity acquisition at once, and to mark the locations on a planning map for field reference, but not worry about marking the new stations for reoccupation. This also reduces the footprint of a gravity campaign to foot and tire prints!

2.7.2 Station Repeat Schemes

Since the acceptable accuracy of exploration projects is typically 0.05 mGal to 1 mGal, fewer repeat occupations are needed to correct for non-linear instrument drift. Thus, typical exploration projects can get away with 2-3 measurements on a local base per day, with no repeated stations during the day. This allows covering 15-30 stations per day, rather than the 10-15 of a gravity monitoring project. Note that the larger areas covered in exploration projects will reduce the station coverage, due to longer transport times.

2.7.3 Reference Stations

Unlike gravity monitoring, the primary job of the reference station in exploration projects is to provide a tie to an absolute gravity value from the relative gravity values measured by a CG-5 (or other) meter. Thus, all exploration projects must include at least one station with a known absolute gravity value, and preferably many. Also, the absolute gravity values should be as recent as possible, to track possible long-term changes in gravity at the reference sites.

If attempting to include existing gravity data in the exploration project (always a good idea), be sure to measure some of the old stations to check that the gravity values derived in the new survey tie to the old values, or construct a mapping (typically a static shift) to integrate new values into the existing database.

Existing gravity stations for the U.S. is available from the National Geospatial Intelligence Agency (formerly DMA) through the National Geodetic Survey of NOAA, the Pan-American Center for Earth Sciences (PACES) at the U of Texas-El

Paso (`http://research.utep.edu/Default.aspx`), and individual workers with copies of the UTEP or NGS databases. The UTEP PACES database is more up-to-date than the 1999 NGS version and therefore includes more gravity data since the NGS version. Whatever database is used, it will likely have to be reformatted to be suitable for use in OASIS Montaj, USGS processing flow, or whatever analysis system will be used.

2.7.4 Acquisition Time

Since the accuracy requirements for exploration stations is so relaxed compared to monitoring projects, the time on each station can be significantly reduced. In practice, a minimum station collection time of 5-6 min appears adequate for exploration projects with target accuracies of 0.05 mGal. The acquisition setup is identical as for monitoring projects, just cut the time in half.

Moreover, the lower accuracy allows the use of less-precise GPS systems, including averaging versions of hiking GPS receivers and the survey-grade receivers from Trimble, etc. that include ArcPad. Follow the directions of the receiver manufacturer for acquiring sufficient accuracy elevation values; this may require post-processing to a nearby geodetic-grade base station.

Recall that the typical free-air gradient is -0.3086 mGal/m, which means that an exploration project seeking 0.1 mGal accuracy must know the station elevations to 0.3 m or better (1 ft). This is achievable with a Trimble hand-held unit that is post-processed, according to Trimble. Other alternatives could be an L1-only unit set on the faceplate or a fixed-height tripod for an L1/L2 unit recording for only 5-10 minutes, often in a kinematic or real-time kinematic mode. Regardless, the trade-off between time-on-station and vertical accuracy will typically be solved by accepting less vertical accuracy to keep the time-on-station to 10-15 min or less; otherwise the coverage of extensive exploration areas at reasonable station spacing requires more field time than available.

2.7.5 Processing

Data processing is unchanged from monitoring projects, and the use of the high-precision techniques allows improved exploration results compared to many older schemes. However, the processing does not stop with the reduction from raw data file to relative gravity values.

Relative gravity values need to be differenced to a known gravity value to get an absolute observed gravity value at each station. This is most easily accomplished by referencing field data to a station with a known absolute gravity.

2.7.6 Anomaly Computations

The most common interpretative anomaly for gravity is the Complete Bouguer Anomaly, which requires terrain, Bouguer, and free-air corrections to the theoretical gravity at each station. An excellent recent paper on the standards for computing these corrections and the basic theoretical gravity values is *Hinze et al.* [2005].

2.7.6.1 Terrain Corrections

Terrain corrections are an important part of the exploration gravity processing; without terrain corrections, the simple Bouguer anomaly will partly reflect terrain variations. Terrain corrections for areas closest to each gravity station need to be done by hand, using calculation tables or programs for aid. *Hammer* [1939] and Hayford-Bowie [*Hayford and Bowie*, 1912] systems require hand-computation for A-C (0-54 m) or A-B (0-68 m) zones. Hand computation can be avoided if 1-3 m digital elevation data is available, such as from LIDAR surveys; calculation of the inner-zone terrain correction by block-based or prism models is then straight forward.

Hand computation is most easily done by converting actual topography, recorded when at a station, into a set of (displaced) half-slopes and -cones; estimating the average elevation difference from the station for a sector of an annulus is very difficult to do accurately when in the field. Each half-slope or -cone is computed separately, and the total inner-zone terrain correction is the total sum.

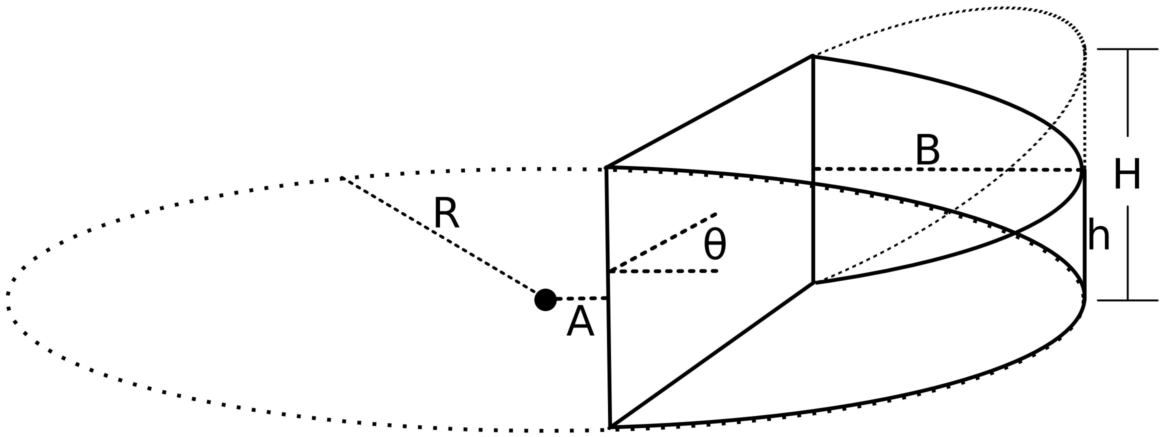

Figure 2.16. Geometry and field data needed for a displaced half-slope terrain correction. The calculation is the difference between two slopes; one from the start (A) to the edge of the zone, and one from height h to the edge of the zone.

The equation to compute the gravity effect of a displaced half-slope is taken from an unpublished USGS open-file report [written communication, USGS, 1993]. A difference of triple integrals is used to compute the effect of a half-slope starting at a distance A from the station, rising (or falling) at an angle θ, to a maximum height h or distance from the zone boundary B. The zone boundary distance, R, is taken as either 54 m for a *Hammer* [1939] or 68 m for a *Hayford and Bowie* [1912] system. In the field notes, it is necessary to specify A, θ, and either B or h. Given either B or h, the other can be computed from R and θ; given B, $h = (R - A - B)\tan\theta$, or given h, $B = R - A - h/\tan\theta$.

The first integral term is the slope from the start to the edge of the zone; the second term removes the portion from h to the edge of the zone. Figure 2.16 shows the geometry of measurements for the calculations. The integrals can be evaluated analytically from 3 to 1 dimension, and the last integration done numerically. For compactness, the numeric integral is presented with some intermediate terms:

$$
\begin{aligned}
H &= (R - A)\tan\theta \\
l &= \frac{H^2(x - A)^2}{(R - A)^2} \\
c &= h + \frac{H - h}{B}(x - R + B) \\
\alpha &= \sqrt{R^2 - x^2}
\end{aligned}
$$

$$\beta = \sqrt{R^2 + l}$$
$$\zeta = \sqrt{R^2 + c^2}$$
$$\xi = \sqrt{R^2 + h^2}$$

The terrain correction using the above terms is:

$$\delta g = G\rho \left[\int_A^R \ln \left(\frac{-(R+\alpha)(\alpha-\beta)}{(R-\alpha)(\alpha+\beta} \right) dx - \int_{R-B}^R \ln \left(\frac{(\alpha+\xi)(\alpha-\zeta)}{(\alpha-\xi)(\alpha+\zeta)} \right) dx \right] \quad (2.18)$$

where G is the universal gravitation constant, and ρ is the density (2670 kg/m^3). The integrals can be computed using Rhomberg or trapezoidal integration over the ranges.

The truncated, or displaced, half-cone is found from the difference between a full, enclosing cylinder, and the cone below the station. The calculated effect of the cylinder and cone are halved, to generate a half, rather than full, cone. Figure 2.17 shows the geometry and distances used in the calculations. The technique of using a difference between the enclosing cylinder and frustum is taken from an unpublished USGS open-file report by Robbins & Oliver [written communication, USGS, 1970], but the following equations are from a more recent USGS program [written communication, USGS, 1993]:

$$\delta g = \frac{\delta g_{cylinder} - \delta g_{frustum}}{2} \quad (2.19)$$

Now,

$$\delta g_{cylinder} = 2\pi\rho G(L + R - \sqrt{R^2 - L^2})$$

where ρ is the density (2670 kg/m^3), G is the universal gravitation constant, L is the height of the cone, and R is the diameter of the inner zones (54 m for Hammer or 68 m for Hayford-Bowie schemes).

And,

$$\delta g_{frustum} = 2\pi\rho G \left\{ L - r - \cos^2\beta \left[D + r\sin\beta \ln \left(\frac{L + \cos\beta(D + r\sin\beta)}{r\cos\beta(1+\sin\beta)} \right) \right] \right\}$$

where r is the radius on the top of the cone at the station, β is the angle of the cone from the vertical (90-θ), and $D = \sqrt{L^2 + (r + L\tan\beta)^2}$.

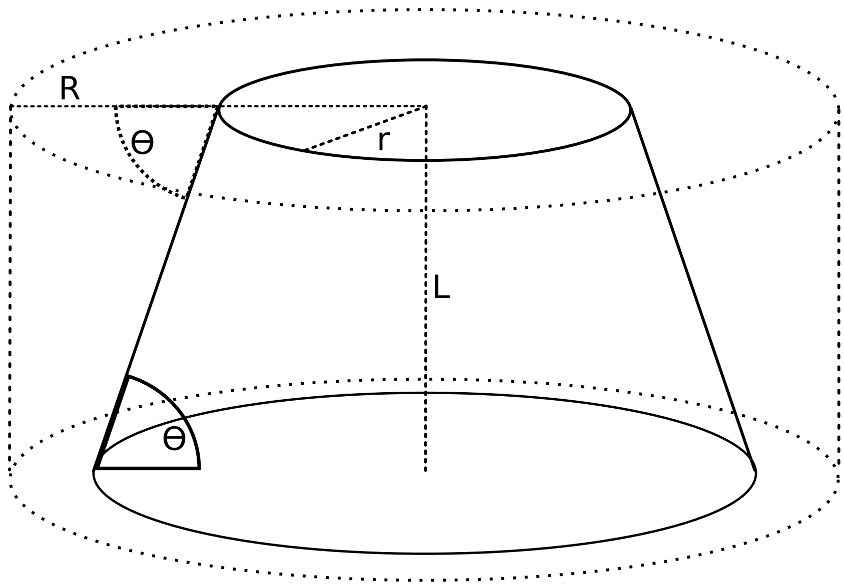

Figure 2.17. Geometry and field data needed for a displaced half-cone terrain correction. The calculation is the difference between the vertical cylinder to the edge of the inner zones and a frustum of a cone with top radius r, height L, and angle from the horizontal θ. The terrain correction is halved to account for a half, vs. full, cone.

Terrain corrections from the inner-zone boundary to the maximum radius of 166.7 km are most easily calculated using a DEM and program. As part of this project, a new computation scheme was implemented to allow terrain corrections of any station location, not just those in the U.S., as was the case with some earlier programs and digital map files [e.g. *Plouff*, 1977]. To allow correction anywhere, a global grid of spherical diamonds with inter-center spacing of 468 m was generated using the Discrete Global Grid software of *Sahr et al.* [2003]. The resulting 2 684 354 560 polygons were then filled using Shuttle Radar Topography Mission (SRTM) data [*Farr et al.*, 2007] for the land polygons from 57 S to 60 N, GLOBE data [*Hastings et al.*, 1999] for land areas from 57 to 90 S and 60 to 90 N, and ETOPO1 data [*Amante and Eakins*, 2009] for the remaining polygons (ocean and land). Cells filled from ETOPO1 were also used to create an ocean mask for use in computing terrain corrections near oceans. Due to the number of polygons, the geometry (corner coordinates, center coordinate) is kept separately from data values for each polygon (elevation, ocean/land flag, etc.). This allows many data sets to be referenced to a single geometry file. The geometry file for all polygons takes 221 GB on disk, the ocean mask file is 26 GB, and the elevation list takes 31 GB.

Each polygon within 166.7 km of a gravity station adds to the total terrain correction using a slightly modified form of the Gauss-Legendre quadrature of *Asgharzadeh et al.* [2007]; since the quadralaterals of the DGG are not aligned north-south in all cases, the algorithm in *Asgharzadeh et al.* [2007] is modified to interpolate the latitude extents depending on the longitude quadrature points. Also, the quadrature order is set according to the larger of the height difference and the maximum horizontal dimension across the polygon. Orders in all three dimensions (latitude, longitude, radius) are set to the maximum of any dimension.

Each polygon in range is treated as a stack of spherical prisms. The prism height is set to the elevation difference between the polygon and the gravity station. Polygons in the ocean use two prisms; one from sea level to the station (filled with air), and one from the ocean floor to sea level (filled with sea water); the height of the seawater prism is scaled to reflect the density difference between water and air (1035 vs $\sim$0 kg/m^3); the prism radial center is set to half the ocean depth. The sum of all polygons within range is added to the hand-computed inner-zone terrain correction to get the total terrain correction. Terrain corrections are computed for a density of 2670 kg/m^3; the total terrain correction is then scaled to a desired reduction density by multiplying by $\rho/2670$.

Comparing the new algorithm reported here to the published total terrain correction for the UTEP PACES database of stations results in figure 2.18. Total terrain corrections computed using the new code for all 1 258 462 stations in the PACES database are differenced from the UTEP results; stations with differences of $\pm$5 mGal or larger are collected in the last bins ($\pm$5 mGal). The distribution is not symmetric, with more stations showing a negative difference (new total terrain correction less than the UTEP result). Just over 65% of the stations have differences within 0.2 mGal of zero. A total of 16 710 stations have an absolute difference of 5 mGal or larger, a total of 1.33% of the database. Inspection of stations with

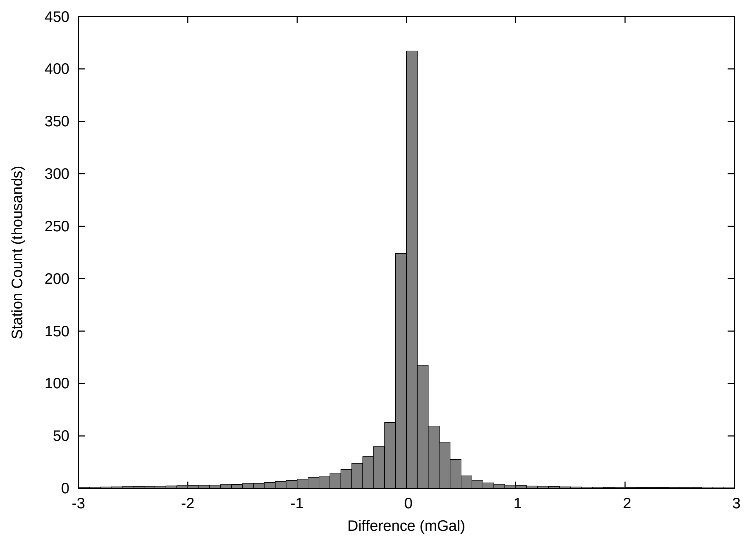

Figure 2.18. Histogram of differences between the terrain correction code presented here and the total terrain correction results given in the UTEP PACES database. All 1 258 462 UTEP PACES stations used in the comparison. A total of 16 710 stations (1.33%) have a difference of 5 mGal or larger.

large (>5 mGal) differences indicates that large differences are due to particular circumstances at each station, such as a mismatch between the station elevation and the nearest DEM polygon of multiple meters. Individual stations must be fixed either in the official database or per project. Stations with large differences are easily caught by inspecting a map of terrain corrections or anomaly values; the individual stations are single-point extrema.

CHAPTER 3

DATA FUSION IN GRAVITY MONITORING OF DUTCH FLATS, NEBRASKA

3.1 Introduction

Management of groundwater resources is of increasing interest, particularly in the western U.S. Methods of tracking groundwater change are an important component of management strategies, and geophysical techniques can play an important role in projects with large areal extent and limited well data. There are a variety of geophysical techniques that are sensitive to ground water changes, such as repeated gravity [e.g. *Chapman et al.*, 2008; *Gettings et al.*, 2008; *Leirião et al.*, 2009], electromagentic (EM) surveys [e.g. *MacLennan and Li*, 2011], and seismic surveys [e.g. *Landrøand Strønen*, 2003].

As part of a long-term investigation into management techniques and strategies, the U.S. Geological Survey in Lincoln, Nebraska has been using the Dutch Flats study area since 1995 for testing geophysical techniques to track ground water changes due to irrigation and canal leakage [*Verstraeten et al.*, 2001]. To this end, the USGS established an extensive nested well network in the Dutch Flats study area for tracking water levels with monthly measurements. Various geophysical techniques have been tested on the site to see how well inferred changes match measurements in the nested wells. Repeated gravity as a tracking method was tested with a gravity monitoring project between July and October 2003.

The Dutch Flats study area is in westernmost Nebraska (see figure 3.1). As is clear from aerial photography, the entire area is covered with irrigated agriculture,

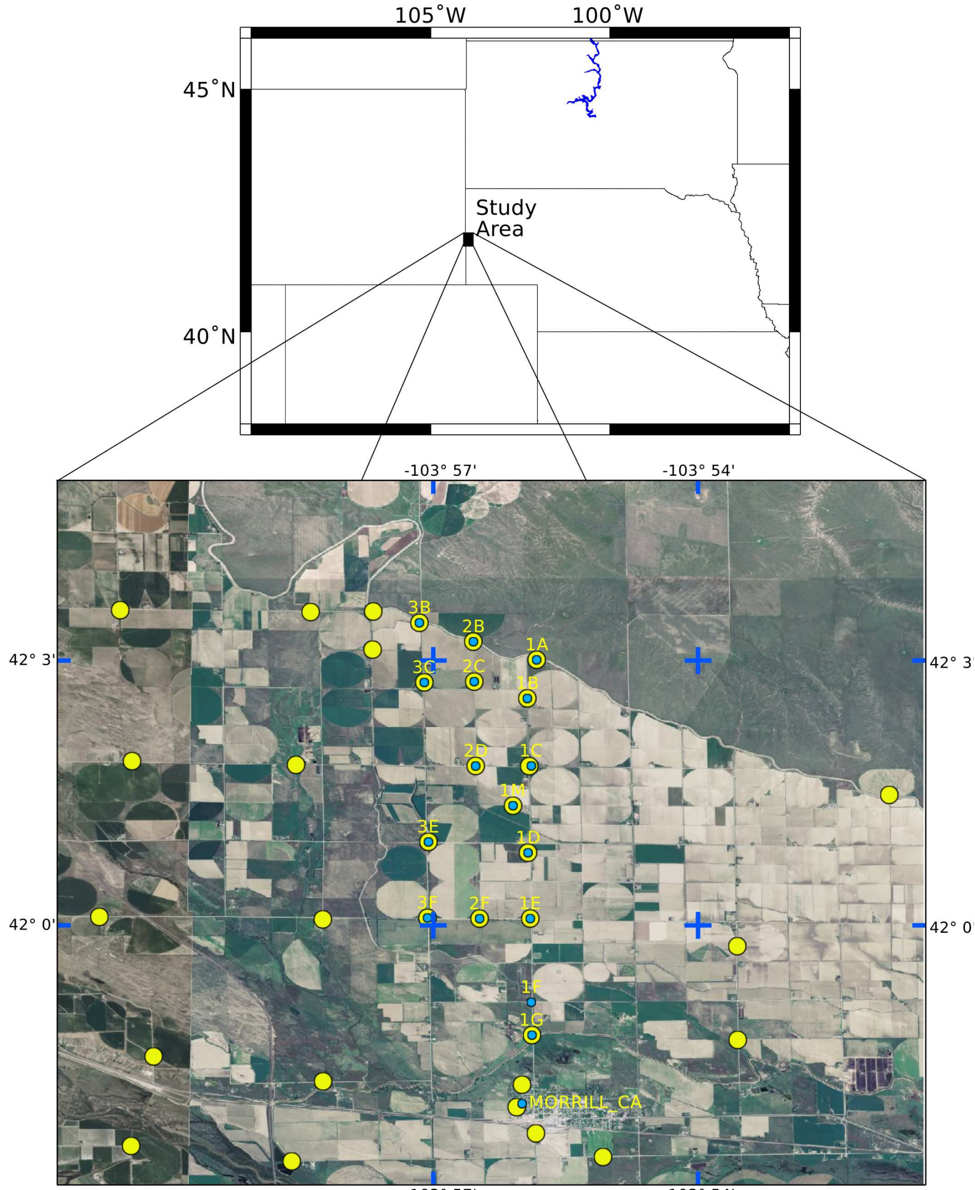

Figure 3.1. Study area map, with aerial photos from 2009. Monitored wells shown by yellow circles, gravity stations shown by blue circles. Gravity stations labelled by name of the coincident well.

and extensively drilled for irrigation and monitoring. Monitoring wells in the study area are shown on figure 3.1 as yellow circles; note the extensive network surrounding the gravity stations shown by blue circles. As the area is actively farmed, irrigation continued during the gravity monitoring.

In the gravity study area, the surface geology is sandy soil, underlain by predominantly sandy alluvium [*Verstraeten et al.*, 2001]. This alluvium forms the dominant shallow aquifer that provides the bulk of ground water supply in the gravity monitoring area. Underneath the alluvium is basement composed mostly of sandstone. Permeability of the basement is poor in general, although local areas can have enhanced permeability from fractures [*Verstraeten et al.*, 2001].

Surface elevation of the study area, taken from the USGS Seamless DEM data set [*Gesch*, 2007], ranges from 1203 m to 1388 m; elevations are lowest at the southern end, and steadily rise to the north as shown in Figure 3.2. Overall hydraulic gradient is thus to the south, from the higher elevations in the north towards the low point at 4642 km northing. Inferred basement elevations range from 1150 m to 1320 m, following the same general trend as the surface elevations. Basement elevations imply sediment thicknesses that generally increase from 20-30 m in the north to >70 m in the south.

A S-N cross-section at 588.5 km easting is shown in Figure 3.3. Surface elevations are shown with the solid black line. All gravity stations have been projected onto the cross-section at appropriate elevations and northing values; hence the stations apparently in the air or below ground level. Basement elevations are taken from the gridded basement map shown in Figure 3.2b. The water table elevation is interpolated from monitoring well levels in July 2003, at the start of monitoring. Note the clear hydraulic gradient to the south, and the areas with basement higher than the water table; such regions are assumed to have little storage change and are found to have little to no water table change during 2003.

The alluvial aquifer is unconfined in the study area, and recharged from precipitation, surface irrigation, and leakage from canals. Due to the permeability of the unlined canal bottoms, and the semi-arid climate of the region, recharge is

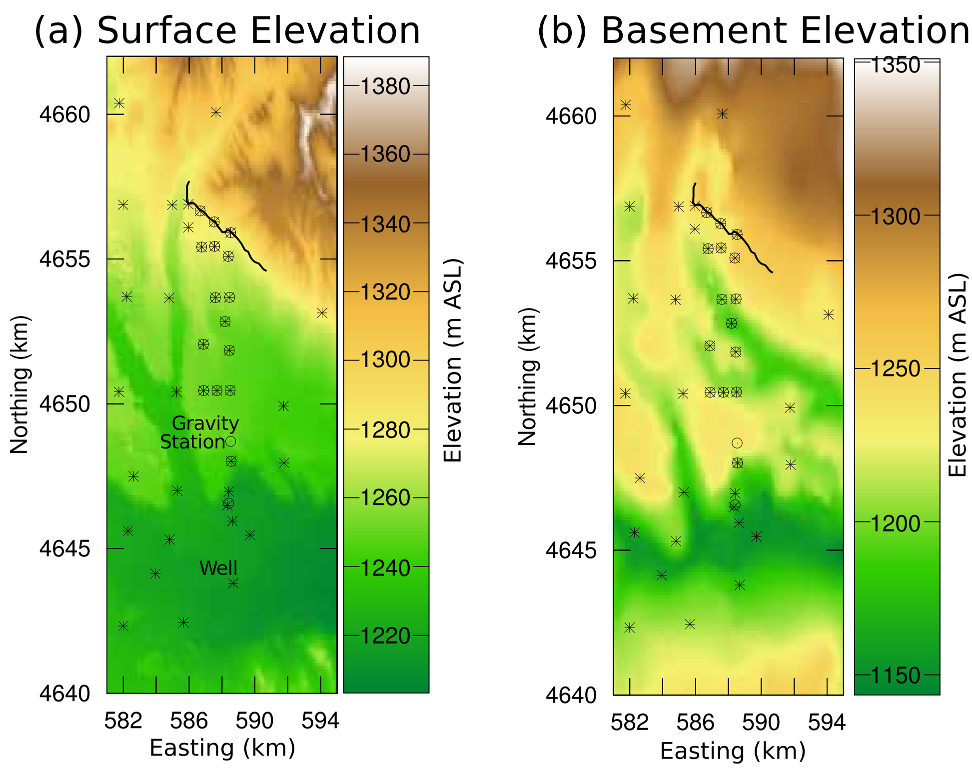

Figure 3.2. (a) Surface elevation of the study area; colorbar indicates range of elevations above WGS84 ellipsoid. Gravity stations are denoted by circles; monitored water wells by stars, and the irrigation canal in the area next to the gravity monitoring by a solid black line. (b) Elevation of basement-sediment contact, inferred from airborne EM results supplied by the USGS. Gravity stations and monitored wells indicated as in (a). Note the increasing sediment (and hence aquifer) thickness to the south.

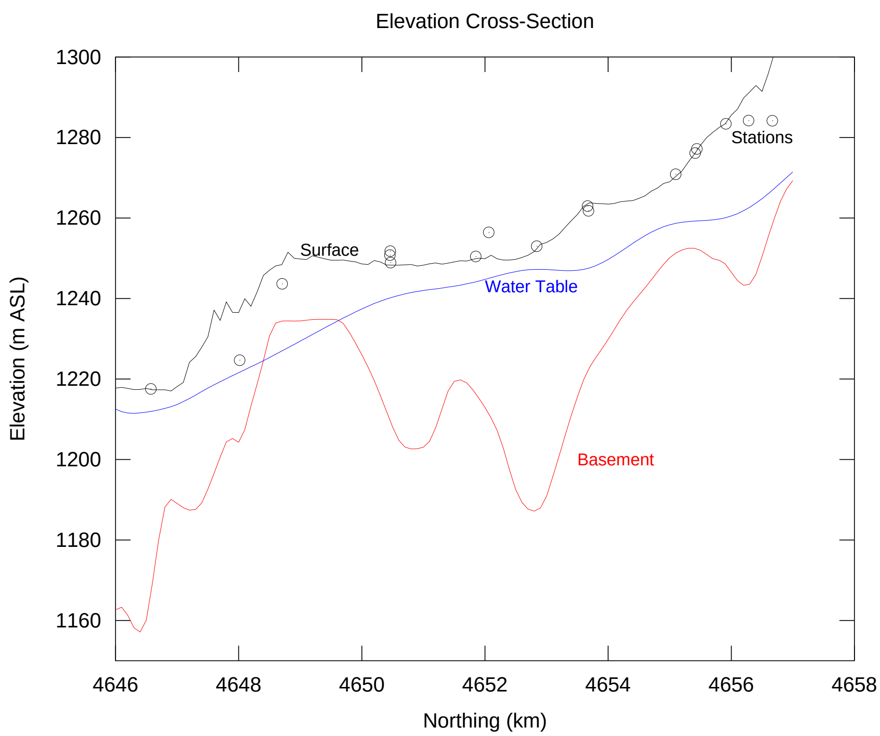

Figure 3.3. South-to-north cross-section at 588.5 km easting. Surface elevation shown in solid black. All gravity stations projected onto the cross-section line at thier elevations and northings. Water table elevation interpolated from July 2003 monitoring data. Basement elevations from gridded map in Figure 3.2b. The overall hydraulic gradient and zone of basement storage are clearly visible.

dominated by irrigation and canal leakage. Thus, when the canals are filled, water drains into the aquifers raising the water table near the canals. The water table near the canals then drains once canal flow ceases at the end of the growing season in late summer or early fall. Irrigation dominates the shallow water table across the study area, whether from well or surface supply.

The gravity monitoring data, combined with irrigation allotments and helicopter-borne EM measurements for basement topography, are used to investigate a method of dealing with the non-uniqueness in gravity interpretation by incorporating multiple data sets into a single numerical model. Interpretation of the irrigation, gravity change, and well change data provides simple checks on the numerical model results for plausibility.

3.2 Data Acquisition

Gravity data were acquired on all stations once per month, between July and October 2003; actual survey dates are 23 July, 26 August, 23 September, and 28 October. Data were acquired using a CG-3M gravimeter with a field protocol as detailed in *Gettings et al.* [2008]. Station occupations have a minimum of 12 min time series each time, with a minimim of two occupations per survey for intrument drift control. Instrument drift is removed using a staircase drift function, as described in *Gettings et al.* [2008]. Vertical deformation control from geodetic GPS receivers (Trimble 4700 systems) run in a post-processed, rapid-static mode showed no elevation changes greater than 2 cm during the monitoring project. Thus, gravity changes are attributed entirely to mass change, and not to deformation.

Stations MORRILL_CA and SBNM (Scotts Bluff National Monument) are used to remove inter-campaign instrument drift. Measurements of absolute gravity at both stations in July and September 2003 by the National Geodetic Survey show no significant change: -1.8±1.9 μGal at SBNM, and 11.6±6 μGal at MORRILL_CA. Thus, apparent gravity differences between campaigns have been shifted to hold the average gravity changes at SBNM and MORRILL_CA at 0.

Water levels in the monitoring wells co-located with gravity stations were measured by the Lincoln USGS personnel during the gravity campaigns. Water levels in surrounding wells were measured within 1 week of gravity campaigns; water levels have been interpolated from bracketing measurements to the campaign dates.

The U.S. Geological Survey acquired and processed a helicopter-borne EM survey over the Dutch Flats study area. Contours of basement elevation from processed EM data were provided [pers. comm. James Cannia, 2010].

3.3 Results & Discussion

Gravity and well data, differenced from the initial 23 July campaign, are shown in figure 3.4. Gravity and water level data have been interpolated onto a 100 m regular grid using an equivalent sources algorithm [*Cordell*, 1992], and the grids differenced. Grids are limited to the areas covered by data points; thus the well grids are much more extensive due to the greater spatial coverage. Also note that the east-west extent is 3 km compared to the north-south extent of 13 km; east-west grid cells are shown 4x wider than north-south. This makes changes appear dominantly horizontal.

Multiple techniques were tried for gridding the observed data, including cubic splines, linear interpolation, nearest-neighbors, kriging, and equivalent sources. Cubic splines, due to the sparse and irregular well locations, introduce artificial extrema between the wells. Nearest-neighbors and linear interpolation result in grids with discontinuities or sharp corners. Given that the well levels represent a potential surface, there should be no sharp corners in the gridded result. Kriging introduced large extrema in regions without wells; the empirical variogram does not match the assumed gaussian variogram very well (see figure 3.5). Equivalent sources produced continuous smooth grids for gravity and well data. By construction, the equivalent source grids are potential fields and match the observed data at all data points. Areas with little to no control (such as the extreme SE corner of the water table grids) show some artifacts; these artifacts are consistent between campaigns and thus differenced out.

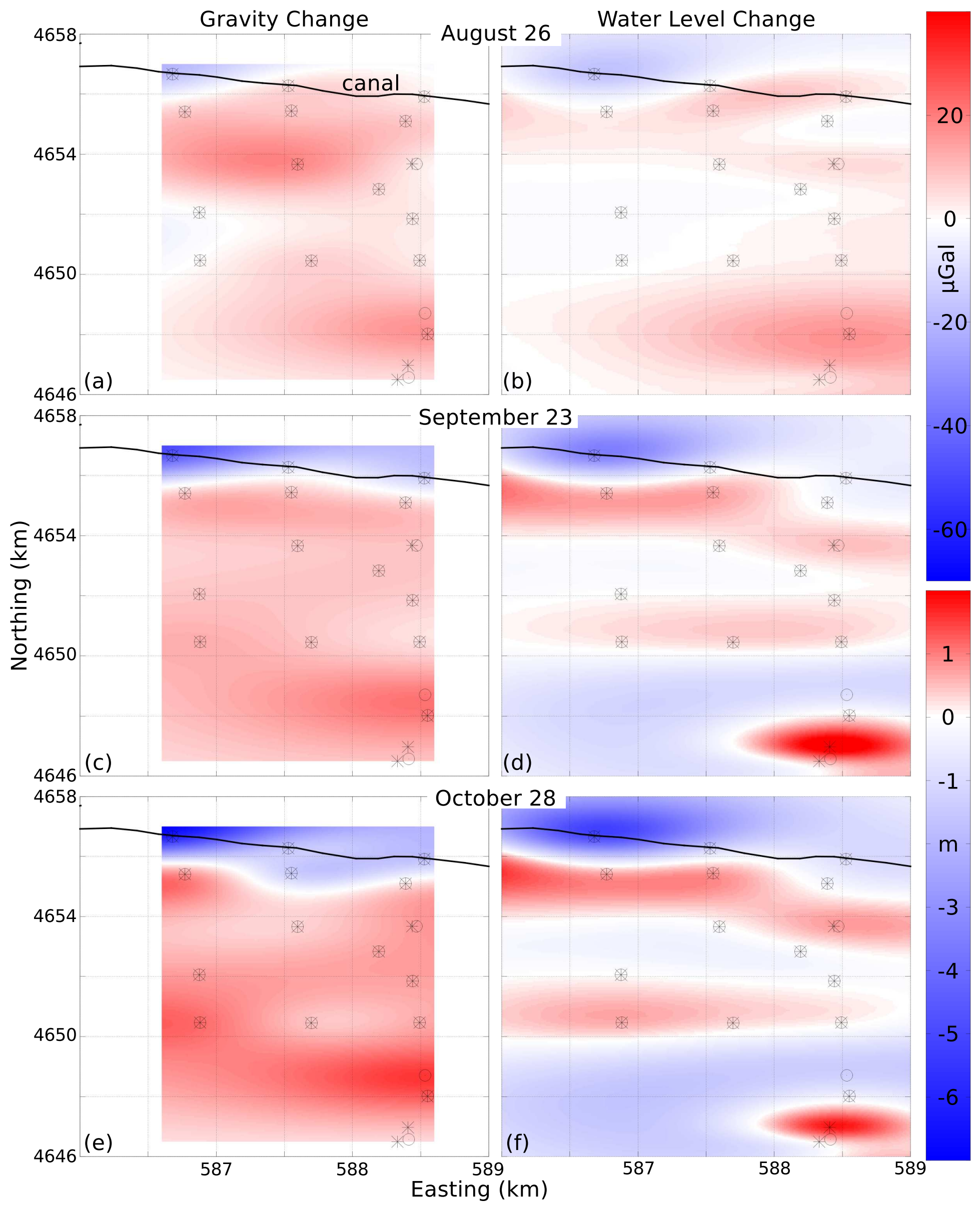

Figure 3.4. Gravity and water level changes from 23 July. Data at wells (stars) and gravity stations (circles) were interpolated to a 100 m grid using equivalent sources [*Cordell*, 1992].

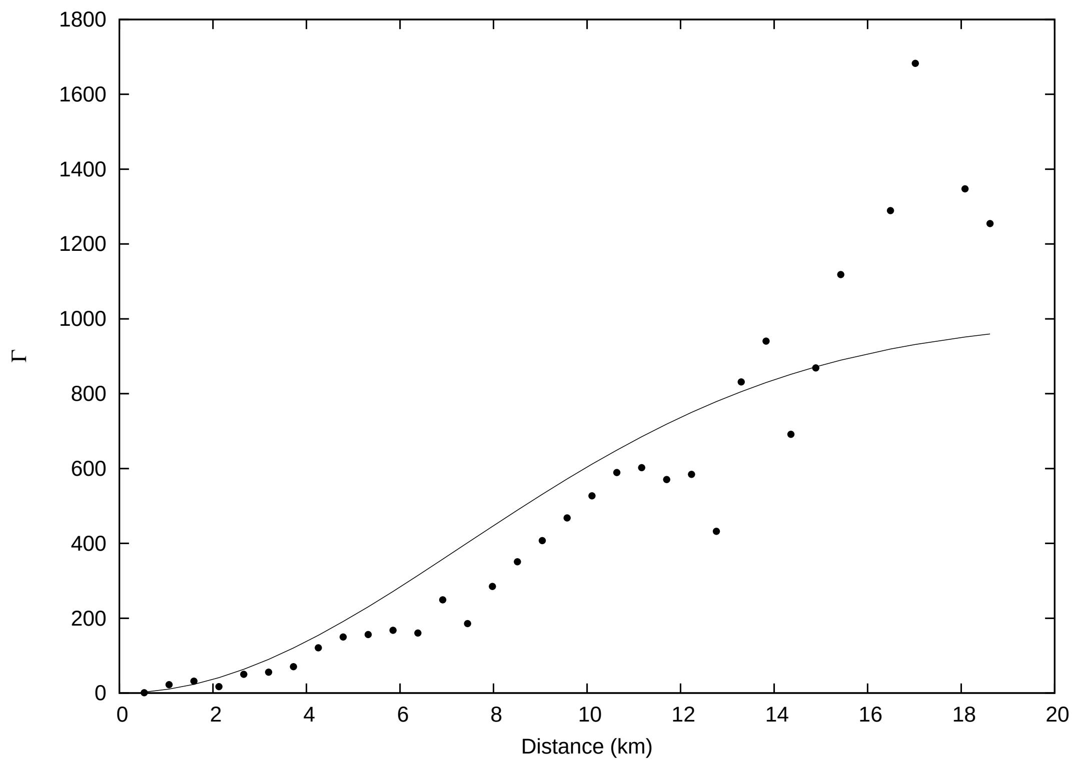

Figure 3.5. Variogram of well levels vs. inter-well distance used for kriging. Symbols denote actual variogram values for different well pairs, while the solid line is the best-fit gaussian variogram. The two do not agree very well, and is the cause of significant extrema in areas without wells.

August changes range from -21 to +19 μGal, with negative changes around the northwest corner, and a single positive region in the center of the field area. Water levels show similar small changes from July to August (-1.71 to +0.85 m) with much of the region showing change of less than 0.5 m. Maximum water level increase is seen coincident with the main gravity high in the SE corner, and the maximum water level drop coincides with maximum observed gravity decline. The gravity high in the center of the field (well 2D) is attributed to local irrigation at the site not reflected in the well data.

Change from July to September range over a larger range (-50 to +22 μGal), but generally similar pattern to August-July. Additional gravity decrease on the northern edge is consistent with a lowered water level due to irrigation shutoff. A water level high in the SE corner of the field is not reflected in the gravity measurements, but the nearest gravity stations are displaced from the maximum water level increase. Gravity change due to the ground water high is seen in the nearest station to the north.

October gravity changes range from -70 to +31 μGal, with maximum decline in the NW corner, consistent with the maximum ground water level drop (-5.27 m). Maximum water increase is in the SE corner, just north of MORRIL_CA; gravity stations to the north show gravity increase.

3.3.1 Quantative Interpretation & Modeling

Gravity data, whether spatial anomalies or temporal changes, are non-unique; an infinite number of subsurface density distributions (or changes) will produce the observed data. However, only a small number of the mathematically-correct solutions will also be consistent with plausible geology and rock properties. Thus, quantative interpretations of gravity changes must use additional information to restrict the solution space to a plausible range in the rock parameters of interest.

In a project such as Dutch Flats, the parameters of interest are hydrologic, such as water mass in place, porosity, permeability, and specific yield. Given the gravity and water level data available, the quantitative interpretation in this project is for total mass changes and average in-situ specific yield, rather than permeability; permeability interpretation suffers from the large inter-station distance for a 3-month monitoring data set.

An effective total mass change can be computed from the gravity change surfaces (grids) and Gauss' Theorem,

$$\int_S g \cdot dA = -4\pi GM \tag{3.1}$$

The gravity change maps are discretized, thus the surface integral can be replaced with a summation over all grid areas. Since the map is only half the total surface, the integral must be doubled. Also, the desired number is the total excess mass (M), so Gauss' Theorem can be recast to a summation,

$$M = \frac{1}{2\pi G} \sum_{i}^{N} g_i \cdot dx \cdot dy \tag{3.2}$$

where g_i is the gravity anomaly in the i'th grid cell, the cell sizes are dx and dy in the east and north directions, and there are N total grid cells.

To enhance interpretation of irrigation and drying signals, the integration is carried out only over cells with either positive or negative gravity changes; both such regions are bounded by a zero-change region or the edge of the grid. Gaussian integration for excess mass yields computed excess masses shown in Table 3.1.

Table 3.1. Excess mass by campaign

Campaign	**+M (Mt)**	**-M (Mt)**	**+Area (m^2)**	**-Area (m^2)**
Aug	3.4765	-0.2467	19990000	2270000
Sep	4.8288	-1.1761	19460000	2800000
Oct	6.2451	-1.8650	18450000	3810000

Excess mass estimated for the August vs. July campaigns is an addition of 3.476 Mt. Total irrigation flow, taken from water rights records maintained by the Nebraska Department of Natural Resources, for the same period implies a maximum irrigation total of 33.967 Mt. Flow records for the Tri-State Canal, which supplies the surface irrigation water to the study area, indicates flows of around 1200 cfs into the study area, but flows of 20-60 cfs down stream from the study area. This corresponds to a maximum-allowed irrigation takeout in the study area of 1120 cfs during the July to August irrigation season. Thus, the gravity monitoring excess mass of 3.476 Mt implies that 10.2% of irrigation water in August 2003 was not used by the crops, and reached significant depths beyond the active root zone. This water eventually reached the saturated zone, as shown by the correlation of high positive gravity change and high water table change at the wells.

Note that between the September-July total is indicative of an additional 1.352 Mt of water reaching the water table in the study area. This excess mass represents additional irrigation from groundwater pumping. The gravity decrease due to groundwater pumping is apparently being more than offset by the same mass being added to the near-surface soil at the gravity stations. Since pumping total are not available for the study area, a quantitative comparison of the September and

October gravity and irrigation mass changes is not possible. Negative mass change due to "drying" of the near-surface around the canal is of greater interest.

Negative mass changes start much smaller (-0.247 Mt from July to August), but then quickly grow through the end of monitoring. This mass loss represents decreasing gravity signal from dewatering the near-surface sediments as saturated ground near the canal drys with water flowing to deeper levels. Thus, the negative mass change does not represent mass "lost", just deeper and thus with a smaller surface gravity signal.

Note the initially small decrease (-0.247 Mt) in the first month, as the irrigation canal was full until the week before the August campaign, decreasing to shut off on the day of the August campaign. The irrigation canal was then dry until the end of the monitoring. Thus, the September apparent mass drop of -0.929 Mt represents the initial desaturating of the sandy soil under the canal, and the -0.689 Mt drop in October shows the slowing due to a deepening saturated zone, and thus less gravity decline for a given mass change.

As a first pass at determining an effective in-situ specific yield of the near-surface aquifer, the gravity decline at the canal can be used with a Bouguer slab approximation. By rearranging the equation for the gravity effect of a Bouguer slab, the effective specific yield can be computed from the well level drop, gravity change, and constants:

$$\phi = \frac{\delta g}{2\pi \rho G \Delta z} \tag{3.3}$$

where ρ is 1000 kg/m^3, Δz is the well level change, and δg is the measured gravity change. Since there is uncertainty in the gravity changes, a maximum and minimum specific yield are calculated in addition to the average. Comparing maximum and minimum specific yields for the three near-canal stations (1A, 2B, and 3B), all gravity and water level changes can be explained by a uniform specific yield of between 0.20 to 0.35.

Ideally, an optimum specific yield is found for the entire study area by inversion. For 3- and 4-dimensional problems, formulation of an analytic inversion scheme is extremely tricky and often requires numerical approximation. By choosing an appropriate numerical model, forward model computation is fast, so this project avoids analytic complexity by employing a grid search for an optimum field-wide average specific yield.

The USGS-supplied EM-derived basement topography isolines were converted to the same grid as observed data; UTM-projected isoline coordinates, along with the elevations, were used as a set of control points for a multiquadric surface fit [*Hardy*, 1971]. Once the coefficients of the multiquadric surface were determined, the elevation at the grid points used in gravity and water level grids were computed. As a check on the fitting and gridding algorithms, the 100 m grid points were contoured at the same levels as the original isolines, and the original control points plotted on the same plot (figure 3.6). Note that the original isoline points lie on top of the contours, indicating agreement between the basement grid and original isoline points. Some small features are mis-connected compared to the original isolines due to the 100 m grid spacing, but these differences will not affect modeling or optimization.

The numerical models for the specific yield grid search were built using the water level and basement topography grids, and consisted of a large number of variable-sized blocks. The entire gridded region plotted in figure 3.4 was broken into columns centered on the grid points. Columns started at the elevation of the water level grid, and descended to one of two bottom elevations: (1) a deep constant-depth bottom, or (2) a bottom following the basement topography grid.

Each 100 m square model block has a height set from the distance between the top and bottom elevations, with the center half-way between. Due to truncation of the moment series when computing gravity effects of the model blocks, blocks with a north or east width greater than 20 times the height are inaccurately computed; thus blocks with heights less than 10 m were broken into an array of 10 m square blocks of the appropriate height. The density contrast of each block is set by the assumed specific yield, multiplied by 1000 kg/m^3. An example model of both types, from the 28 October campaign and assuming 20% specific yield, is shown in figures 3.7 and 3.8. Note that for models using the basement topography, areas with a

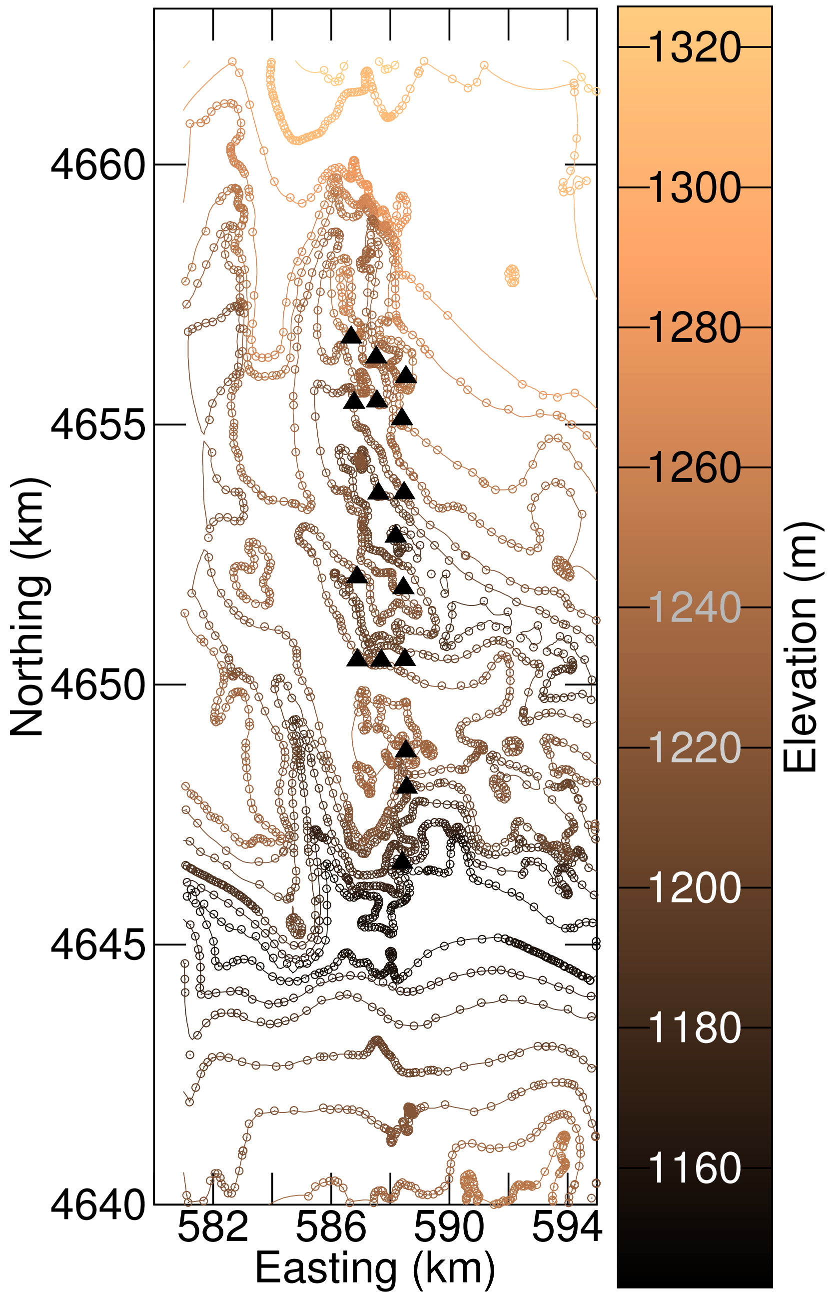

Figure 3.6. Contoured gridded data and original isoline points. Basement isoline points shown as circles, color-coded by elevation. Gravity stations shown as triangles for reference. Contours are from the 100 m gridded data from a multiquadric surface fit to the isoline points. Note the agreement between original points and contoured grid data.

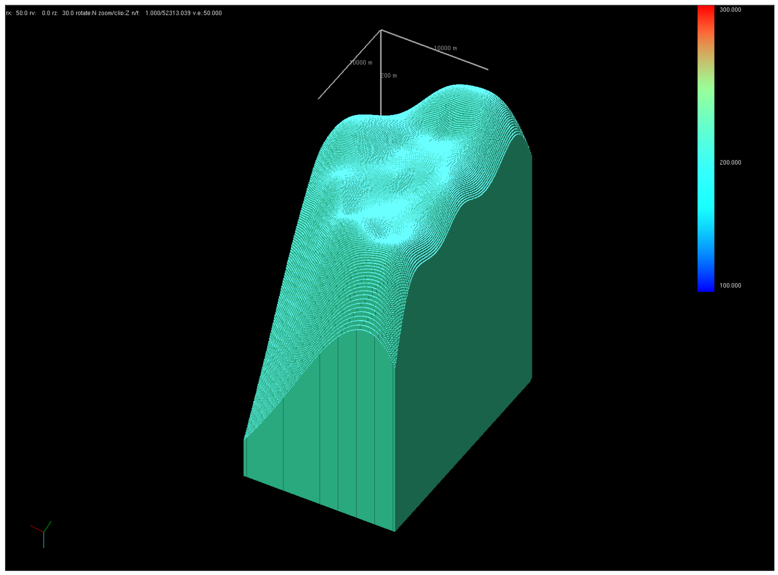

Figure 3.7. Fixed base model for water levels of 28 October 2003. Gridded water level elevations are used for the top surface, and the bottom set to an arbitrary, deep level (700 m ASL). Density contrast set to 200 kg/m^3 (Φ=20%).

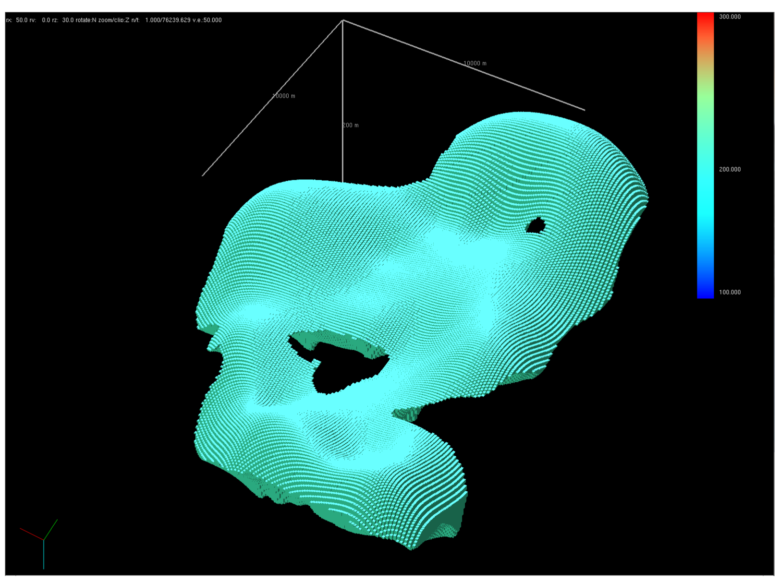

Figure 3.8. Variable base model for water levels of 28 October 2003. Gridded water level elevations are used for the top surface, and the bottom set to the basement topography grid; areas with basement elevations at or above water elevations have no model blocks. Density contrast set to 200 kg/m^3 (Φ=20%).

basement elevation within 30 cm or above the water table have no model blocks; storage in the dominant basement aquifer (Brule formation) is generally negligeable [*Verstraeten et al.*, 2001]. Models with a fixed deep base had 31 161 blocks; those with basement topography typically had between 90 000 and 105 000 blocks due to regions with heights less than 10 m.

Alluvial soils compact when buried, which reduces the porosity at increasing depth. The assumption of a constant porosity for the gravity models could be poor if the burial depth extends over a sufficient depth. Using the 30 m DEM grids available from the U.S. Geological Survey and the gridded basement isolines, the depth to basement was calculated across the study area. Maximum depth was just 95 m, with an average of 32 m. Compaction of porosity for modern floodplain sands follows an exponential form: $\phi = \phi_0 \exp(-kz)$ for $k = 0.12$, z in km [*Sheldon and Retallack*, 2001]. For burial depth of 100 m, a surface porosity of 0.30 drops to 0.296; thus compaction is irrelevant to this project, and a constant saturated porosity is sufficient.

The gravity effect at each gravity station position (north, east, elevation) is computed from the generated model blocks, and then differenced to the 23 July values. The gravity effect of blocks are computed according to the method of moments presented in *Grant and West* [1965]. The predicted differences are then gridded identically to the measured gravity changes. The gridded predicted differences are compared to the measured gravity changes by computing a RMS difference from all grid points.

The RMS difference between the predicted and measured gravity change grids depends on the assumed alluvial aquifer specific yield. Thus, a grid search of specific yields determines a best-fit specific yield for all campaigns. The RMS difference by porosity is plotted for models with basement topography and fixed-depth models in figure 3.9. The plotted RMS misfits have been scaled by the range of observed gravity changes for each campaign, allowing direct comparison of misfits for campaigns with larger and smaller ranges. Note that the porosity is the

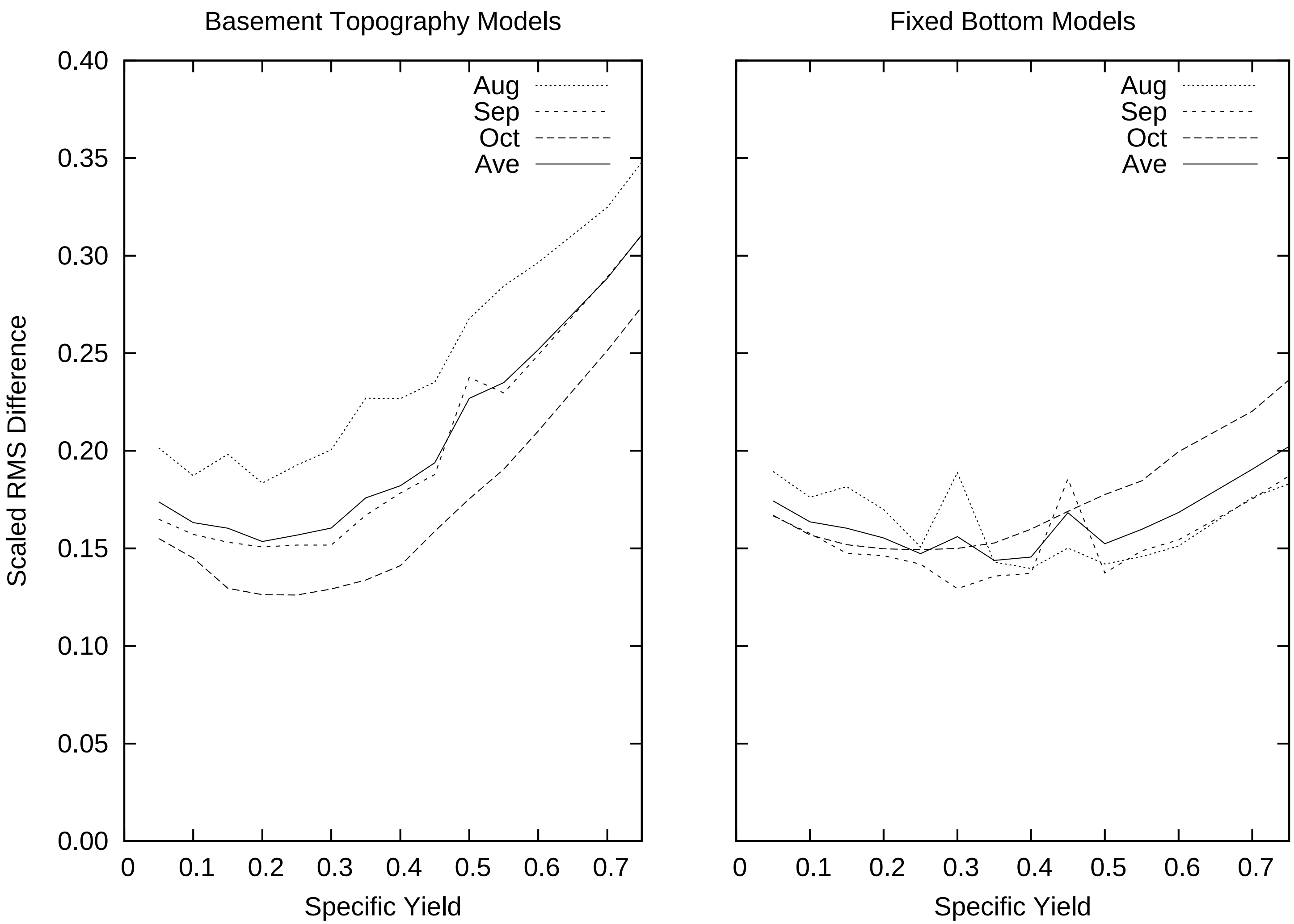

Figure 3.9. Scaled RMS difference by porosity for models with a fixed-depth basement and with basement topography. RMS difference is scaled by the range of the observed gravity grid for each campaign.

effective, field-wide porosity being filled or drained; this is, of course, the average specific yield of the field.

For models with a fixed bottom at great depth, the predicted grids at all porosities better match observed grids in August and September than the predicted grid for a model with basement topography, but do not match as well in October. Minimum average RMS differences are nearly identical for both types of models, but the models with basement topography show a sharper misfit curve. Fixed-depth models show misfits within measurement error (3 μGal) of the minimum (10.34 μGal at 0.25) for specific yields between 0.05 and 0.60, whereas basement-topography models show misfits within error of the minimum for specific yields between 0.05 and 0.35. Thus, basement topography models are more sensitive to specific yield. Minimum RMS specific yields for both types of models are reasonable; 0.20 for topography models, and 0.35 for fixed-bottom models.

Inversion of the observed gravity data to predict a best-fit specific yield is analytically intractable. The forward model is straight-forward, but difficult to formulate in matrix form for direct inversion, as the matrices would take 5 GB of memory to store. Thus, it is faster in total time to perform a grid search rather than attempt to find an analytic shortcut or representation for a conventional inversion scheme. If the generated models used variable porosity, the rock type and hence porosities would be varied using a Monte Carlo approach rather than attempting an analytic inversion.

The ability to “uncontour” data - to go from isolines to a regular grid - opens up many existing interpreted data to use in modeling and analysis, such as GIS layers of potential field anomaly isolines, isopach maps, or geologic maps. Treating the input isoline points as data points for a general gridding algorithm (such as cubic splines or nearest-neighbor averages) is a flexible method of making a grid from the points, but one that doesn’t take into account the type of data; the results are therefore typically poorly representative of the original data that generated the isolines. For example, grids generated with polynomial splines tend to introduce artificial extrema, and grids generated with nearest-neighbor averages tend to have discontinuities.

In the case of this project, the isolines are of topography (albeit buried), and thus the use of a multiquadric surface fit makes an efficient algorithm for gridding the isolines that results in a smooth gridded surface without artifacts. In a gravity or other potential field application, an algorithm that honors potential fields will produce a best grid, e.g. equivalent sources (as used in this project) or minimum curvature. An application using a geologic map could use a nearest-neighbor algorithm (without averaging) to convert polygons of geologic units to a regular grid of rock types for model building.

3.4 Conclusions

Given the inherent non-uniqueness of gravity change interpretations, additional information will always be necessary to reduce the infinite solution space that mathematically matches the observed data to a small solution space of geologically-plausible (or at least consistent) models that best match the observed data. In this project, the water level changes and basement topography leave only an assumed specific yield free to vary. Thus, a best-fit study-wide specific yield can be found by a simple grid search; the speed of forward model computation and the complexity of formulating a full inversion scheme for these models pushes for using analytically simple, but computationally expensive, schemes to optimize the specific yield.

Gravity changes in August, September, and October campaigns qualitatively agree with water level changes in the colocated wells. Comparison of computed excess mass across the field area with irrigation allotments implies that 10% of the irrigation water reaches aquifers below the active ET zone. Quantitative agreement depends on choosing the correct specific yield for the type of model used. Simple estimates of specific yield for the drying vadose zone after the canal shutoff results in specific yields of 0.2 to 0.35. Interpretation based on numerical models results in more precise optimal estimates.

Models incorporating basement topography are more sensitive to the specific yield , and achieve optimum fit at a lower specific yield (0.20) than models assuming a deep uniform saturated zone (0.35). *Verstraeten et al.* [2001] reported a specific yield of the alluvial aquifer in the study area of 0.32, based on an aquifer test, and that unpublished specific yield tests in the alluvial aquifer south of the field area varied by up to an order of magnitude locally. Thus, an effective specific yield for the entire study area of 0.20 to 0.35 agrees with the aquifer test.

Although both optimum specific yields are plausible for the shallow alluvial aquifer at the study site, the higher sensitivity of basement topography models to specific yield makes them a better choice for determining effective in-situ aquifer specific yield. Incorporating geology from well logs, if available, into the numerical models would provide a basis for a variable specific yield model reflecting local sediment package changes.

CHAPTER 4

4-D GRAVITY AT THE GEYSERS

4.1 Introduction

Repeated high-precision gravity measurements can be used to track mass changes of engineering interest, for example groundwater or steam-field changes [*Pool and Eychaner*, 1995; *Gettings et al.*, 2002; *Sugihara and Ishido*, 2008]. Gravity change is sensitive to elevation and mass changes in the reservoir and cap; when coupled with GPS measurements to determine surface deformation, the gravity changes can be corrected to reflect only the mass changes under a station. Thus, gravity and GPS monitoring can provide insight into saturation, temperature (via thermal contraction), mass balance, and steam-field boundary changes over time. While these changes can be detected in other ways (e.g. production well monitoring, microseismic networks, or InSAR), gravity monitoring can play a crucial role in projects with challenging access, large spatial extent, or deep sources. At The Geysers geothermal system in northern California, all three difficulties are present. Despite being the largest produced geothermal system in the world, The Geysers does not have a particularly well-defined boundary for the overall system. Multiple operators and a long production history combine to make delineation of the maximum extent of production changes, reservoir boundaries, and well interference difficult at best. To help address the challenges of where and how The Geysers reservoir is changing at depth and on the surface, gravity and GPS monitoring began in fall 2000.

In this paper, we present initial interpretations of the gravity and GPS monitoring campaigns from 2000 to 2011. As more production and injection data, groundwater levels, and more refined GPS solutions become available, our interpretations will subsequently be updated. The data available currently are sufficient for a first look at the gravity changes, but detailed analysis will require the well-by-well production and injection data.

4.2 Station Network

Data collection started in September 2000 with an initial network of 50 gravity stations on the main production field and off-field valleys. We attempted to use stations from the 1970s precision gravity campaigns [*Isherwood*, 1977] wherever possible; however, construction and weathering made recovery of most benchmarks from those early campaigns impossible. Subsequent campaigns extended the network to 58 stations in April 2001, 108 stations in September 2001, and 120 stations in 2006 and 2011. However, due to loss of stations between campaigns, we have actually occupied 166 sites total over 5 campaigns, but only 120 remain viable in the 2006 and 2011 surveys.

Various stations were lost due to road construction and other factors, so absolute station count does not necessarily reflect that only 2 stations were lost over the 5 campaigns. Over the entire monitoring period, 46 stations have been lost or abandoned in the production field and surrounding region. Most were lost due to construction (e.g. road widening, hill sculpting, sidewalk replacement), but 10 have been abandoned because the station could not be relocated or the abandoned station replicated a nearby, better station.

The full station network, shown in figure 4.1, extends across the current production zone of the The Geysers, with a nominal spacing of 1 km. We have also established some stations extending from the production field to the surrounding valleys; one line from the SE corner extends to the SW, one line extends to the SE, and a line of stations extends to the NE from the northern edge of the field. A sparse ring of stations on the NE edge of the current production will capture upcoming production-induced changes in the newly explored high-temperature reservoir.

To help remove instrument drift and investigate seasonal signals at the reservoir, six regional stations in the valleys around The Geysers are measured each campaign.

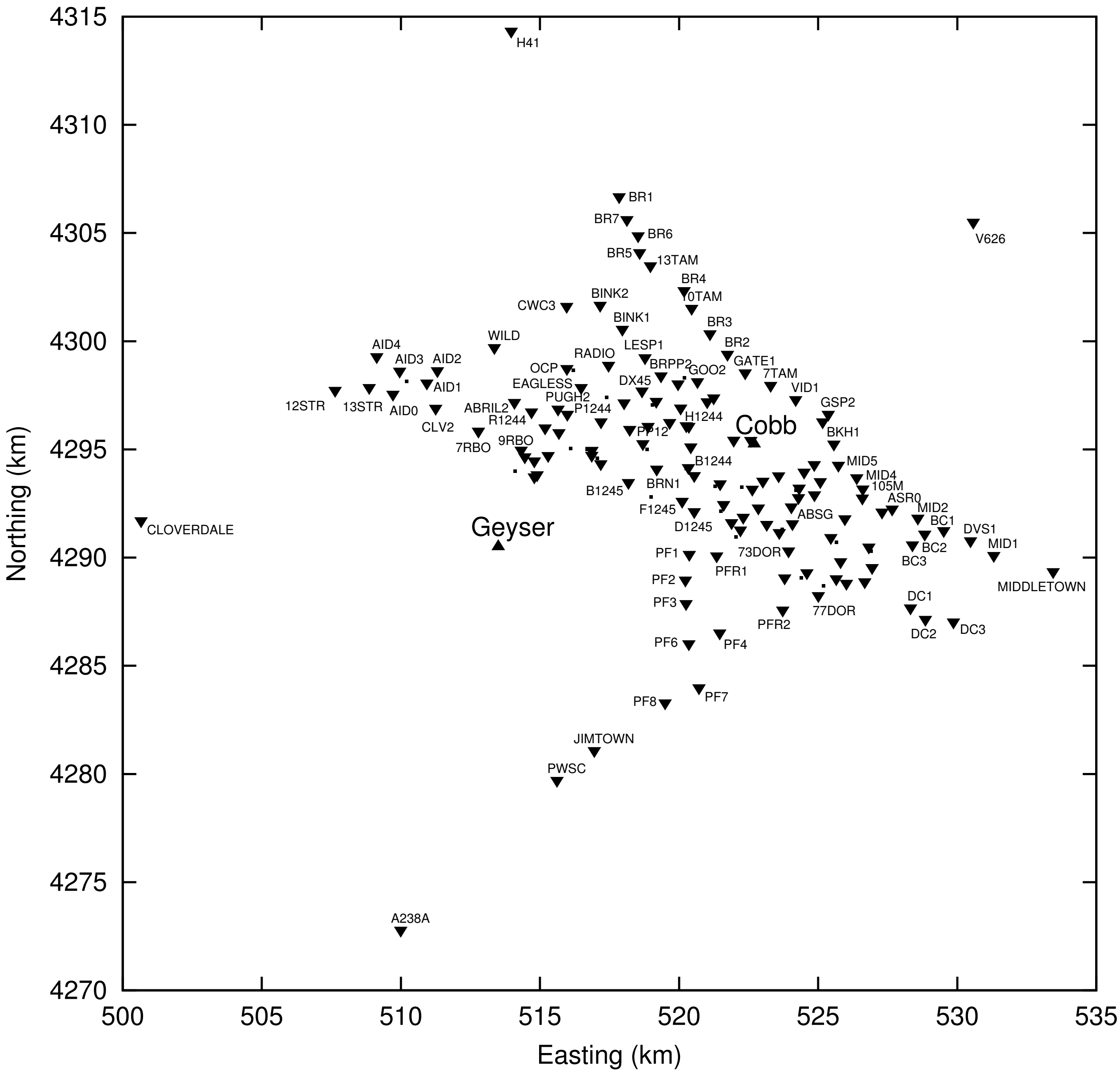

Figure 4.1. Station network at The Geysers. Gravity stations shown as downward-pointing triangles, power plants as squares, and mountain peaks as upward–pointing triangles. All stations are named, but many on the production field are omitted for clarity. Power plants and peaks form a convenient reference frame for interpreting gravity change maps.

Stations H41 (Kelseyville, CA), CLOVERDALE, A238A (Healdsburg, CA), JIMTOWN, V626, and MIDDLETOWN fully surround the production field, but are at least 1000 m lower in elevation than the stations on the field. This elevation difference precludes fully capturing the precipitation-caused gravity changes on the field, as the precipitation on the field is noticeably different than in the surrounding valleys.

4.3 Data Collection

Measurement techniques able to achieve precision and accuracy of 5 μGal have been developed over the past few decades, taking advantage of recording gravimeters and time-series analysis; for the campaigns presented here the data are collected and processed according to *Gettings et al.* [2008]. Campaigns from 2000 to 2006 used a Scintrex CG-3 gravimeter; the 2011 campaign used a CG-5 gravimeter. Gravity change precision varies between 3 and 7 μGal for all stations in all campaigns.

Gravity measurements were conducted on all stations on each campaign, along with high-precision GPS. Campaigns in 2000 and 2001 used GPS occupations of 30 and 60 minutes in a rapid-static mode. A continuous local GPS base was established at H1244 for the 2000 and 2001 campaigns, with precise coordinates computed from all the data on H1244 referenced to the continuous station HOPB in Hopland, CA. Precise H1244 coordinates were used to compute precise coordinates for all campaign stations, with estimated accuracy of 3 cm vertical. Starting in 2006, GPS data were collected for a minimum of 8 hours, using NGS continuous reference stations (CORS) for post-processing. Vertical accuracy is estimated at better than 1 cm for 2006 and 2011 positions.

4.4 Gravity Changes from 2000 to 2011

Corrected gravity changes are presented in figure 4.2, in μGal, for each campaign compared to the immediately preceeding one. Changes have been corrected for instrument drift, elevation change, and estimated near-surface water changes.

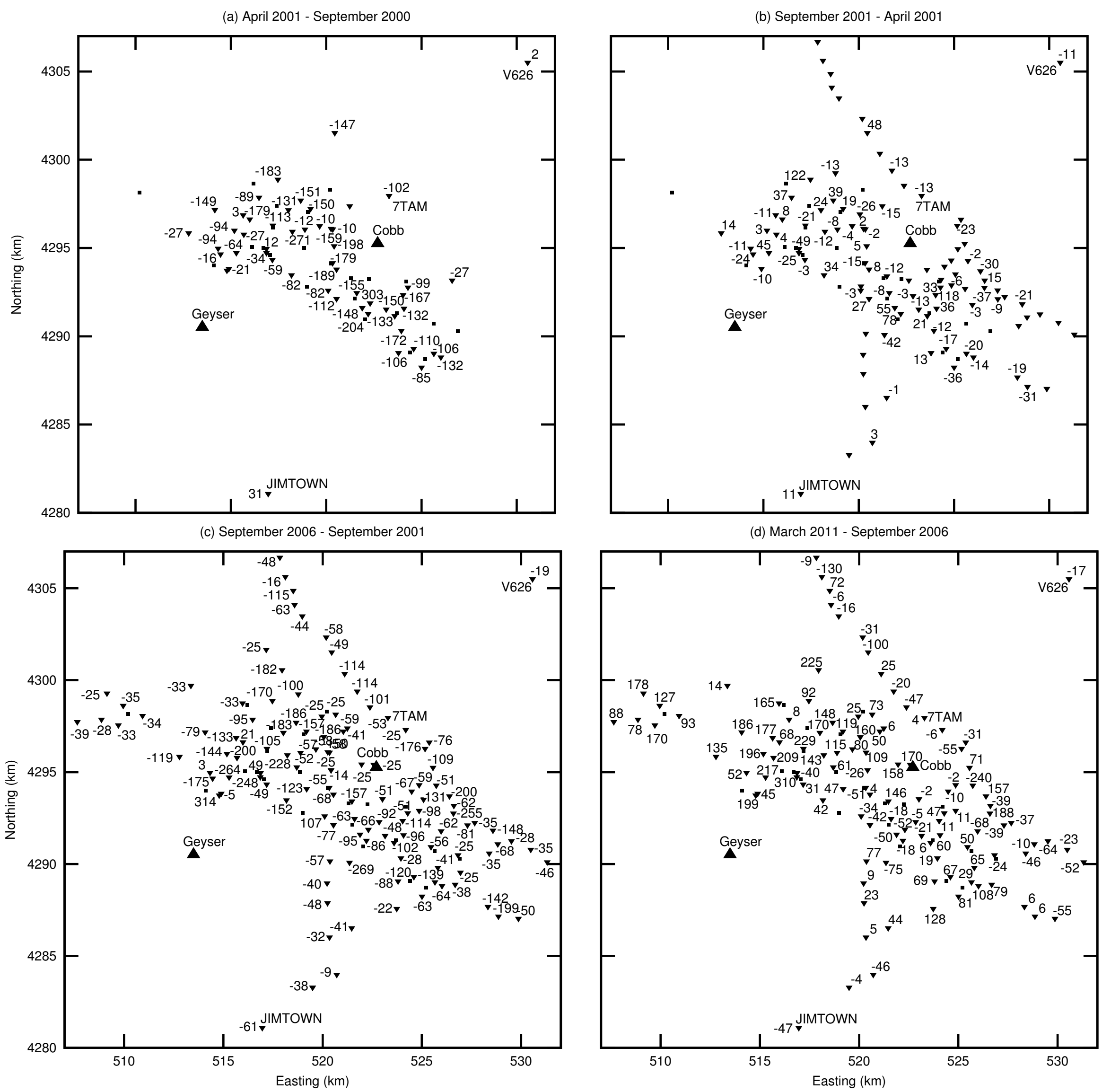

Figure 4.2. Gravity changes, in μGal, between campaigns. Stations are marked with downward-pointing triangles with gravity change shown next to the marker. Power plants are shown as squares, and mountains as upward-pointing triangles. See figure 4.1 for station names. Gravity changes corrected by -25 (2006) and -80 (2011) μGal for estimated groundwater effects (see text for details).

Instrument drift is removed during campaigns by a daily drift function built from repeated occupations, as detailed in *Gettings et al.* [2008], and between campaigns by updating gravity changes such that the average change of stations CLOVERDALE, H41, and JIMTOWN is zero. Holding the average of stations at zero change also removes a groundwater signal, although not the exact signal on the production field. Without well level measurements across the production field, it is not possible to accurately predict the groundwater-caused gravity changes, so some residual groundwater signal will be present in gravity changes on the field.

Gravity changes by -308.6 μGal/m of vertical change; we use the GPS results to determine vertical change at each station, and then compute a gravity correction from the free-air gradient (-308.6 μGal/m). Elevation changes from GPS results are shown in figure 4.3. Differences are shown in mm; stations without changes shown are uncorrected due to a lack of data during a particular campaign. Note the changes between campaigns, which are consistent with observable surface cracks on roads and hills across the production field and surrounding region. Since GPS measurements yield differences at the surface, elevation changes are a combination of near-surface motion due to landslide, water, etc. as well as pressure and temperature changes in the deep reservoir from production and injection. Separating the near-surface and deep deformation signals is not trivial, and work is ongoing.

Water table elevation changes for wells near JIMTOWN, CLOVERDALE, MIDDLETOWN, and H41 are shown in figure 4.4, converted to a gravity change relative to October 2000. Changes in water table elevation can be converted to an estimated gravity change by assuming a porosity (0.25) and that water table changes act as an infinite slab; the gravity change is then 10 μGal/m of water level change. JIMTOWN has the largest changes, ranging from -20 to +80 μGal. Kelseyville wells (near H41) show the second largest changes (up to +60 μGal), but with much less variability after 2002. Cloverdale (and Healdsburg) wells show small gravity changes (-10 to +10 μGal), due to very stable water levels. Both Cloverdale and Healdsburg are in the valley bottom, near the Russian River, so water levels are expected to be fairly stable even with some pumping. Note the variability in water

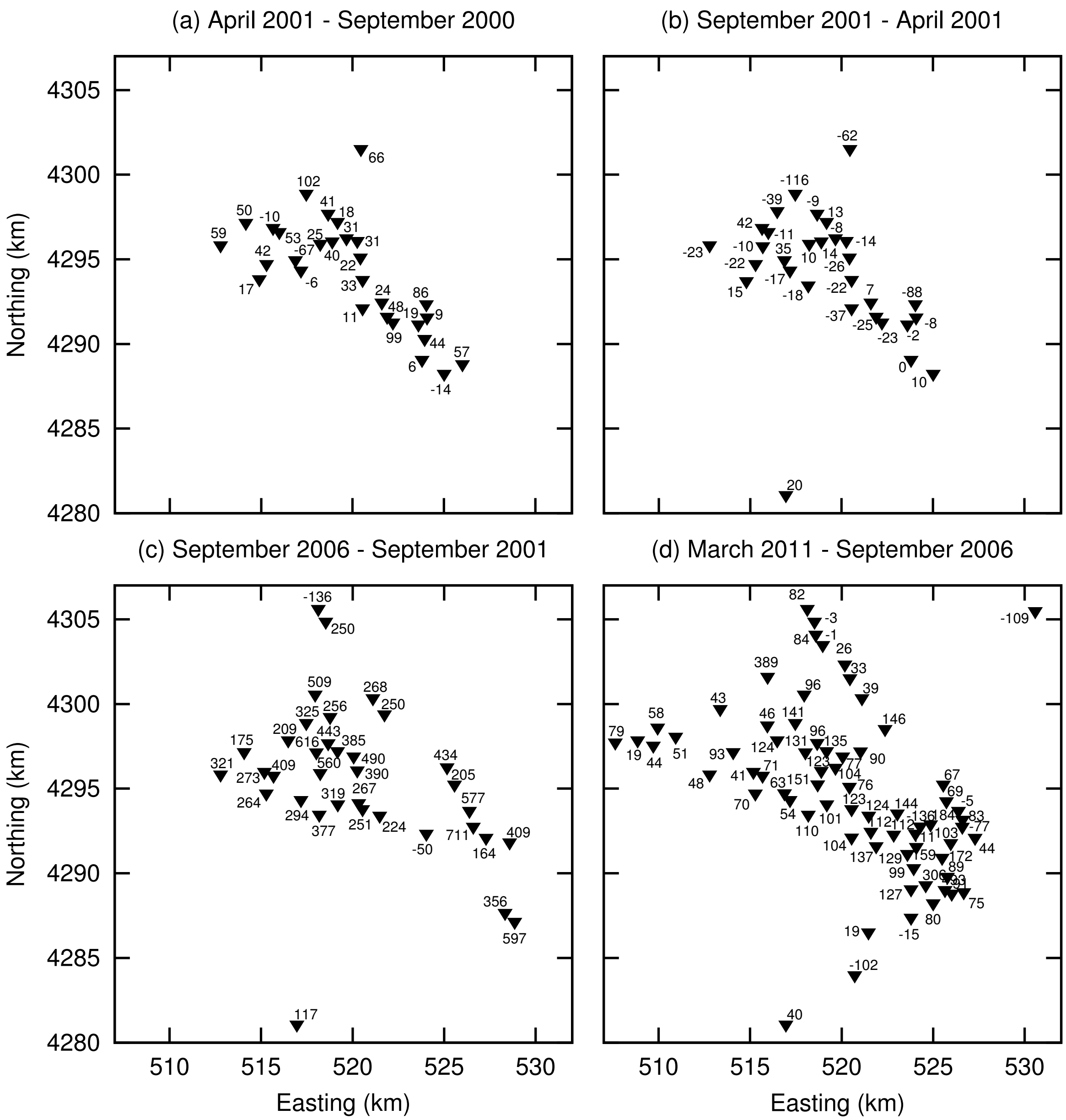

Figure 4.3. Elevation change, in mm, between campaigns. Elevation changes are measured via GPS positions on the surface, and thus represent changes in the near-surface and deep reservoir. Gravity measurements are corrected for elevation change assuming the standard free-air gradient of -308.6 μGal/m.

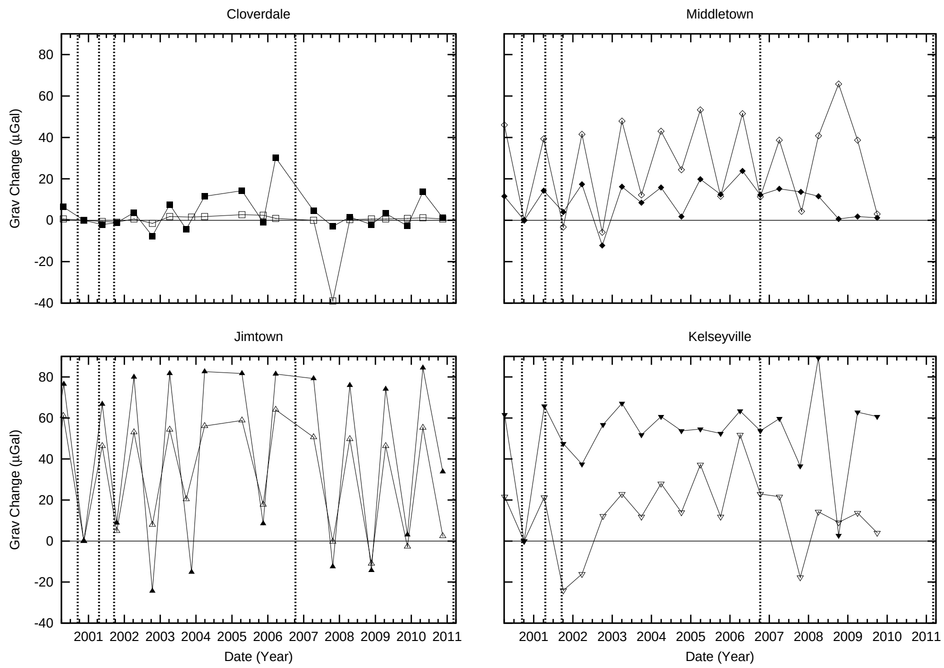

Figure 4.4. Water table elevation changes from October 2000, converted to gravity changes using an infinite slab assumption with 0.25 porosity. Vertical dotted lines show dates of gravity campaigns. Wells are chosen as being the closest available with data covering the monitoring period. Wells are a mixture of irrigation, domestic, and unused. All data from the California Department of Water Resources website (http://www.water.ca.gov).

levels, and hence estimated gravity effects, for JIMTOWN and Kelseyville despite the wells being within miles of one another. Given the variability and size of water level changes, it is possible for a groundwater signal on the production field to exceed 80 μGal peak-to-trough between the dry part of the year (September/October) and the wet (March-May). JIMTOWN is near a canyon mouth and next to a large stream; the station will have gravity effects from stream stage increases, and the estimated gravity effects are thus a lower bound on gravity signals at JIMTOWN.

Gravity changes from April 2001 to September 2000 are generally negative, with large decreases in the northern and southern production zones. Net mass loss over the entire field during September 2000 to April 2001 is 20.55 Mt (20.55x10^9 kg); all production and injection data are taken from the California Division of Oil, Gas, and Geothermal Resources website (http://www.conservation.ca.gov/dog/Pages/Index.aspx). Using an infinite slab formula for a reservoir with an assumed area of 40 km^2

[*Allis et al.*, 2001], 20.55 Mt of production equals an average gravity change of -21 μGal across the field. Without detailed production and injection data, which are currently unavailable, only bounds of gravity effects can be calculated for stations on the field. Production mass loss from September 2000 to April 2001 was 42.68 Mt, with 22.13 Mt of injection. If all mass change occurred at a single station, at the depth of the bottom of the well casing (1250 m), the station should see a gravity change of -186 and +95 μGal for production or injection respectively. Thus, gravity changes on the order of -100 μGal can be easily attributed to local production. Stations with near-zero and positive gravity changes are believed to reflect local conditions where injection dominates production.

Gravity changes from September 2001 to April 2001 are much smaller, in keeping with a production mass loss of 20.21 Mt and injection gain of 7.90 Mt; predicted gravity changes range from +34 μGal for pure injection at a point to -86 μGal for pure production, with a reservoir-wide average predicted of -12 μGal; the average of all repeated stations is -6 μGal, indicating a 6 μGal difference, barely beyond the measurement error bounds of 5 μGal. Most gravity change is again clustered around the production areas. The large number of stations with zero gravity change are stations newly occupied in September 2001. Groundwater-induced gravity change should be negative due to summer drought, and could add tens of μGal to the production signals. Most stations are slightly negative, although the positive cluster in the NW of the field may be injection and local groundwater signals. Once detailed, well-by-well injection and extraction data are available, more detailed interpretations of the gravity changes can be made.

Differences between the 2006 and September 2001 surveys are shown in figure 4.2c. Cumulative extraction and injection masses between 2001 and 2006 are 313.16 Mt and 217.89 Mt, respectively. Estimated maximum gravity signals from production and injection are -1337 μGal and +930 μGal; a field-wide average for the difference between extraction and injection is -95 μGal. To help account for groundwater change between 2001 and 2006, -25 μGal has been added to all stations; inspection of gravity changes at stations off the production field but nearby, with the reference stations held at zero, found a typical drop of 26 μGal between 2006 and 2001. Although a suitable groundwater change is not seen at the CLOVERDALE and Healdsburg wells to account for a 26 μGal shift, changes at JIMTOWN and Kelseyville wells could easily give a 26 μGal signal due to groundwater drop. Average gravity change across the field is -73 μGal, 22 μGal higher than predicted. Whether this difference from field-wide predicted is due to temporal and spatial sampling, incomplete groundwater-effect removal, or local production and injection details remains to be investigated with detailed mass flow data.

Between 2011 and 2006, gravity changes on the production field are convolved with significant groundwater-induced changes due to seasonal differences; JIMTOWN and Kelseyville well changes imply that seasonal groundwater changes could produce gravity signals of 80+ μGal at stations. Since the 2011 campaign was conducted in February and March 2011, compared to the September/October campaign of 2006, a uniform shift of -80 μGal has been applied to all stations in 2011 to remove much of the seasonal groundwater signal. Production data is only available to December 2010 currently, so predicted gravity changes from production and injection are lower bounds. Extraction and injection between December 2010 and September 2006 were 254.90 Mt and 196.48 Mt, respectively. These mass totals predict maximum gravity changes of -1089 and +839 μGal, with a field-wide average of -58 μGal. Average gravity change across all stations is 39 μGal. The 97 μGal difference between average measured change and predicted average change is currently unattributed. Claiming all the difference is due to groundwater effect indicates a seasonal signal of 170-180 μGal, which seems unlikely based on well changes in the valleys around the field. *Goodkind* [1986] found changes of such magnitude, which was attributed to seasonal changes of a single year, rather than 5 years of groundwater change in addition to the seasonal signal (March 2011 versus October 2006). It is thus possible that a better groundwater effect estimate could be 180 μGal; additional water well information on the production field would be extremely helpful in deconvolving geothermal reservoir gravity signals from the near-surface groundwater signals, although such data are not currently available to the authors.

4.5 Discussion & Conclusions

Ten years of gravity changes between 2001 and 2011 show generally good agreement with predicted bounds from production and injection data. In particular, 2001 campaigns are in good agreement with changes of appropriate magnitude, sign, and location for the production areas. Changes in 2006 are more varied and will need well-by-well reservoir data to determine how well gravity changes match the known mass changes and depths. The mismatch in measured versus predicted changes between 2011 and 2006 may well be due to underestimates of the groundwater effects on the production field or high injection during early 2011 just before the gravity campaign; an ongoing search for groundwater levels somewhere on the production field, and additional production data, should allow partitioning of the difference between predicted and observed gravity changes.

Currently, only aggregate production data are available on a monthly basis, preventing detailed interpretation of gravity changes between campaigns for individual portions of the monitoring network. Well-by-well data for September 2000 to April 2011 would allow such detailed interpretation; such data are being prepared by the operators for use in gravity interpretation, but are not yet available to the authors. Additionally, well temperature and pressure data may become available, which will allow incorporation of all geophysical data in a reservoir simulator that spans the production field and surroundings.

4.6 Acknowledgements

The authors wish to thank Calpine Corporation and Northern California Power Agency for their field and data support of this project. The initial campaigns were funded by U.S. Department of Energy. The CG-5 gravimeter in 2011 was provided by Utah Geological Survey. GPS equipment was provided in 2006 by UC Berkeley and 2011 by UC Riverside.

CHAPTER 5

SUMMARY

High-precision gravity measurements can be made for a variety of projects, requiring only the use of a high-precision automated gravimeter and the acquisition and processing techniques of chapter 2. Specific station reoccupation schedules, and the use of time-series data for each occupation make routine accuracies of 5 μGal or better achievable for most projects.

Projects which can accept lower precision can trade station reoccupation for additional station coverage, pushing exploration gravity precision to 50 μGal easily for daily coverage of 20-40 stations. Large projects will need multiple field teams or long field campaigns, but both options are practical for exploration targets.

Processing time-series of gravity readings for each station occupation is complex if done by hand, but straight-forward when using an automated processing flow, such as the software included in appendix A. While the processing package requires training to use well, the automated processing, quality control, and output options make the training time insignificant compared to manually processing time series of data for more than one project.

Interpretation of gravity data, whether spatial anomalies or temporal changes, depends critically on understanding the system under study. The non-uniqueness of gravity signals can only be reliably handled by reducing the infinite mathematical solutions to the (relatively small) set of solutions which are geologically plausible and consistent with any and all other data available for a study.

Thus, computing an effective field-wide specific yield for Dutch Flats, NE field area is best done when gravity change, water level, and basement topography information can be integrated to produce the best numerical models available. Qualitative interpretation can be done from simple gridded maps of observed data, but quantitative interpretation of 2-, 3-, or 4-dimensional data requires numerical models able to predict gravity change for comparison with observed data.

The enormous computing power currently available in commodity desktop computers makes such numerical modeling tractable. The challenge now lies in choosing reliable (and efficient) methods of generating a model for computation, rather than in the gravity calculations themselves. To this end, gravity change data at Dutch Flats, NE was used as a test case for techniques to grid sparse data, and bring water level, topography, and geologic information into the model building procedure.

Automated model generation, starting from data files of water levels, basement topography isolines from airborne EM, and depth inferred from DEMs, allowed a quick grid search for a best-fit specific yield that honors all the information available for the study area.

Application of gravity monitoring techniques to The Geysers in northern CAlifronia allows tracking of gravity changes due to steam field production and deep recharge. Gravity changes between 1977 and 2011 track aggregate mass flows quite well, with definite evidence for spatially-variable field response due to production and injection.

With improved spatial and temporal resolution in the mass data, it is expected that a quantitative tracking of gravity changes in all regions of the field will be seen.

APPENDIX

MICROGRAV SOFTWARE PACKAGE

A.1 Introduction

The processing techniques described in chapter 2 have been embodied in a software package for precision gravity processing. The software package, called `micrograv` is freely available, and this appendix is the main documentation on using the package. This software requires a Python interpreter, C compiler, and graphical interface. A postscript viewer is highly recommended.

To start, this appendix describes how a CG-5 gravimeter should be configured to make best use of the software package.

A.2 Setting up the CG-5 Gravimeter

This manual will not explain how to run a CG-5; see the Scintrex Operator's Manual for the appropriate button sequences to push.

For precision gravity field measurements, set the instrument settings as follows:

- SURVEY HEADER menu
  - Station Designation system: **XYm** (but we will ignore the line number!)
  - Survey name: Appropriate to the project
  - Operator: Appropriate for the operator
  - Client: Ignored
  - Latitude: ignored, but set to the rough center of a project network if using the meter's Earth Tide Correction (ETC) for field comparisons.
  - Longitude: ignored, but set to the rough center of a project network if using the meter's Earth Tide Correction (ETC) for field comparisons.

  - Zone: ignored
  - GMT difference set correctly for the **clock on the meter**
- AUTOGRAV SETUP menu
  - Tide Correction: **YES** or **NO**; reduction programs will apply a more accurate tide correction, but field comparison of readings will be greatly aided by a rough ETC from the meter.
  - Continuous Tilt: **NO**
  - Auto Rejection: **YES**
  - Terrain Correction: **NO**
  - Seismic Filter: **NO**
  - Save Raw Data: **NO**
- DEFINE THE OPTIONS menu
  - Read Time: 30
  - Factory Flag: 80 (this apparently can't be less than the read time+20 or so ?)
  - # of cycles: 99998 (effectively infinite)
  - Start Delay: 1
  - Line Separation: 0 or 1; the line number will be ignored in processing, so don't worry about line separations or new lines.
  - Station Separation: 1
  - Auto station inc.: **NO**
  - Record Ambient Temp: **YES**

Note that the other settings can be set by operator preference or ignored.

A.3 Downloading the CG-5

As Scintrex provides comprehensive download instructions in their manual (starting on page 3-59), only additional notes will be presented here. So far, only the USB download has been made to work with the UGS and U of Utah laptops. The USB download setup using the Scintrex-supplied SCTUTIL program and Scintrex USB driver has been verified to work on Windows XP running natively on a laptop, and also as a virtual machine on a Macbook under VMWare Fusion.

SCTUTIL is available for free from Scintrex; look under the Support link at the bottom of the download page. Also get the Scintrex USB driver if setting up a download computer.

Install the SCTUTIL program according to the on-screen instructions or Scintrex's manual. Install the Scintrex USB driver as per its instructions.

Turn on the computer, and let it boot to the desktop. Make sure nothing else is running in the foreground; operators have reported problems with downloading if other programs are running along with SCTUTIL, and no problems if SCTUTIL is the only program on the task bar.

Connect the USB cable as per Scintrex's instructions; see page 3-60 in the CG-5 manual.

Run SCTUTIL and setup for a USB download, as per Scintrex's instructions.

Make sure to produce a text (.TXT) file of the data, as this is the only file type that can be processed with the reduction software!

A.4 Installing the Reduction Software

A.4.1 Installing the Python Software

From the CD, install *Python-2.5.4.msi* first. Then, install *numpy-1.3.0-win32-superpack-python2.5.exe*. Finally, install *scipy-0.7.0-win32-superpack-python2.5.exe*. All installers can be run from the CD by double-clicking the icon.

These installers will setup a working Python 2.5.4 installation, with Tkinter (a GUI builder). Be sure to select all the options when installing the Python package (all options are on by default). The *numpy* and *scipy* packages should be installed using the Python 2.5.4 installation you installed first.

Python versions other than 2.5.4 can be used if you acquire new versions of the *numpy* and *scipy* packages; as of April 2009, pre-built binary packages are only available for Python 2.5.

Installation of Python, *numpy*, and *scipy* should only take a few minutes total, and does not require a reboot.

A.4.2 Installing Micrograv

Extract the ZIP archive of the programs into a directory. Or, copy the *micrograv* folder from the CD to the hard disk.

A.5 Preparing to Reduce Gravity Data

Create a folder for the entire project if it doesn't exist. This folder should have a useful name, such as *WeberRiverASR*. Inside this folder (directory) will eventually be many other folders, one for each campaign. This allows for easy copying of all data and results, but reduces the chance of accidently overwriting data and results.

After downloading the data from the CG-5, create a new directory (folder) for this campaign within the project folder. Preferably, name the folder after the date(s) of the campaign, such as *2009-03* for a campaign in March 2009. All the following files will be placed in the campaign or project folders, to allow for results to be kept from all campaigns at once, without overwriting each other.

Copy the downloaded data, in text format, to the campaign folder. This makes a backup of the data file and makes it easier to import the file into the reduction software. The reduction software defaults to choosing data files with a `.dat` extension, so this extension is recommended for the text data files.

A.5.1 Preparing a "Name" File

Create a text file, using Notepad, Wordpad, or similar, that has the station number and station name, one per line. An example:

```
1 WBB115
2 WRP12
3 WRP17
4 WRP18
...
```

Save this file in the campaign folder. Call it something recognizable, such as "names".

A.5.2 Preparing a "Coordinates" File

To process the gravity data, we need to have accurate coordinates for each station. Thus, at least once for each project we need to build a file with station names, latitudes, longitudes, and elevations. The file also includes a field for elevation changes, if they are known. In general, the elevation change field will be left at 0.

Using a text editor (Wordpad using *Save as text*, Notepad, emacs, etc.), create a file with station name, latitude in decimal degrees (north positive), longitude in decimal degrees (east positive), elevation in meters, and elevation change in centimeters. An example:

```
# Coordinates from GPS and map interpolation
WKRP         41.141159  -111.808245 1459.990 0.0
WRP01 41.135807 -111.921265 1400 0.0
WRP02        41.132546  -111.921041 1362.037 0.0
WRP03 41.135875 -111.937339 1400 0.0
WRP04 41.135290 -111.923927 1400 0.0
WRP05        41.138707  -111.913560 1363.735 0.0
WRP06        41.144369  -111.927628 1360.311 0.0
WRP07        41.142176  -111.933948 1355.781 0.0
WRP08        41.130724  -111.912758 1343.950 0.0
WRP09        41.128914  -111.923269 1362.535 0.0
WRP10        41.135192  -111.929902 1354.874 0.0
```

```
WRP11        41.132578  -111.926417 1360.375 0.0
WRP12        41.132591  -111.928806 1359.063 0.0
```

Lines that start with # are ignored as comments. Fields must be separated by a space, but can be separated by many spaces or tabs. There must be all 5 fields on each line, in the order given above: name, lat, lon, elevation, elevation change. Do not add units or direction letters (e.g. N or E) to the fields.

Note that west longitudes are represented by negative longitudes, and southern latitudes are indicated by negative latitudes.

Give latitude and longitude coordinates to 6 decimal places if possible, and elevations to 3 decimal places (mm). Elevation changes, which are in cm, will rarely be known to better than 1 decimal place (mm).

This file should contain all stations ever used in a project, so it can be built once for a project and then used for each campaign.

Save this file into the **project** folder, not the campaign folders. The reduction software looks for a `.coord` extension on coordinate files by default, so it's easiest to use `.coord` as the extension on your coordinate files.

A.5.3 Preparing a "Skip" File

If there are stations or single occupations that should be skipped, due to bad or irrelevant data, place them in a text file in the campaign folder. Call the file something recognizable, such as *skips*.

The file can hold either a station ID or station name on each line. If a station name, **all** occupations of the station name will be skipped in processing. If a station ID, only that single occupation will be skipped.

An example:

```
64.
36.
WBB101A
```

This file will be used to instruct the reduction package to skip station IDs 64., 36., and all the occupations of station WBB101A regardless of ID.

Save this file in the campaign folder.

A.5.4 Making a Parameter File

Once the campaign folder has the name file, the project folder has a coordinate file, and the campaign folder has a skip file (if necessary), we are ready to make the **parameter file** which will hold all the information needed for the reduction program.

Two utilities are provided by the Micrograv package to make the parameter file from the 3 files noted above: *make_parm_file.py* (command-line) and *makeparameters.py* (graphical file choosers). *make_parm_file.py* is run from a command-line (*cmd* on a Windows PC, *Terminal* on a Mac); e.g. `make_parm_file.py names coordinates skips stations.par`.

makeparameters.py is more friendly, as it allows for choosing each of the files from dialog boxes. The order, as noted in the dialog box titles, is ID-name file, coordinate file, skip file (cancel if no skip file), and output file. The resulting parameter file is written to the output filename; name the parameter file with a `.par` extension, which is the default in the reduction software. After an info window noting success, the program dies. The program will fail if there are stations in the ID-name file without coordinates in the coordinate file.

Save the parameter file in the campaign folder; use an extension of `.par` as the reduction software expects this extension by default.

A.6 Reducing Precision Gravity Data

With the parameter file and raw data files, we are ready to reduce the data to single gravity values at each station. The program that will do all the heavy lifting is called *reduce.py*, and it can be run in two different modes: interactive with windows, or as a batch process that uses only files. Interactive mode is useful for the first reduction run of a campaign, as it allows immediate feedback and interactive setting of options. Batch mode is most useful for automated processing of results or re-running a reduction with the same parameters as before. Batch mode processing will not be discussed here; see section A.8 for some notes on batch processing of gravity data.

- Run *reduce.py* (**in the campaign folder if possible**) and wait for the first dialog box to appear. Multiple windows appear when running the reduction; there is a status window which will have all the messages from the program about what it is doing, and any problems that are encountered. This information will also be written to a **log file** in the current directory, called *reduce.log*. If there are problems reducing data, start by reading through the text log file to see where the problem occurred.

- Unless the campaign was collected with a meter different than a CG-5, accept the default meter type of CG-5. *reduce.py* can also process data obtained with CG-3(M) meters and Aliod-equipped LaCoste & Romberg gravimeters; notes for using those meter types are included in chapter 2.

- Select the gravimeter data file, which is the text file obtained from SCTUTIL.

- Select the parameter file you created from the name file, coordinate file, and optional skip file.

- Check the Station Parameters window to make sure the station names, coordinates, and repeat occupations are correct according to the field notes, etc. The parameter window should look something like:

```
  ID  |    STATION NAME    |REPEAT|  LATITUDE  | LONGITUDE  | ELEVATION|  dZ
     2|WBB101A             |     8|  40.7651770|-111.8495850|  1436.300|  0.0
......|....................|     9|............|............|..........|
     3|LC11                |     5|  40.5975500|-111.8021860|  1477.104|  0.0
......|....................|     7|............|............|..........|
     4|LC12                |     6|  40.6024590|-111.8042980|  1475.164|  0.0
     5|LC11                | None |  40.5975500|-111.8021860|  1477.104|  0.0
     6|LC12                | None |  40.6024590|-111.8042980|  1475.164|  0.0
```

```
7|LC11                   | None |  40.5975500|-111.8021860|   1477.104|  0.0
8|WBB101A                | None |  40.7651770|-111.8495850|   1436.300|  0.0
9|WBB101A                | None |  40.7651770|-111.8495850|   1436.300|  0.0
```

ID are the station IDs read from the parameter file that must match the station IDs in the data file. STATION NAME is taken from the parameter file, and should be checked against the field notes. REPEAT shows the station ID of the next repeat occupation of the station, if any. Note that stations with multiple repeats will have extra lines, one per additional repeat, with dots for all fields but the repeat. Check the station repeat list against the field notes, to help catch transcription errors. Also note that repeated occupations of a station are listed, but they do not have repeats listed, as the processing compares all repeats to the first occupation, not to the previous. LATITUDE and LONGITUDE are the supplied lat/lon coordinates, in decimal degrees. ELEVATION should be in meters above sea level, in a common datum for all stations; typically use WGS84 for easy import and comparison to GPS data. dZ is an elevation change of this station occupation; it is unique to each occupation to allow for elevation corrections when station occupations are on unstable ground, and different occupations could have slight elevation changes between them.

- When asked for the tare database file, select the previous output file to re-read tares entered from a previous reduction run. Otherwise, cancel the dialog, which will result in no tares being initially applied. The tare database file is almost always ignored.
- Select the reduction options; the defaults are typically correct unless there is a problem with the data or the data came from a meter other than a CG-5. For the first run for each campaign, the defaults are almost certainly correct; after inspecting the reduction log and results, re-run with different options if necessary. All the reduction options are detailed below, including when changes might be necessary. There is almost never a reason to turn off

the non-linear instrument drift corrections, as residual instrument drift is the dominant noise source in gravity campaigns.

- Choose an appropriate reference type in the reduction options. The reference value will be entered in the `Reference gravity/station ID` box below the reference type options.

  For exploration surveys, choose the `fixed value` option and enter the difference between known absolute gravity at some station (e.g. 978032.674 mGal) and the measured gravity at the same station (e.g. 3827.654 mGal). The difference (-974205.020 mGal in this example) will be negative, as the reference value is subtracted from the measured gravity. Use of a fixed value reference may take two reduction runs: a first run with a zero reference value to determine the meter value at the absolute station, and then a second run with the appropriate difference.

  For repeat gravity projects, choose the `station ID` option, and enter a station ID in the box below. Choose some station as the reference for reduction of all campaigns. The choice of station is not critical, as any station will remove most of the meter drift between surveys, and further corrections to hold some station or set of stations stable will be applied to the reduced data during interpretation. The average of the entered station ID and all its repeats will be used as the reference gravity value.

  The reference gravity value will be put in the output file, as a comment, for future reference.

- If performing instrument drift corrections, the program will present 4 windows with plots. These are critical plots, and they should always be studied in detail to determine the quality of a campaign and the functioning of the instrument. See the next section (A.6.1) for details of interpreting the plots and assessing the campaign quality.

It is generally best to save the plots using the `Save` button in the instruction window. The plots are all written at once, to fixed filenames of *dg_none.ps*, *dg_drift.ps*, *drift.ps*, and *repeats.ps* for the pre-drift arrow plot, post-drift arrow plot, drift function plot, and station repeat plot, respectively. The plots are saved as color Postscript (level 2) files, which should be directly printable on most modern printers, or viewable in various software on the reduction computer; Adobe Illustrator, Ghostview, and GIMP are known to work on Windows, and Preview will work on an OS X computer.

- If desired, the mouse can be used in the `Figure 2` window to add tares to the data. This will introduce a static gravity offset at a specified time to all station occupations after that time. To enter a tare, press the `Tare Entry` button, and follow the instructions. Existing tares can be edited by pressing the `Tare Edit` button and using the newly opened window to change the settings of each existing tare. The tares entered here will be saved to the output file, if written, in a format suitable for reading into *reduce.py* for the next reduction run.

  Note: the staircase drift function will automatically handle a tare in the data set by introducing a large offset at the appropriate time. Thus, tare entry is almost never used except in uncommon cases where station repeats are lacking, but a tare is known to have occurred. In general, **do not** enter tares into the data.

- When done with the instrument drift plots and (highly optional) tare entry, press the `Done` button in the instruction window to continue with reduction.

- Wait for the reduction process to complete, and choose an output file. Select a filename in the **campaign** folder.

- Assuming *reduce.py* claims the output file was written, the reduced gravity data will be in the specified output file, in text format. This file will be the basis of further analysis for interpretation, gravity change computations, etc.

A.6.1 Instrument Drift Plots & Tare Entry

There are four plots made by the instrument drift computations: a plot of gravity station repeats before any drift correction, a plot after drift correction with the staircase function, a plot of the staircase and polynomial drift functions, and a plot of the stations, repeats, and their time spans. Each of the four plots has a particular purpose, and all should be inspected for each reduction.

A.6.1.1 Drift Function Plot

The window `Figure 1` is a plot of the staircase and polynomial drift functions vs. time in hours. An example, taken from real field data, is shown in Figure A.1. Functions are only computed at station occupations, and connected with straight lines, so non-linear polynomials may show aliasing effects in the plotting. The staircase function is plotted with a black line, with individual station occupations marked with a large black X. Polynomial functions of varying orders are shown as solid colored lines without points. Polynomial functions are shown for comparison, as the field data are corrected using the staircase function.

In general, there is no reason the instrument drift function should be smooth or continuous. However, most of the literature uses polynomial drift functions, so they are computed for comparison.

A.6.1.2 Pre-drift Arrow Plot

The window labelled `Figure 2` is the plot of gravity stations and their repeats before drift correction. Figure A.2 shows an example plot saved from the reduction program. The plot shows each station and its repeats as a connected set of points, starting at the time of the first station in the repeat string. Gravity values are differenced to the reading at the first station in the string. Thus, each connected string of points starts at 0 relative gravity, and then shows the changes in gravity for each repeated occupation, in μGal.

Note that the gravity differences do not have error bars for clarity. Inspection of the pre-drift arrow plot can show possible changes in instrument drift rates,

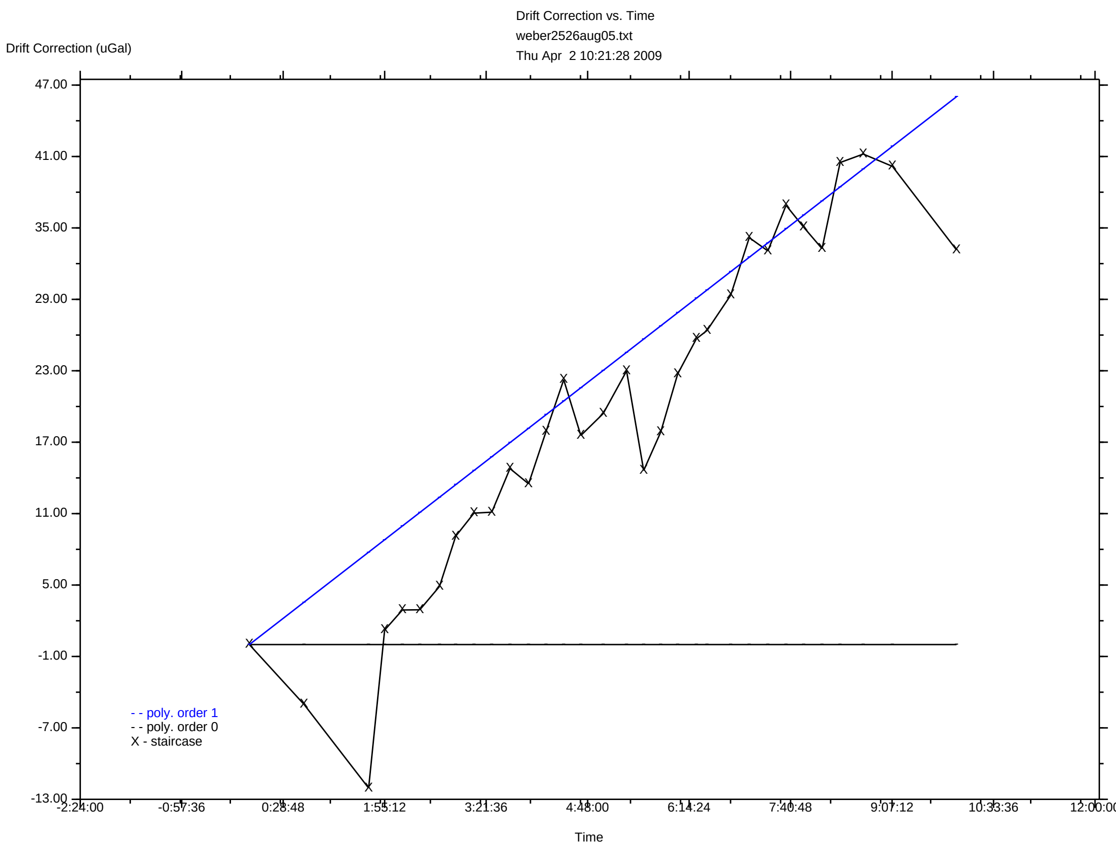

Figure A.1. Example drift function plot, with all functions shown as solid lines. Station occupations are shown as black Xs for the staircase drift function. Polynomial functions are shown without points. Drift functions are required to start at 0 at the first repeated station. Polynomials are shown for comparison, but corrections are only taken from the staircase function.

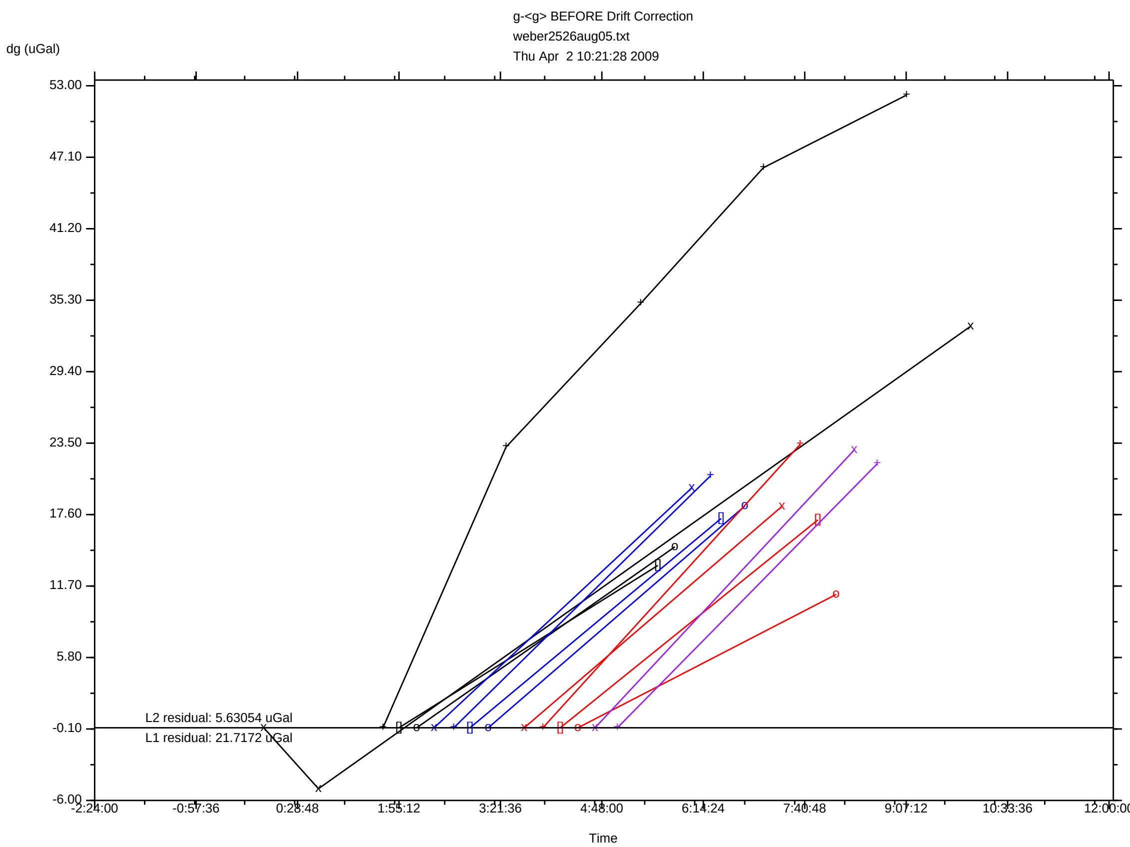

Figure A.2. Example pre-drift station repeat arrow plot, with stations and repeats shown as connected strings of stations; markers and line color differentiate the strings. L1 and L2 show the L1 and L2 norms of the repeats; smaller numbers indicate smaller overall drift. All station strings start at 0 relative gravity, as gravity values are referenced to the first station in a string. Times are in hours since the first station in the data. Gravity differences represent instrument drift, residual Earth tides, etc.

tares due to shocks, and significant Earth tide residuals. A good field day will have consistent slopes to all repeats. For CG-5 data, the instrument drift may be predominantly linear and possibly large; the drift rate of the instrument is dominantly linear, but the instrument's supplied drift rate may be incorrect for the current actual drift rate. Hence, field data may show linear drifts of 10s to 100s of μGal/day, either positive or negative. The example plot, in Figure A.2, shows a consistent linear drift of $\sim$120 μGal/day; this is due to an old drift constant in the meter, and does not indicate poor data.

Random or sudden shifts in drifts for similar time intervals generally indicates shocks to the meter due to handling or transport. Sudden or sporadic changes in the slopes of the arrows can also indicate electronic or sensor errors in an instrument. Thus, good field data has consistent or **slowly** varying, even if large, slopes for repeats. Note that slow variation in slopes likely indicates a residual Earth-tide-like signal in the data, which may be due to errors in the Earth tide positions or GMT offsets.

A.6.1.3 Post-drift Arrow Plot

The window `Figure 3` reproduces the pre-drift arrow plot (window `Figure 2`), but after the staircase drift function is removed. Figure A.3 shows an example using the same data as Figure A.2. Note that the arrows now all lie along the zero line, and the residuals are 10^{-13} μGal or less. The non-zero (but tiny) residuals are due to the weighted fit of the drift function. If this plot shows a non-zero residual of more than 1-2 μGal, one of the occupations is likely quite poor, and should be inspected carefully.

A.6.1.4 Station Repeat Plot

The window `Figure 4` plots stations and their repeats vs. time; Figure A.4 is an example plot for the same data as the other examples. This plot is similar to the arrow plots, but there is no gravity information shown. Instead, the plot shows a station, with the station ID, and then station IDs of the repeats as a connected

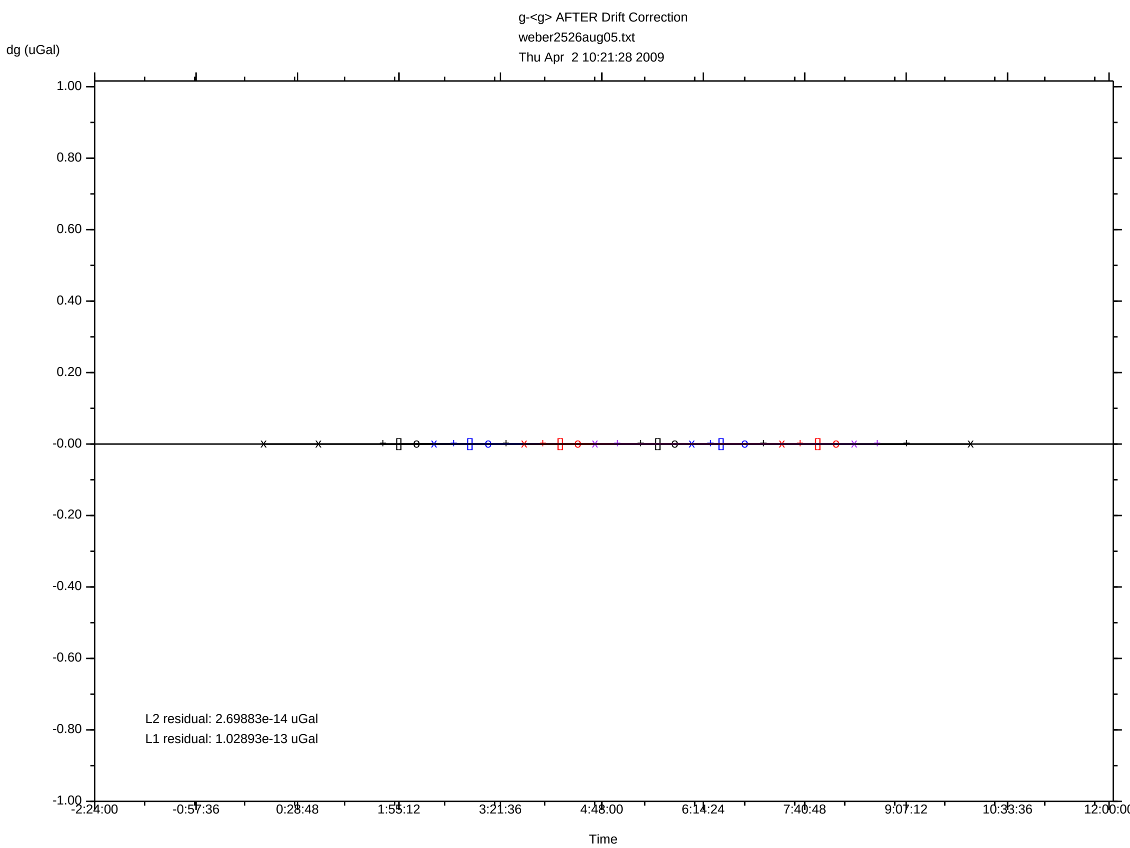

Figure A.3. Example post-drift station repeat arrow plot, with stations and repeats shown as connected strings of stations. All strings start at 0 relative gravity, as gravity values are referenced to the first station in a string. Times are in hours since the first station in the data. The drift correction is taken from the staircase drift function, which typically results in zero differences after correction. Note the residuals in the range of 10^{-14} μGal.

string of occupations. The repeat strings are offset vertically for clarity. The plot visually depicts the looping schedule of the data, and also allows easy identification of particular stations in the arrow or drift plots for further inspection. Note that the lines connecting stations accurately represents the time interval covered by the loop, and thus what portion of the drift function will be influenced by the loop.

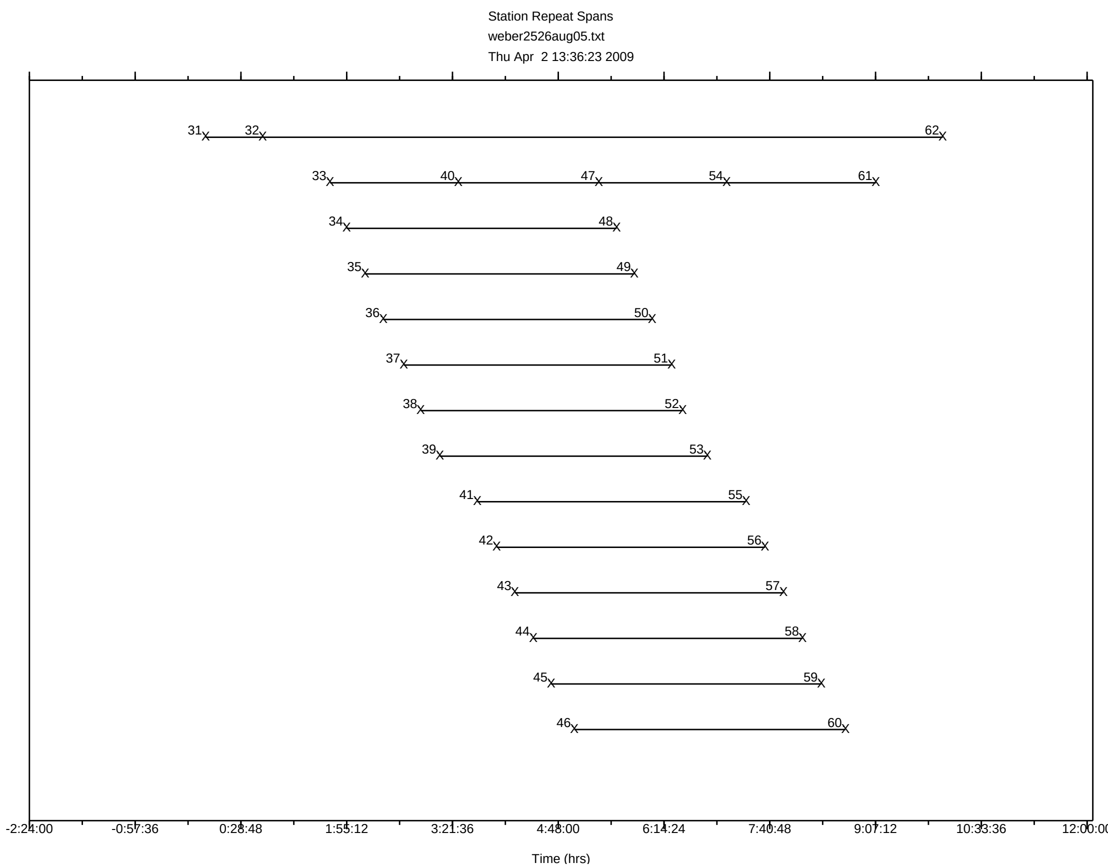

Figure A.4. Example station repeat plot, with stations and repeats shown as connected strings of stations. Station occupations are labelled with the station ID from the data file. Connected stations are repeats of the first station. Vertical offset is for clarity only. The station labels allow this plot to be used as a map between the arrow and drift plots and the station IDs in the data file for quality checking or data inspection.

A.6.2 Reduction Options

Here is a description of each of the processing options available in *reduce.py* with notes on choosing values.

- **DATA INPUT** options
  - **Meter Type** - Set interactively at the beginning of the program run, or in the command file with the token `meter_type`. This option determines what format the raw data are in, and thus how to import data for processing. The default is "CG-5," and should only be changed if data were collected with a CG-3/CG-3M or Aliod.
- **PLOT DATA TIME-SERIES** options
  - **Plot uncorrected raw data** - If true, a simple data plotting utility will be launched to allow plotting of raw time-series, broken apart by station ID. All the station data is available for plotting, including gravity, standard error, tilts, temperature, etc. The data viewer is reasonably friendly to use, but is designed for working plots and not publication-quality graphics. This option is normally not used except if there are suspected problems with a time-series. It is generally easier to use the stand-alone program *cg5view.py* to look at raw data series.
  - **Plot corrected time-series data** - If true, a simple plotting utility will be started after time-series corrections (Earth tide, etc.) but before time-series averaging/analysis. This allows plotting of the data series broken apart by station ID, but after the Earth tide and other time-series corrections. This option is not used, except in cases where a data series is considered suspect from inspection of a previous reduction run.
- **CORRECT RAW READINGS** options
  - **Remove meter-applied Earth Tide correction?** - If true, any Earth tide correction applied by a CG-5 or CG-3 meter will be removed from the data series before any other processing is done. This option defaults to true, and should be left true unless the Earth tide correction in the data file is correct for all stations (which is extremely rare) or the Earth

tide correction listed in the data file is not the correction that was applied (which has never yet happened).

– **Remove meter-applied linear drift?** - If true, a linear drift term subtracted by the meter will be restored to the raw data before time-series analysis. This option defaults to false, and is only used to check the overall drift rate of the instrument. If the meter-applied linear drift term is removed, the non-linear instrument drift corrections will incorporate the (large) linear drift, and will likely grow to very large values. Also note that removing the linear drift may cause station time-series to show linear trends in quality assurance, so be careful with the QA options, below.

– **Apply Tamura ETC w/parameter file lat/lon?** - If true (default), the Earth tide correction from *Tamura* [1987] using the latitude, longitude, and elevation from the parameter file will be applied to each reading before time-series analysis. **Do not set to true unless the meter-applied ETC is removed!**

– **Correct to fixed atmospheric pressure?** - If true, the code will ask for a file of atmospheric pressure vs. time and will interpolate a gravity correction for changing atmospheric pressure, relative to the supplied base pressure. This correction is so small, it is ignored unless some campaigns are being performed in the middle of hurricanes or typhoons.

– **Base Atmospheric Pressure (mbar)** - The reference pressure, if correcting for atmospheric pressure changes. Given in units of millibar.

– **Force ALL(!) GMT offsets to: (hrs E of GMT)** - If blank (default), the GMT offset encoded in the data file header will be used for computing the Earth tide corrections. If a number is entered here, **all** readings will use the entered value. Note that for areas west of GMT, the offset is negative. This may be a floating point number, if that will help remove residual Earth tide signals.

- **Correct for meter tilt (Aliod ONLY)?** - If true, convert the Aliod tilt measurements into a gravity correction. Aliod measurements are not automatically corrected for instrument tilt, which this corrects. If using a CG-5 or CG-3, **do not turn this option on!** The default is false, where it should stay.

- **STATION OCCUPATION CORRECTIONS** options

  - **Correct for elevation change listed in parameter file?** If true, convert the `dZ` entries in the parameter file to gravity corrections using the global vertical gradient of -3.086 μGal/cm. As most parameter files leave the `dZ` column at 0, this option defaults to off. In some cases, the local vertical gradient is significantly different from the global, in which case the corrections should be done after processing.
  - **Non-linear instrument drift corrections?** - If true (default), compute a non-linear instrument drift function from repeated station occupations, and remove from the occupation gravity values. This option should be left on.
  - **Use weighted fit for drift functions?** - If true (default), both staircase and polynomial drift functions will be found by a weighted inversion, using the occupation standard errors for the weights. This option should be turned off only if a particular occupation has a large standard error, but is somehow actually quite good anyway.
  - **Minimum order for polynomial drift functions** - Enter a number here that is the minimum order for the comparison polynomial drift functions. The default value is 0, which results in a zero line on the drift plot.
  - **Maximum order for polynomial drift functions** - Enter a number here that is the maximum order for the comparison polynomial drift functions. Typical maximums are 3-7 for a single day campaign.

- **TIME-SERIES PROCESSING** options
  - **Use Thiele extrapolation instead of weighted averages?** - If true, gravity time-series readings will be converted to an occupation gravity value using a rational function extrapolation; see section 2.5.3.6 for the math behind the extrapolation.

    The default is off, which is correct for CG-5 and CG-3 meters. Turn on for Aliod data.
  - **Time-series data are samples, not averages?** - If true, raw data series are sets of individual samples, not sets of averages and standard deviations. The default is false, which is correct for CG-5 and CG-3 data. Set to true for Aliod data.
  - **Sample decimation filter radius, in data points** - This number, default of 30, is the half-width of the window to use in despiking and decimating sample time-series before applying Thiele extrapolation. This setting only matters if analyzing sample time-series with Thiele extrapolation. In that case, the default window size is considered a good trade between despiking ability and computation time. Alter only after understanding the math behind the filtering; see section 2.5.3.4 and following.
  - **Thiele extrapolation equality tolerance** - This setting has no meaning unless using Thiele extrapolation for time-series analysis. In that case, leave the tolerance at $1x10^{-7}$ unless you understand the math behind the Thiele extrapolation; see section 2.5.3.4 and following.
  - **Skip how many minutes at beginning of time-series when using weighted averages?** - This setting determines how many minutes of data, counted from the reading times, are tossed from the beginning of an occupation to remove transient effects of transport and handling. For CG-3 and CG-5 meters, the default of 3 minutes is fine. Increase the value for meters with long-lived transport effects, but longer times will

increase the standard error in occupation gravity values due to decreased readings in the averages. Decrease from the default for meters with extremely short transport relaxation times or projects with no transport noise (perhaps vertical gradient measurements).

  - **Maximum # of readings for weighted averages? (-1 to use all)** - If set to a positive number, n, no more than n readings will be used in a weighted average, after removing readings prior to the skip-time set above. The default is -1, and it should rarely be changed. This setting applies to all stations, so remove problematic readings for a particular station by editing the data file.

- **TIME-SERIES QUALITY ASSURANCE** options

  - **Correct tmperatures outside threshhold to running average?** - If true, temperature readings in each time-series that are outside a threshhold (see next option) will be replaced with a running window average of in-threshhold data points. The gravity reading will be updated using the new temperature correction and the data file temperature coefficient. This setting should only be used when data has been taken from a CG-3 or CG-5 meter with a malfunctioning temperature readout circuit which mostly works, but occasionally records incorrect temperatures. This option will almost always be left off, the default.
  - **Temperature correction threshhold for correction (mK)** - Enter the threshhold for correction. The absolute value of the temperatures is used for threshhold comparisons, so readings with temperatures outside + or -threshhold will be corrected. This option has no effect unless the previous setting is true.
  - **Remove raw data with temperatures outside threshhold?** - If true, time-series readings with temperature values outside a threshhold will be dropped from the time-series. This may result in the complete removal of a station! The default is false, as the temperature readout

circuits typically work. This option is a more harsh, but preferred, version of the temperature correction option. If possible, remove data rather than correct it, but some data sets may not be able to survive temperature removal without unacceptable loss of stations. In those cases, use the previous correction option instead of this one.

– **Temperature threshhold for removal (mK)** - Set this box to the threshhold, in mK, to remove data from the time-series. Note that both the correction and removal options can be true, and each has its own threshhold. Temperature correction is done after removal, which allows the use of the two options together. This option does not have any effect unless the previous option is true.

– **Reading s.d. warning threshhold (mGal)** - Time-series readings with standard deviations larger than this number will be flagged in the Quality Assurance portion of the reduction for checking. The default (0.050) is typically acceptable for most field data. Set the value larger for noisy campaigns, if the level of warning messages is distracting. This option only controls when warnings are printed for readings; it does not alter the time-series data in any way.

– **Occupation time-series detrend threshhold (uGal/hr)** - This option controls when an occupation time-series will be detrended using a linear fit to all but the first *skip time* minutes of data (see *Skip how many minutes at the beginning...* above for setting this time). Time-series with slopes larger than this value will be pivoted about the data point after *skip time* minutes to bring them to zero slope. This effectively removes trends due to varying tilt without introducing error from transport effects. The default (97.2) has been empirically chosen by inspecting a large number of CG-3 field stations with and without visually-apparent trends. Typical field data is suitably handled with the default slope; set this number to >90 000 if using Aliod data! Otherwise, modify only if time-series inspection warrants it.

- **REFERENCE GRAVITY** options
  - **Reference station gravity values to**...
    - **fixed value** - If true, all stations will have a fixed value subtracted from the drift-corrected gravity value.
    - **station ID** - If true, the designated station and its repeats will be averaged to compute a reference gravity value, which will be subtracted from all stations. This is the default option, as repeat gravity surveys will need some station assumed fixed.
    - **abs. gravity station** - If true, the designated station and its repeats will be averaged to compute a gravity value which will then be differenced from the absolute gravity value entered. This difference will be subtracted from all stations, which will bring them all to absolute gravity readings based on the absolute gravity value for the chosen station ID.
  - **Reference gravity** - Enter the gravity value to subtract for a fixed value reference, or the absolute gravity value for the selected ID for an absolute gravity station reference in this box. Note that gravity values can be positive or negative, and are in mGal.
  - **Reference station ID** - Enter the station ID of the reference station for station and absolute gravity station reference options. Station IDs are strings, and must match the station ID of an occupation, not a station name! If the station ID cannot be found, the reference gravity will be set to 0!

A.6.3 Checking Reduced Data

A.6.3.1 Quality Check of Reduced Data

Reduced data should always be inspected using the instrument drift plots and reduction log file. Pay attention to the linear detrending in time-series quality assurance; detrended occupations are more suspect. Also, if computing instrument drift, compare the linear daily rates for stations and repeats. The rates will fluctuate even on good days, due to the extrapolation of short intervals to 24 hr periods. However, pairs with drift rates that are differing signs or more than 30 times different than all the other pairs are suspect.

The most useful plots for checking the reduction results is the pre-drift arrow plot. For a typical field day, this plot should show station pairs following one of 2 patterns: (1) small random drift at the 10-20 μGal level, or (2) predominantly linear drift over the entire day (parallel pairs) with random shifts at the 10-20 μGal level. Station pairs with radically different arrows than the others are suspect.

Before worrying about data, check the scale of the arrow plot; the plot is scaled to the maximum data range, and thus changes each time. Drifts less than 10 μGal are approaching instrument noise (2-5 μGal precision in each station) and should be ignored.

Drifts of milligals (1000s of μGal) generally indicate a naming problem; if the name-ID map file is incorrect, the constructed parameter file (with the repeat information) will claim that two different stations are repeats of one. This will cause an apparent drift of milligals. Hence, if such a giant drift is seen, use the *Station Repeat Span* plot to find the station IDs, and check the field notes to see if the repeats are correct. In one case, this check has led to noting that the field book was wrong! After finding what stations should be repeats, fix the name-ID map file and regenerate the parameter file, then re-run the reduction from scratch.

Other station pairs that are suspect need to be inspected individually. Use the program *cg5view.py*, included in the reduction package, to look at time-series data for each station. The program breaks apart the input data file by station ID, and then plots the various values (gravity, tilt, temp, meter ETC) for each station ID. Use the control window to find the stations under question, and compare the time series. Any current plot can be saved to a Postscript file using the `Save` button, if desired. Typically, it is best to run multiple copies of *cg5view.py*, so each one can be plotting a different station in the repeats.

Inspection of the raw time-series may help explain why a station pair shows a large drift. In some cases, station IDs were not changed between measurements, so one station ID has multiple occupations. In other cases, particular occupations are noticeably worse than others due to external factors such as traffic or weather.

In the case that multiple stations have been recorded to one station ID, the only fix is to edit the raw data file and change the station IDs. This should be done with a text editor (e.g. Notepad), not Excel or Word. Note that the reduction code doesn't care about order of station IDs when processing, so choose an unused number for the new station ID. In the field, when recording station IDs, always opt to skip IDs if there is a question as holes are even easier to ignore.

A.6.3.2 Troubleshooting Problematic Data

Name-ID map errors are fixed in the name-ID map, which is then used to regenerate the parameter file. Then restart the data reduction with the new parameter file.

Station occupations that have been combined into a single ID (by forgetting to increment the station ID before reading) can be fixed by changing the ID of one of the stations in the data file. Be very careful to maintain the format of the data file when editing. It is also best to save an untouched copy of the data before editing. Document the changes to the data file in your own notes.

Stations with poor-quality data can be dropped by adding their station ID to the `[SKIPS]` section of the parameter file and re-running the reduction. Repeat info, etc. will all be automatically updated after removing the skipped station in the reduction run. This is only really viable if there is a good occupation of the station, and a different occupation is clearly problematic (erratic gravity values, etc.). Always choose the best station time-series to keep, even if the kept station is the repeat of the first occupation.

If more than 10% of stations in the data file have problems due to intermittently faulty measurements, it is unlikely to be possible to simply skip stations and not lose all occupations of some stations or cripple the drift computations with few repeats. In this case, try fixing the data using the temperature correction/removal option (for faulty temperature readings) or the linear detrending (for faulty tilt measurements). Note that if the gravity readings are possibly faulty, skip the station(s) and redo the campaign if necessary.

Due to time constraints, it is not uncommon to have field data with no start or ending measurement at the gravimeter storage site. In this case, the data can be added to the data file by copying the lines from the bracketing long-term drift files. Ideally, the drift files should run right up to meter's transport to the field, and then start immediately upon return to storage. Add the data points and make sure they have unique station IDs, add the IDs to the name-ID map file, add the position of the storage location to the coordinate file, and regenerate the parameter file. Then re-run the reduction with the added data and check the drift based on the long-term data that brackets the field campaign. Note that enough data must be added to allow for losing at least one measurement at the beginning (due to the *skip time* option) and still produce a time-series; generally adding at least 10 measurements is best.

A.7 Reduced Gravity Data Output Format

Reduced data is output in an ASCII format, suitable for direct processing or import into Excel, etc. The format is fixed width, with spaces between fields. Comments start the line with "`#`"; they are for reference and generally not necessary for interpretation.

At the top of the file is a block of comments with the various settings of the reduction run. There is also a timestamp, to help determine if the output file is up-to-date.

Each station has a single line, with the following fields:

- Station name
- Station ID
- Final gravity (mGal)

- Gravity uncertainty (mGal) [2 standard errors]
- Date (year/month/day)
- Time (hours:minutes:seconds)
- Longitude (dec. degrees, E positive)
- Latitude (dec. degrees, N positive)
- Elevation (m)
- Δz (cm)
- Δz correction (mGal)
- Drift correction (mGal)
- Uncorrected gravity (mGal) [gravity after time-series corrections, QA, and analysis; no drift or elevation corrections]
- Unc. gravity uncertainty (mGal) [2 standard errors, from time-series analysis]

Due to the size of the fields, lines are 151 characters long.

A.8 Batch Processing of Gravity Data

reduce.py can be run interactively (the default), or as an automated batch process. In batch mode, the program gets input from a command file, which sets the processing parameters and data sources. The results are written to disk, as with interactive mode. The benefit is that a reduction run may be reproduced exactly using the command file prepared by *reduce.py* when it completes a run.

At the end of a reduction run, after writing output data to disk, *reduce.py* will write a command file in the current directory named `reduce.cmd`. This file contains all the settings and options that were chosen by the operator for the previous reduction run. Thus, the file can be used to reproduce the last reduction run without operator intervention.

Batch mode precludes the use of a mouse for interactive tare input, and will not allow for plotting of data. Batch mode will, by default, prepare Postscript versions of the drift and repeat plots in the current directory, just as if the `SAVE` button was pressed in the drift plot command window.

To run *reduce.py* in batch mode, use the command-line argument `-F` *command_file*, where *command_file* is a filename for the appropriate command file. To replicate the last run, from the same directory, use:

```
reduce.py -F reduce.cmd
```

A log file, `reduce.log`, will be created in the current directory, just as with interactive use. The command file `reduce.cmd` will be overwritten by *reduce.py*.

A.8.1 Command File Format

Command files are lines of key, value pairs. All entries are in plain text. Strings need not be quoted. All options have a default value, which may not be valid for a complete run (e.g. raw data file). The various options, with their meanings, are as follows:

- atm_file - Name of the atmospheric pressure file, if correcting to a base pressure. Can be `NONE` if not correcting to a base pressure.
- atmosphere - If `yes` or 1, correct for atmospheric pressure change.
- base_pressure - Base pressure value for corrections, in mBar.
- batch_drift_plot - If `yes` or 1, save a copy of drift and repeat plots in the current directory.
- detrend - List of station IDs to detrend; generally automatically generated. Separate IDs with commas.
- drift - If 1 or `yes`, remove the instrument-applied drift function.
- dz - If 1 or `yes`, compute a gravity correction from the elevation change column of the parameter file and the global free-air gradient of -0.3086 mGal/m.

- gmt_offset - If set to something other than "None", override the GMT offset of a data file with this value. All stations will have the GMT offset overridden!
- grav_samples - If `yes` or 1, raw data are samples, not averages.
- instrument_drift - If `yes` or 1, compute a non-linear staircase drift function from station repeat info.
- longman - If `yes` or 1, remove a meter-applied Longman ETC, if present.
- max_recs - Use no more than this number of records in processing average time series. If -1, use all records.
- meter_file - Filename of meter information file for Aliod data processing.
- meter_type - Type of raw data. Should be one of `CG-5`, `CG-3`, or `ALIOD`. Case doesn't matter.
- order - Maximum order to use for comparison polynomial drift functions.
- out_name - Output filename for processed gravity data. May have a full path.
- parm_file - Filename for parameter file. May have a full path.
- processed_view - If `yes` or 1, view corrected time-series. Requires a display for plotting.
- raw_file - Filename of raw data. May have a full path.
- raw_view - If `yes` or 1, view uncorrected time-series. Requires a display for plotting.
- ref_type - Type of gravity reference; 1 is fixed value, 2 is station ID, 3 is absolute station (set ID and value).
- ref_id - Station ID for reference, string - must match data file station ID.
- ref_val - Gravity reference value, in mGal

- sigma_threshhold - Threshhold for warning messages of reading s.d. in time-series quality checking.
- skip - Number of minutes to skip at the beginning of a station occupation when using weighted averages to analyze time-series.
- slope_threshhold - Threshhold, in mGal/day, for linear detrending in time-series quality checking.
- start_order - Starting polynomial order for comparison drift functions.
- tamura - If `yes` or 1, apply a Tamura ETC to the data.
- tare_file - Filename for tare information. May have a full path.
- temp_correct - If `yes` or 1, correct readings with temperatures outside the threshhold to a moving average of accepted temperatures.
- temp_correct_debug - If `yes` or 1, provide a printout of temperature corrections in the output file.
- temp_remove - If `yes` or 1, remove readings with temperatures outside a threshhold.
- temp_threshhold - Threshhold for temperature correction.
- temp_threshhold_drop - Threshhold for temperature filtering.
- thiele - If `yes` or 1, apply Thiele extrapolation to time-series, rather than weighted averages.
- thiele_filt_radius - Radius, in data points, for filtering time-series for spikes and decimation when using Thiele extrapolation.
- thiele_tolerance - Equality tolerance for Thiele extrapolation.
- tilt - If `yes` or 1, correct tilt errors using `xe` and `ye` entries. Does not currently work.

- tilt_corr - If `yes` or 1, correct for tilt using constants in the meter file. Useful only for Aliod data!
- weighted_drift - If 1 or `yes`, use weighted fits in drift function inversions.
- xe - Error in X tilt sensor; not currently used.
- ye - Error in Y tilt sensor; not currently used.

REFERENCES

Allis, R., and T. Hunt (1986), Analysis of exploitation-induced gravity changes at the Wairakei Geothermal Field, *Geophysics*, *51*(8), 1647–1660.

Allis, R., P. Gettings, W. Isherwood, and D. Chapman (2001), Precision gravity changes at the Geysers geothermal reservoir, 1977–2000, in *Proceedings, Twenty-Sixth Workshop on Geothermal Reservoir Engineering, Stanford University, January 29-31, 2001.*

Amante, C., and B. W. Eakins (2009), ETOPO1 1 arc-minute global relief model: Procedures, data sources and analysis, *Technical Memorandum NESDIS NGDC-24*, NOAA.

Andres, R. S., and J. R. Pederson (1993), Monitoring the Bulalo geothermal reservoir, Phillipines, using precision gravity data, *Geothermics*, *22*(5/6), 395–402.

Arnet, F., H.-G. Kahle, E. Klingele, R. B. Smith, C. M. Merteens, and D. Dzuirsin (1997), Temporal gravity and height changes of the Yellowstone caldera, 1977-1994, *Geophysical Research Letters*, *24*(22), 2741–2744.

Asgharzadeh, M. F., R. R. B. von Frese, H. R. Kim, T. E. Leftwich, and J. W. Kim (2007), Spherical prism gravity effects by Gauss-Legendre quadrature integration, *Geophysical Journal International*, *169*, 1–11, doi:doi: 10.1111/j.1365-246X.2007.03214.

Ballu, V., M. Diament, P. Briole, and J.-C. Ruegg (2003), 1985-1999 gravity field variations across the Asal Rift; insights on vertical movements and mass transfer, *Earth and Planetary Science Letters*, *208*(1-2 (15 Mar)), 41–49.

Battaglia, M., C. Roberts, and P. Segall (1999), Magma intrusion beneath Long Valley caldera confirmed by temporal changes in gravity, *Science*, *285*, 2119–2122.

Budetta, G., and D. Carbone (1997), Potential application of the Scintrex CG-3M gravimeter for monitoring volcanic activity: results of field trials on Mt. Etna, Sicily, *Journal of Volcanology and Geothermal Research*, *76*(3-4), 199–214.

Butler, D. K. (1984), Interval gravity-gradient determination concepts, *Geophysics*, *49*(6), 828–832.

Chang, W.-L., R. B. Smith, C. Wicks, J. M. Farrell, and C. M. Puskas (2007), Accelerated uplift and magmatic intrusion of the Yellowstone Caldera, 2004 to 2006, *Science*, *318*, 952–956.

Chapman, D. S., E. Sahm, and P. Gettings (2008), Monitoring aquifer recharge using repeated high-precision gravity measurements: A pilot study in South Weber, Utah, *Geophysics*, *73*(6), WA83–WA93.

Cordell, L. (1992), A scattered equivalent-source method for interpolation and gridding of potential-field data in three dimensions, *Geophysics*, *57*(4), 629–636.

Dragert, H., A. Lambert, and J. Liard (1981), Repeated precise gravity measurements on Vancouver Island, British Columbia, *Journal of Geophysical Research*, *86*(B7), 6097–6106.

Farr, T. G., et al. (2007), The Shuttle radar topography mission, *Reviews of Geophysics*, *45*, 33 pages, doi:doi:10.1029/2005RG000183.

Ferguson, J. F., T. Chen, J. Brady, C. L. V. Aiken, and J. Seibert (2007), The 4D microgravity method for waterflood surveillance II – Gravity measurements for the Prudhoe Bay reservoir, Alaska, *Geophysics*, *72*(2), I33–I43.

Furuya, M., S. Okubo, W. Sun, Y. Tanaka, J. Oikawa, and H. Watanabe (2003), Spatiotemporal gravity changes at Miyakejima Volcano, Japan: Caldera collapse, explosive eruptions and magma movement, *J. Geoph. Res.*, *108*(B4), doi:10.1029/2002JB001,989.

Gesch, D. B. (2007), *Digital Elevation Model Technologies and Applications: The DEM Users Manual, 2nd Edition*, chap. The National Elevation Dataset, pp. 99–118, American Society for Photogrammetry and Remote Sensing, Bethesda, Maryland.

Gettings, P., R. N. Harris, R. G. Allis, and D. S. Chapman (2002), Gravity signals at The Geysers geothermal system, in *Proceedings: Twenty-Seventh Workshop on Geothermal Reservoir Engineering, Stanford University*.

Gettings, P., D. S. Chapman, and R. Allis (2008), Techniques, analysis, and noise in a Salt Lake Valley 4D gravity experiment, *Geophysics*, *73*(6), WA71–WA82.

Goodkind, J. M. (1986), Continous measurement of nontidal variations of gravity, *Journal of Geophysical Research*, *91*(B9), 9125–9134.

Grant, F. S., and G. F. West (1965), *Interpretation Theory in Applied Geophysics*, McGraw-Hill Book Company.

Hammer, S. (1939), Terrain corrections for gravimeter stations, *Geophysics*, *4*(3), 184–194.

Hardy, R. L. (1971), Multiquadric equations of topography and other irregular surfaces, *Journal of Geophysical Research*, *76*(8), 1905–1915.

Hastings, D. A., et al. (1999), The global land one-kilometer base elevation (GLOBE) digital elevation model, version 1.0, *Tech. rep.*, National Oceanic and Atmospheric Administration, National Geophysical Data Center, 325 Broadway, Boulder, Colorado 80305-3328, U.S.A., digital data base on the World Wide Web (URL: http://www.ngdc.noaa.gov/mgg/topo/globe.html).

Hayford, J. F., and W. Bowie (1912), The effect of topography and isostatic compensation upon the intensity of gravity, *Special Publication 10*, U.S. Coast and Geodetic Survey.

Hinze, W. J., et al. (2005), New standards for reducing gravity data: The North American gravity database, *Geophysics*, *70*(4), J25–J32.

Hunt, T. M., and W. M. Kissling (1994), Determination of reservoir properties at Wairakei Geothermal Field using gravity change measurements, *Journal of Volcanology and Geothermal Research*, *63*, 129–143.

Isherwood, W. (1977), Geothermal reservoir interpretation from change in gravity, in *Proceedings: Third Workshop, Geothermal Reservoir Engineering, Stanford University.*

Jachens, R., D. Spydell, G. Pitts, D. Dzurisin, and C. Roberts (1981), Temporal gravity variations at Mount St. Helens, March-May 1980, *USGS Professional Paper Report: P 1250*, pp. 175–181.

Jousset, P., S. Dwipa, F. Beauducel, T. Duquesnoy, and M. Diament (2000), Temporal gravity at Merapi during the 1993-1995 crisis; an insight into the dynamical behaviour of volcanoes, *Journal of Volcanology and Geothermal Research*, *100*(1–4), 289–320.

Keysers, C. J., H. J. Kuempel, and J. Campbell (2001), Local seasonal gravity changes in the Lower Rhine Embayment, Germany, *Acta Geodaetica et Geophysica Hungarica*, *36*(3), 313–326.

Landrø, M., and L. K. Strønen (2003), 4D study of fluid effects of seismic data in the Gullfaks Field, North Sea, *Geofluids*, *3*, 233–244.

Leirião, S., X. He, L. Christiansen, O. B. Anderson, and P. Bauer-Gottwein (2009), Calculation of the temporal gravity variation from spatially variable water storage change in soils and aquifers, *Journal of Hydrology*, *365*, 302–309.

Longman, I. (1959), Formulas for computing the tidal accelerations due to the Moon and Sun, *Journal of Geophysical Research*, *64*(12), 2351–2355.

MacLennan, K., and Y. Li (2011), Signal extraction from 4D transient electromagnetic surveys using the equivalent source method, *Geophysics*, *76*(3), F147–F155.

Merteens, C., R. Smith, W. Chang, C. Puskas, and T. V. Hove (1998), GPS-derived deformation of the western U.S. Cordillera, Wasatch Front, Utah, and Yellowstone, *EOS Trans. Amer. Geophys. Union*, *79*(45), f203.

Nordquist, G., J. A. P. Protacio, and J. A. Acuña (2004), Precision gravity monitoring of the Bulalo geothermal field, Philippines: independant checks and constraints on numerical simulation, *Geothermics*, *33*, 37–56.

Plouff, D. (1977), Preliminary documentation for a FORTRAN program to compute gravity terrain corrections based on topography digitzed on a geographic grid, *Open-File Report 77-535*, U.S. Geological Survey, 43 pp.

Pool, D., and J. Eychaner (1995), Measurements of aquifer-storage change and specific yield using gravity surveys, *Ground Water*, *33*(3), 425–432.

Pool, D. R. (2008), The utility of gravity and water-level monitoring at alluvial aquifer wells in southern Arizona, *Geophysics*, *73*(6), WA49–WA59.

Sahr, K., D. White, and A. J. Kimerling (2003), Geodesic discrete global grid systems, *Cartography and Geographic Information Science*, *30*(2), 121–134.

Sasagawa, G. S., W. Crawford, O. Eiken, S. Nooner, T. Stenvold, and M. A. Zumberge (2003), A new sea-floor gravimeter, *Geophysics*, *68*(2), 544–553.

Sheldon, N. D., and G. J. Retallack (2001), Equation for compaction of paleosols due to burial, *Geology*, *29*, 247–250, doi:10.1130/0091-7613(2001)029¡0247:EFCOPD¿2.0.CO;2.

Stenger, F. (1993), *Numerical Methods Based on Sinc and Analytic Functions*, 285–291 pp., Springer-Verlag.

Sugihara, M. (1999), Continuous gravity measurements for reservoir monitoring, in *Proceedings, 24th Workshop on Geothermal Reservoir Engineering, Stanford University.*

Sugihara, M. (2001), Reservoir monitoring by repeat gravity measurements at the Sumikawa geothermal field, Japan, in *Proceedings, 26th Workshop on Geothermal Reservoir Engineering, Stanford University.*

Sugihara, M., and T. Ishido (2008), Geothermal reservoir monitoring with a combination of absolute and relative gravimtery, *Geophysics*, *73*(6), WA37–WA47.

Tamura, Y. (1987), A harmonic development of the tide-generating potential, *Bulletins d'Informations Marées Terrestres*, *99*, 6813–6855, Bruxelles.

Verstraeten, I., G. Steele, J. Cannia, D. Hitch, K. Scripter, J. Böhlke, T. Kraemer, and J. Stanton (2001), Interaction of surface water and ground water in the Dutch Flats area, western Nebraska, 1995-99, *Water-Resources Investigations Report 01-4070*, U.S. Geological Survey.

Vigouroux, N., G. Williams-Jones, W. Chadwick, D. Geist, A. Ruiz, and D. Johnson (2008), 4D gravity changes associated with the 2005 eruption of Sierra Negra volcano, Galápagos, *Geophysics*, *73*(6), WA29–WA35.

Wenzel, H. (1996), Accuracy assessment for tidal potential catalogues, *Bulletin d'Informations Marées Terrestres*, *124*, 9394–9416, Bruxelles.

Whitcomb, J. H., W. O. Franzen, J. W. Given, J. C. Pechman, and L. J. Ruff (1980), Time-dependant gravity in southern California, May 1974 to April 1979, *Journal of Geophysical Research*, *85*(B8), 4363–4373.